THE INFLUENCE OF ATMOSPHERIC CIRCULATION ON SNOWMELT AND CARBON FLUXES IN THE CANADIAN LOW ARCTIC

A Thesis Submitted to the Committee on Graduate Studies in Partial Fulfillment of the Requirements for the Degree of Master of Science in the Faculty of Arts and Science

TRENT UNIVERSITY

Peterborough, ON, Canada

Environmental and Life Sciences MSc. Graduate Program

January 2024

ABSTRACT

The Influence of Atmospheric Circulation on Snowmelt and Carbon Fluxes in the Canadian Low Arctic

Alexandra Stephanie Lind Braid

This study examines the atmospheric (synoptic) controls on snowmelt and snow-free season carbon dioxide (CO_2) fluxes at Daring Lake, Northwest Territories. Atmospheric circulation patterns were derived from 500 hPa geopotential height and classified using the self-organizing maps artificial neural network. Snowmelt timing was not found to be influenced by atmospheric circulation patterns or large-scale teleconnection indices, but a shift from meridional to zonal atmospheric circulation marked the transition from pre-melt to melt period. Multiple linear regression identified heating degree days and incoming solar radiation as the most important meteorological predictors of melt length; however, the model would have benefitted from additional variables. Analysis of CO_2 (net ecosystem exchange, NEE) during the snow-free season highlighted a strong correlation between NEE and temperature anomalies. Like the snowmelt period, no atmospheric circulation patterns were found to significantly influence NEE; however, these findings prompt further questions regarding snowmelt and CO_2 fluxes in the Canadian low Arctic.

Keywords: Carbon fluxes, atmospheric circulation, synoptic patterns, self-organizing maps, net ecosystem exchange, snowmelt

ACKNOWLEDGEMENTS

I would like to thank Dr. Peter Lafleur for the incredible amount of kindness and support over the past few years. Dr. Lafleur has also offered unwavering expertise; his knowledge and passion consistently inspired me to produce my best work. I will forever be thankful to Dr. Lafleur for taking me on as a student, especially on short notice. I would also like to extend my thanks to Dr. Lafleur and Dr. Elyn Humphreys for the years of data collection at the Tundra Ecosystem Research Station. This thesis would not have been possible without access to years of valuable data and research. A big thanks is also extended to Colin Burgin, the Tundra Ecosystem Research Station manager, for making my time in the Arctic unforgettable.

I also owe deep gratitude to Dr. Robert Hember and Dr. Julian Aherne for sitting on my committee and providing a wealth of valuable advice and feedback. Their contributions were instrumental in the development and completion of this research.

The completion of this thesis would not have been possible without the collective support and mentorship of these wonderful individuals. I am sincerely thankful for their contributions to my thesis and overall academic development.

TABLE OF CONTENTS

List of Tables

List of Figures

Chapter 1: Introduction

1.1 Climate change and the tundra

The Arctic is warming two times faster than lower latitudes, a phenomenon referred to as Arctic amplification. Such Arctic amplification will likely have significant global implications through surface-climate feedback systems (Intergovernmental Panel on Climate Change [IPCC], 2001; Overland et al., 2015). Furthermore, Arctic regions, including the tundra, are particularly vulnerable to disturbances at both local and global scales (Reynolds and Tenhunen, 1996). Recent observations indicate that river discharge is increasing, vegetation communities are changing, and near-surface permafrost is warming (Box et al., 2019; Stow et al., 2004). Multiple studies have highlighted the significant trends in snow cover extent (SCE) over time, underscoring a general consensus and understanding in its decrease in some Arctic regions over time (Brown et al., 2010; Foster et al., 2008; Yeo et al., 2016).

Feedbacks in the Arctic tundra are complex mechanisms that influence several interconnected systems and thus have potentially wide-ranging impacts (Bonfils et al., 2012; Wookey et al., 2009). For example, decreasing SCE on the tundra has the potential to decrease mean annual albedo (Li et al., 2018; Loranty et al., 2011), intensify permafrost thaw (Wilcox et al., 2019) and alter the distribution and abundance of plant communities (Wipf and Rixen, 2010). Decreasing seasonal SCE and seasonal albedo promote warmer soil and air temperatures, thus influencing active layer depth and permafrost thaw (Lawrence and Swenson, 2011). The active layer refers to the uppermost layer of soil that experiences seasonal freezing and thawing. Variations in permafrost thaw and active layer depth allow shrubs to increase in height and distribution,

which can further alter SCE, albedo, soil and air temperature, and active layer depth (Bonfils et al., 2012). Due to the importance of these processes on a global scale, the feedback systems acting on the tundra have the potential to alter carbon exchange and storage (Wookey et al., 2009), hydrology (Marsh et al., 2010), and energy balances **(**Bonfils et al., 2012; Loranty et al., 2011), further influencing and contributing to climate change.

Although the broad-scale implications of climate change in the Arctic tundra are relatively well understood, and the processes and interactions at local scales have been extensively studied, the connection between the local-scale and large-scale atmospheric drivers are not. This connection is significant as there is growing evidence that atmospheric circulation patterns are likely to undergo changes with climate change, which could further impact the Arctic tundra (Rudeva et al., 2023). To broaden our understanding of the impact and future of climate change in the Arctic tundra, it is critical to develop a general understanding of the large-scale features driving ecosystem-scale processes. To this end, this thesis focuses on large-scale circulation in the atmosphere and its connection to two important environmental processes and their interannual variability: 1) snowmelt timing and duration and 2) carbon dioxide fluxes.

1.2 Snowmelt

Snowmelt is a profound annual event influencing many biotic and abiotic tundra ecosystem processes (Pedersen et al., 2015; Wilcox et al., 2019). The onset, length and termination of snowmelt play crucial roles in Arctic freshwater budgets, the distribution of flora and fauna and surface energy budgets (Box et al., 2019; Derksen et al., 2015;

Pohl and Marsh, 2006). The characteristics of snowmelt are complex and differ depending on geographical location. On the tundra, several ecosystem-scale factors may influence the onset and duration of snowmelt locally, such as slope, aspect, vegetation cover, and water table height (Assini and Young, 2012; Luce et al., 1998). Open areas that lack large stands of vegetation are more susceptible to wind redistribution (Marsh et al., 2010). The redistribution of snow can lead to snow-free patches and causing local heat advection from areas of little to no snow-cover to areas with snow (Pohl and Marsh 2006); however, areas with greater vegetation cover may also see accelerated melt due to radiative outputs from vegetation and decreases in surface albedo (Marsh et al., 2010). Snowmelt is controlled by the surface energy balance, which includes radiation inputs and outputs, turbulent exchanges, subsurface energy transfer, and conductive processes. On the tundra melt is primarily driven by turbulent energy exchanges between the snowpack and atmosphere (Marsh et al., 2010), which are influenced by wind speed and air temperature (Stigter et al., 2018). Once the pack becomes patchy, heat advection may also contribute significantly to the timing and rate of snowmelt (Marsh et al., 2010).

Although there is considerable interannual variability, it is believed that the onset of snowmelt in the Arctic has been advancing in recent decades (Kankaanpää et al., 2018) and will have varying, but uncertain, implications on factors such as the geographic distribution of flora and fauna (Kankaanpää et al., 2018), rate of permafrost melt (Wilcox et al., 2019), and carbon cycling (Aurela et al., 2004; Winchell et al., 2016). It has been demonstrated that earlier spring snowmelt increases springtime carbon uptake in the boreal zone due to increases in season length (Pulliainen et al., 2017). However, evidence from the Arctic tundra is inconsistent. Aurela et al. (2004) first proposed that earlier snowmelt leading to longer snow-free seasons is associated with greater carbon uptake in

Arctic regions, whereas several later studies have found that timing of snowmelt had no effect on and in some cases hindered annual carbon uptake. For example, Humphreys and Lafleur (2011) found that the timing of snowmelt had little effect on summer carbon uptake and instead found that variations in photosynthetic capacity were a more significant contributor due to variations in leaf area. Additionally, Kudo et al. (1999) and Winchell et al. (2016) concluded that earlier snowmelt resulted in a decrease of carbon accumulation.

Not only are snow cover extent and the timing of snowmelt important at the local scale, they also influence processes occurring at the global scale. For example, Li et al. (2018) found that, using satellite measurements spanning 2002 to 2016, a decrease in Arctic snow cover resulted in a decrease in global albedo. Additionally, changes in snowmelt runoff patterns have altered Arctic river discharge rates, which in turn influenced the movement of water masses and freshwater fluxes in the Arctic Ocean. These changes impacting the Arctic Ocean will likely impact global climate systems (Peterson et al., 2002; Rahmstorf, 2002; Semiletov et al., 2016). Although snowmelt is recognized as a profound annual event influencing many ecosystem processes (Box et al., 2019; Derksen et al., 2015), the large-scale atmospheric forces driving its temporal and spatial variability in the tundra remain uncertain.

1.3 Tundra Carbon Exchange

Northern circumpolar permafrost currently holds roughly 50% of the global below ground carbon pool (Tarnocai et al., 2009). Climate change poses a considerable threat to the tundra carbon pool, yet the effects of warming temperatures on carbon fluxes (here

the emphasis is on carbon dioxide, CO_2, fluxes) and the impacts from permafrost thaw in this region are uncertain. Rising air temperatures are likely to accelerate microbial activity, respiration, and decomposition, which may lead to a greater efflux of carbon into the atmosphere (Grosse et al., 2016). Although increasing temperatures may drive the efflux of carbon, they can also promote vegetation growth and lengthen the snow-free season, influencing the influx of carbon (Loranty et al., 2018). Additionally, long-term modelling experiments suggest that future climate change may enhance photosynthetic uptake variability in the short-term, but ultimately result in a net loss of carbon over time due to changes in factors such as soil nutrients and microbial activity (Jiang et al., 2017). Although the fate of the tundra carbon pool is unknown, should it transition from a net sink to a source, surface-climate feedback systems could accelerate the impacts of climate change both in the tundra and globally (Christensen et al., 1999).

Previous studies indicate a high degree of spatial and temporal variability in locally observed CO_2 fluxes (Euskirchen et al., 2012; Lafleur and Humphreys, 2018; Lund et al., 2010; McGuire et al., 2002). Locally, CO_2 uptake is driven by factors such as soil moisture, air temperature and vegetation cover, while emissions are influenced by variables such as air and soil temperature, and vegetation cover (Magnani et al., 2022). While the spatial variability and local-scale processes driving CO_2 fluxes are well studied, there is limited knowledge regarding the large-scale forces that drive the variability in snowmelt timing and CO_2 fluxes in the tundra. Assessing the impacts of large-scale drivers, such as atmospheric circulation, on local-scale processes is crucial in broadening our understanding of the large-scale systems that drive ecosystem-scale processes. Understanding the driving forces behind ecosystem-scale processes has become increasingly important due to the uncertainties associated with climate change.

1.4 Synoptic climatology

Synoptic climatology is the study of how surface-level processes relate to and can be evaluated in the context of large-scale atmospheric circulation patterns (hereafter referred to as synoptic patterns) (Hewitson and Crane, 2002). Synoptic climatology has been used to understand a wide range of environmental processes. More specifically, synoptic climatology has been used to assess how certain atmospheric characteristics, such as troughs or zonal advection, impact environmental processes such as snow-avalanches, flooding, and the movement of air pollutants (Grote, 2020; Martin and Germaine, 2017). The classification of synoptic patterns allows for the examination of the impacts of atmospheric circulation on near-surface weather conditions and, hence, on ecosystem-scale processes. Classification techniques can be either manual or automatic. Technique selection is subjective and depends on the objectives of the research, as larger data sets often benefit from automatic techniques (Dayan et al., 2012; Huth et al., 2008). Manual classification is accomplished with sea level pressure maps and is labour-intensive and inconsistent, but flexible, and it allows skilled forecasters to incorporate their expertise (Dayan et al., 2012). The most common automated classification techniques are correlation-based, such as Principal Component Analysis. Automatic techniques require subjective decision making; for example, researchers are required to determine the desired number of pattern outputs and parameter weights, which can impact the detail provided by each resulting synoptic pattern (Dayan et al., 2012). Yarnal (1993) found that no classification technique is consistently superior to another, and that the technique selected should reflect the available data and the relationships being assessed.

Recently, however, the usage of automated techniques, including artificial neural networks, have become much more widespread (Gibson et al., 2017; Sheridan and Lee, 2011; Zhong et al., 2020).

Self-Organizing Maps (SOMs) are a relatively new classification technique of potentially great value due to their capacity to classify high-dimensional data and their ability to capture spatiotemporal variations in atmospheric circulation (Hewitson and Crane, 2002). SOMs are a class of artificial neural networks used across a broad range of disciplines (Kohonen, 1990). Compared to traditional manual and automatic classification techniques, the SOMs method is more capable of capturing differences in synoptic pattern anomalies and transitional synoptic patterns (Zhong et al., 2020). Furthermore, SOMs possess the ability to represent the data as a continuum, whereas traditional techniques represent discrete synoptic patterns (Sheridan & Lee, 2011; Zhong et al., 2020). The SOM approach is an iterative algorithm used to illustrate and interpret large and complex datasets. SOMs consist of grid processing units referred to as "neurons" that organize the data into an array of two-dimensional nodes (Kohonen, 2013; Sheridan and Lee, 2011).

While not applied to the Arctic tundra, synoptic climatology, and the classification of synoptic patterns has been used to identify relationships between atmospheric circulation patterns, carbon fluxes and snowmelt in other regions. For example, Bednorz (2009) found a relationship between meteorological patterns associated with the North Atlantic Oscillation and rapid snowmelt in the Polish-German lowlands. Additionally, Randazzo et al. (2020) found that a summer storm pattern in the Great Lakes region was associated with a reduction in carbon uptake by temperate forests in Michigan, USA. Liu et al. (2016) studied the impacts of synoptic patterns on carbon dioxide (CO_2) fluxes from

a reservoir in central Mississippi and concluded that frequent synoptic patterns contributed to a 16% increase in the release of CO_2 from the surface. Synoptic climatology holds promise as a useful technique for studying the relationship between the atmosphere and ground-level processes, such as snowmelt and carbon fluxes in a diverse array of regions.

1.5 Study Objectives

This study is the first to investigate the influence of synoptic patterns on snowmelt timing and CO_2 fluxes on the Arctic tundra, with a focus on assessing the relationships between synoptic patterns and net ecosystem exchange (NEE) of CO_2 during the snow-free season. To evaluate these influences, the links between synoptic patterns, snowmelt, and snow-free season CO_2 fluxes (NEE) using an extant collection of on-site data (2004 - 2018) and atmospheric data provided by the National Centers for Environmental Prediction Department of Energy (NCEP-DOE; Kanamitsu et al., 2002) was assessed. As few synoptic climatological studies have evaluated relationships between synoptic patterns and surface processes over long periods of time, the full range of data collected at the study site (2004 - 2018) was used for the purpose of this study. There were two main objectives of this study. First, to assess the relationships between synoptic patterns and the timing and duration of snowmelt, and second, to identify relationships between synoptic patterns and eddy covariance measurements of CO_2 fluxes (NEE) in the snow-free (summer) period. The research questions were:

1. Does the state of the atmosphere change leading up to and during snowmelt?

2. Do certain synoptic patterns exert greater control over snowmelt timing and length than others?
3. Is more positive or negative NEE associated with certain synoptic patterns?
4. Does the state of the atmosphere influence the interannual variability in CO_2 flux?

The remainder of this thesis is presented in four chapters, as follows.

Chapter 2: Methodology. A detailed description of the research site, data sources, methodology for defining SOMs, results of the SOMs analysis, and descriptions of the resulting synoptic patterns.

Chapter 3: Snowmelt on the Tundra. A qualitative analysis of the atmospheric conditions surrounding snowmelt, results of linear regression, and discussion outlining the relationships between synoptic patterns and the timing and duration of snowmelt.

Chapter 4: Tundra CO_2 Flux. A qualitative report on the variability in annual CO_2 fluxes and the variation in synoptic patterns, results of correlation analysis, and discussion describing the relationships between synoptic patterns and snow-free season CO_2 flux.

Chapter 5: General conclusion and future research.

Chapter 2: Methodology

2.1 Study Area

The study area is located near Daring Lake in the low Arctic Ecozone of the Slave Geological Province of the Canadian Shield (64°52.131′ N, 111°34.498′ W), approximately 70 km north of the tree line and 300 km northeast of Yellowknife, Northwest Territories (Figure 1) (Dagg and Lafleur, 2011). The study area is classified as mixed mesic tundra, containing a combination of mesic heath and shrub tussock tundra. Mesic heath and shrub tussock tundra are categorized by graminoids, small shrubs, mosses and lichens and are representative of much of the surrounding region. The study area has coarse mineral soil overlain by an organic layer ranging 1 to 22 cm in depth (Grant et al., 2015; Humphreys and Lafleur, 2011). The region is underlain by continuous permafrost spanning 160 to 350 m in thickness and has an average summer maximum active layer 0.3 to 1 m in depth (Dredge et al., 1999). Winters are long and cold, whereas the snow-free season is short (June to early September) and has an average temperature of 8.6°C (Nobrega and Grogan, 2008).

Research has been carried out surrounding the Tundra Ecosystem Research Station (TERS) since 1994. There are several established study sites surrounding TERS (Figure 1). The Shrub (Sb) site consists predominantly of deciduous shrubs ranging in height from 50 to 100 cm while the Daring Lake (DL) site (a mixed tundra) consists of tussock, sedges, low and dwarf deciduous and evergreen shrubs. The Fen (Fn) site is categorized as a wet sedge tundra and contains graminoids, deciduous shrubs, evergreen

shrubs, and mosses. The Lake Tower (LK) site is categorized as low shrub mixed tundra and contains primarily deciduous shrubs and mosses. For the purposes of this research, the DL site was used to determine the timing and duration of annual snowmelt because it possessed the longest and most complete data record. Additionally, meteorological variables were obtained from the Government of Northwest Territories (GNWT) meteorological tower (Figure 1).

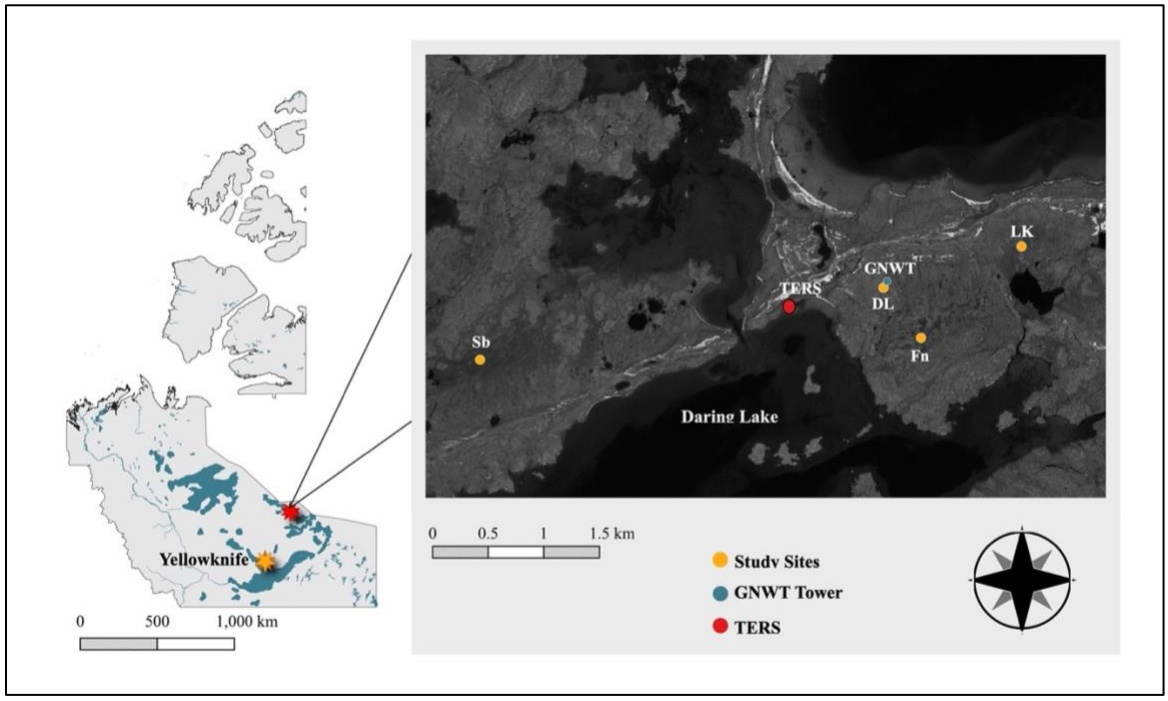

Figure 1. Left: map of Northwest Territories showing the territorial capital, Yellowknife, and the location of the study sites. Right: Expanded view of the study sites and location of the Tundra Ecosystem Research Station (TERS).

2.2 Snowmelt Classification and Meteorological Data

Snowmelt onset, end, duration, and trends have been determined using an array of meteorological data, albedo measurements, and game camera imagery that spanned the study site (Table 1). Meteorological data were obtained from the GNWT tower at a height of roughly 1.3 meters, albedo measurements were obtained from the eddy

covariance station at the DL site, and game camera imagery was obtained from the DL site. Meteorological data, albedo measurements, and data on snow characteristic have been collected near TERS since 2004. Imagery from game cameras have been collected since 2010; however, collection has varied from year to year.

Table 1. Sources and uses of the albedo, meteorological, and imagery data sets.

Data set	Source	Use
Albedo	DL site	Snowmelt classification
Meteorological Conditions - Mean air temperature (°C) - Maximum air temperature (°C) - Incoming solar radiation (Wm^{-2})	GNWT	Snowmelt classification
Game camera imagery	DL site	Snowmelt classification

Snowmelt onset date at the DL site was determined using daily maximum air temperature (°C) and was classified as the day of year (DOY) in which hourly maximum temperatures were above 0°C for three or more consecutive hours in a day and for three or more consecutive days. The end of snowmelt was classified as the DOY in which albedo was less than 0.2 and confirmed using game camera imagery to ensure snowmelt had occurred in the surrounding area. The annual DOYs in which snowmelt began and ended at the DL site were used to classify three melt periods for this study. The pre-melt period consisted of the two-week period leading up to snowmelt onset. The onset period was the 3-day period consisting of the DOY in which onset occurred, the day preceding melt onset, and the day following the melt onset. The length of melt period was defined at the day in which melt onset occurred until the tundra was snow free.

2.3 Carbon Flux Measurements

CO_2 flux data have been collected at the DL site since 2004 using an open-path eddy covariance system. Open-path eddy covariance (EC) systems measure gas and energy exchanges between the surface and atmosphere. With the use of a sonic anemometer and a gas analyzer, the EC system measures wind speed and temperature, as well as fluctuations in gas concentrations, respectively. The statistical combination of these data provides estimates of gas exchange rates (Zhou et al., 2022). The reliability of the open-path EC system was tested in southern Ontario before being deployed in the tundra (Humphreys and Lafleur, 2011, Lafleur and Humphreys, 2008; Lafleur and Humphreys, 2018). Data were collected each year from late winter/early spring until early fall and have been quality checked and gap-filled. Flux measurement methodology and data processing are fully described in Humphreys and Lafleur (2011), Lafleur and Humphreys (2008), Lafleur and Humphreys (2018), and Lafleur et al. (2012). It should be noted that due to extensive gaps in the 2004 data record, only measurements obtained from 2005 to 2018 have been used in this study. For this study, the impacts of synoptic patterns on CO_2 fluxes were evaluated during the snow-free season, the period in the Arctic tundra in which peak carbon cycling activity occurs. The snow-free season was defined as the period following the end of snowmelt until September 30th of each year, after which CO_2 flux measurements were not taken. Although CO_2 exchange at the ecosystem level is composed of two large fluxes (gross ecosystem exchange (uptake) and ecosystem respiration (loss), the EC equipment directly measured the net of these fluxes, in other words NEE. For this study, NEE is used as the metric to assess CO_2 flux at the study site.

2.4 Synoptic Pattern Classification

2.4.1 Data Requirements and SOM Training

To classify synoptic patterns, the SOMs artificial neural network and an average of 4 daily values of 500 hPa geopotential height from the NCEP-DOE Reanalysis 2 data products (Kanamitsu et al., 2002) were used. The spatial domain selected in this study extended from 58° to 71°N and 93° to 125°W (Figure 2). This spatial extent was selected to ensure that the study site was central and to include possible synoptic patterns influenced by the Mackenzie Mountains in the west and the Hudson Bay in the east. SOM grid size determines the number of nodes, or in this case, synoptic patterns in a SOM. For this study, a SOM grid size of four patterns by four patterns (16 total synoptic patterns) was selected through trial and error. SOM grids larger than four patterns by four patterns tended to produce repetitive patterns, whereas smaller SOMs insufficiently captured transitional patterns. All data pre-processing and SOM analyses were completed using the aweSOM, SynoptReg, and Kohonen packages for R in the RStudio interface (Boelaert et al., 2021; Lemus-Canovas et al., 2019; Wehrens and Kruisselbrink 2018).

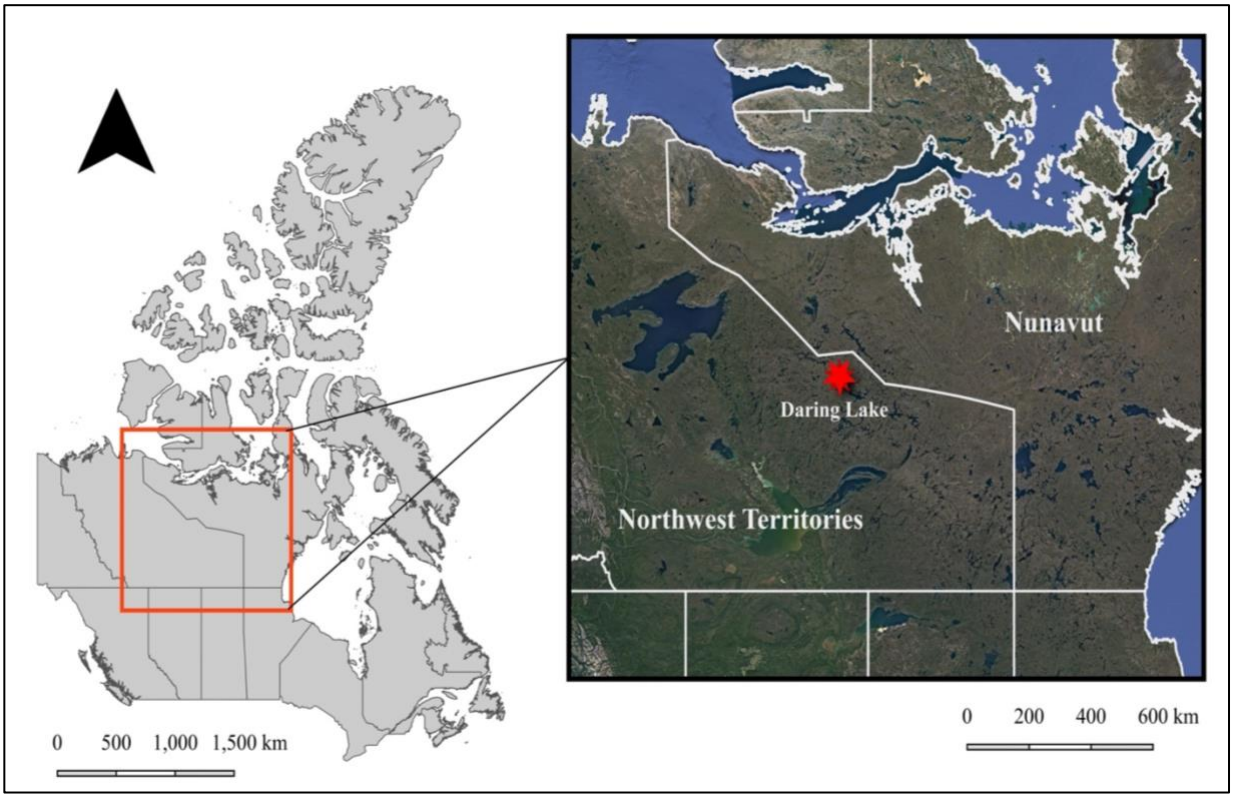

Figure 2. Location and extent of the data used to train the SOM.

A range of SOMs were computed using varying training parameters to select the SOM that best represented the raw data. The SynopReg package was used to train the SOMs and its source code was altered to allow for flexible parameterization of SOM training variables (Lemus-Canovas et al., 2019). Training parameters included SOM topology, learning mode, number of training iterations, neighbourhood functions, and the alpha learning rate.

SOM topologies are traditionally hexagonal or rectangular; however, may be toroidal, or spherical in shape. While spherical and toroidal topologies reduce the impact of edge effects common in rectangular and hexagonal SOMs, they are difficult to interpret and reduce visualization capabilities (Jagric and Zunko, 2013). The edge effect occurs

with rectangular and hexagonal topologies because external nodes are less central to the SOM than internal nodes (Schmidt et al., 2011). Although spherical and toroidal topologies offer a solution to this issue, following Schmidt et al., (2011), they were not tested in SOM training due to the importance of pattern visualization post-classification. A rectangular SOM topology was used for the purpose of this study, as it increased the accuracy of the resulting SOM following training iterations of both rectangular and hexagonal topologies (Table 2).

SOMs traditionally learn via the batch or online methods. In both methods, data is seeded through the nodes of the SOM. Each winning node along with the nodes in its neighbourhood are updated to resemble the input data (Kohonen, 2013). Throughout SOM training the size of the neighbourhood decreases incrementally until only the winning node is altered (Kohonen, 2013). When a SOM learns via the batch method winning nodes are not updated until the entire dataset has been presented to the SOM network, whereas nodes of a SOM trained with the online method are updated after each individual data object has been presented (Wehrens and Kruisselbrink, 2018). The number of training iterations determines the number of times a dataset is presented to SOM and is often selected on the basis of ensuring robust training while preserving computing power. For the purposes of this study, the Online learning method and 1500 training iterations yielded the most favourable SOM results (Table 2).

SOM neighbourhood functions determine the rate at which neighbouring nodes are updated to resemble a winning node (Natita et al., 2016). The most used neighbourhood functions are Gaussian and Bubble. When SOMs employ the Gaussian neighbourhood function, the rate at which a neighbouring node is updated increases with proximity to the winning node. SOMs that employ the Bubble neighbourhood function

will update the entire neighbourhood to the same degree (Chen et al., 2021). Similarly, a SOM's learning rate determines the degree to which an input data object will impact a winning node and its neighbours (Zhang et al., 2018). Learning rates decrease linearly over time and typically range from 0.1 to 0.01 or 0.05 to 0.01 (Zhang et al., 2018). In this study, the Gaussian neighbourhood function paired with a learning rate of 0.1 to 0.01 produced the most optimal SOM outcome (Table 2). An overview of the complete SOM learning process is provided in Figure 3.

Table 2. Parameters used for SOM training (* indicates parameter was selected for the final SOM).

Topology	Learning Mode	Training Iterations	Neighbourhood Function	Learning Rate (alpha)
Rectangular* Hexagonal	Batch Online*	500 1500* 2000	Gaussian* Bubble	0.1 to 0.01* 0.05 to 0.1

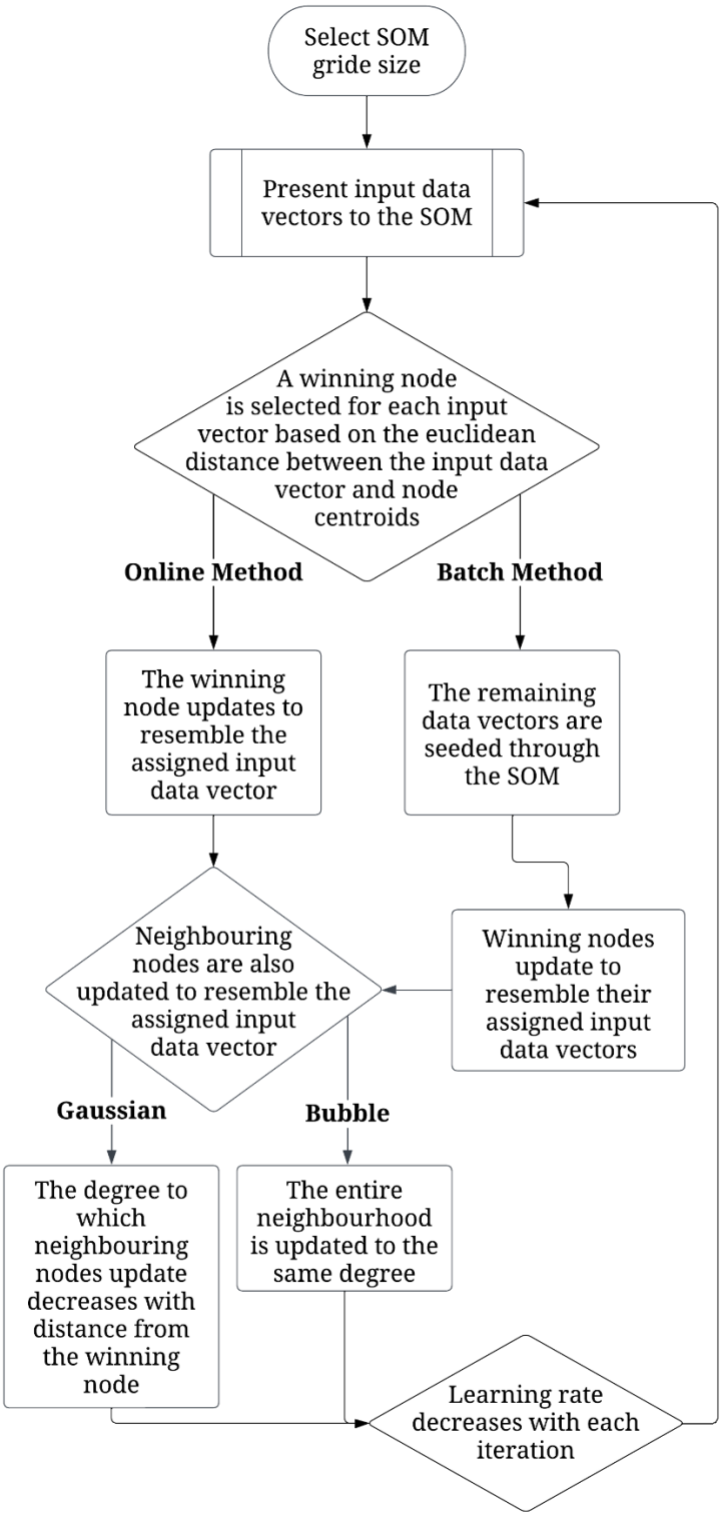

Figure 3. An overview of the SOM learning process with options for Online or Batch learning methods, and Gaussian or Bubble neighbourhood functions.

2.3.2 SOM Results and Synoptic Patterns

Several metrics exist for evaluating SOM performance. Topographical error measures the SOM's ability to self-organize and identifies the first and second-best SOM nodes for each input data vector (Forest et al., 2020). A topographical error occurs when the first and second-best nodes are not neighbours on a map. Topographical errors range from 0 to 1, with lower values indicating a higher degree of topographical preservation (Boelaert et al., 2021; Forest et al., 2020). Quantization error evaluates how well the SOM fits the distribution of the original dataset and measures the mean euclidean distance between the centroid of a winning node and input data vector without accounting for the SOM's topology (Forest et al., 2020; Schmidt et al., 2011). The combined error, established by Kaski and Lagus (1996) incorporates aspects of the topographical and quantization errors. The Kaski-Lagus combined error is defined as the sum of the mean euclidean distance between input data vectors and their winning node and of the mean distance between input data vectors and their second-best node (Boelaert et al., 2021; Kaski and Lagus, 1996). The combined error can range in size, from small such as 0.5 to larger values greater than 55. The measure of these values depends on factors such as SOM shape and the number of training iterations (Le Thi and Nguyen, 2014).

In this study, the Kaski-Lagus combined error was used to select the final SOM, which had a rectangular topology, gaussian neighbourhood, online learning method, underwent 1500 training iterations and possessed a learning rate that declined linearly from 0.1 to 0.01 (Table 2). The SOM had a combined error of 8.12, topographical error of 0.02, and quantization error of 18.74. Additionally, the final SOM explained 80.87% of the variance of the original dataset. The final SOM displayed a range of meridional,

transitional, and zonal patterns with a varying range of height anomalies (deviation of a pattern's geopotential height from the long-term average) (Figure 4; Figure 5). Meridional patterns displayed a north-south flow of atmospheric circulation while zonal patterns displayed west-east atmospheric circulation. Transitional patterns were neither zonal or meridional and occurred at high geopotential heights, while gradient patterns displayed atmospheric circulation over a steep geopotential height gradient. The following is a brief description of each SOM node, with each representing a synoptic pattern.

Pattern 1 was transitional and displayed a more positive 500 hPa geopotential height anomaly compared to all other patterns, a steep ridge, and flow from the west to the southeast. Patterns 2 and 3 were transitional, occurred at relatively high heights with a gentle height gradient, and displayed west to southeast flow. Pattern 4 displayed meridional flow from the north to the southeast and occurred at heights between 5400 and 5600 m. Pattern 5 possessed a steeper height gradient and meridional shape, with flow from the west and northwest to the east. Patterns 6 and 7 both displayed zonal flow from west to east. Pattern 8 was meridional with a gentle height gradient. Like pattern 5, pattern 9 possessed a steep gradient with meridional shape, and flow from the west and southwest to the southeast. Patterns 10 and 11 were relatively similar, displaying zonal flow from west to east and declining height from the south to the north. Flow associated with pattern 12 occurred from the northwest to southeast over a weak height gradient, whereas the flow associated with pattern 13 occurred in the same direction, but over a steep height gradient. Patterns 14, 15, and 16 all possessed a steep height gradient, but differed slightly in shape. Pattern 14 possessed a zonal shape whereas patterns 15 and 16

approached a meridional shape. Pattern 16 occurred at the lowest height compared to all other patterns (Figure 4).

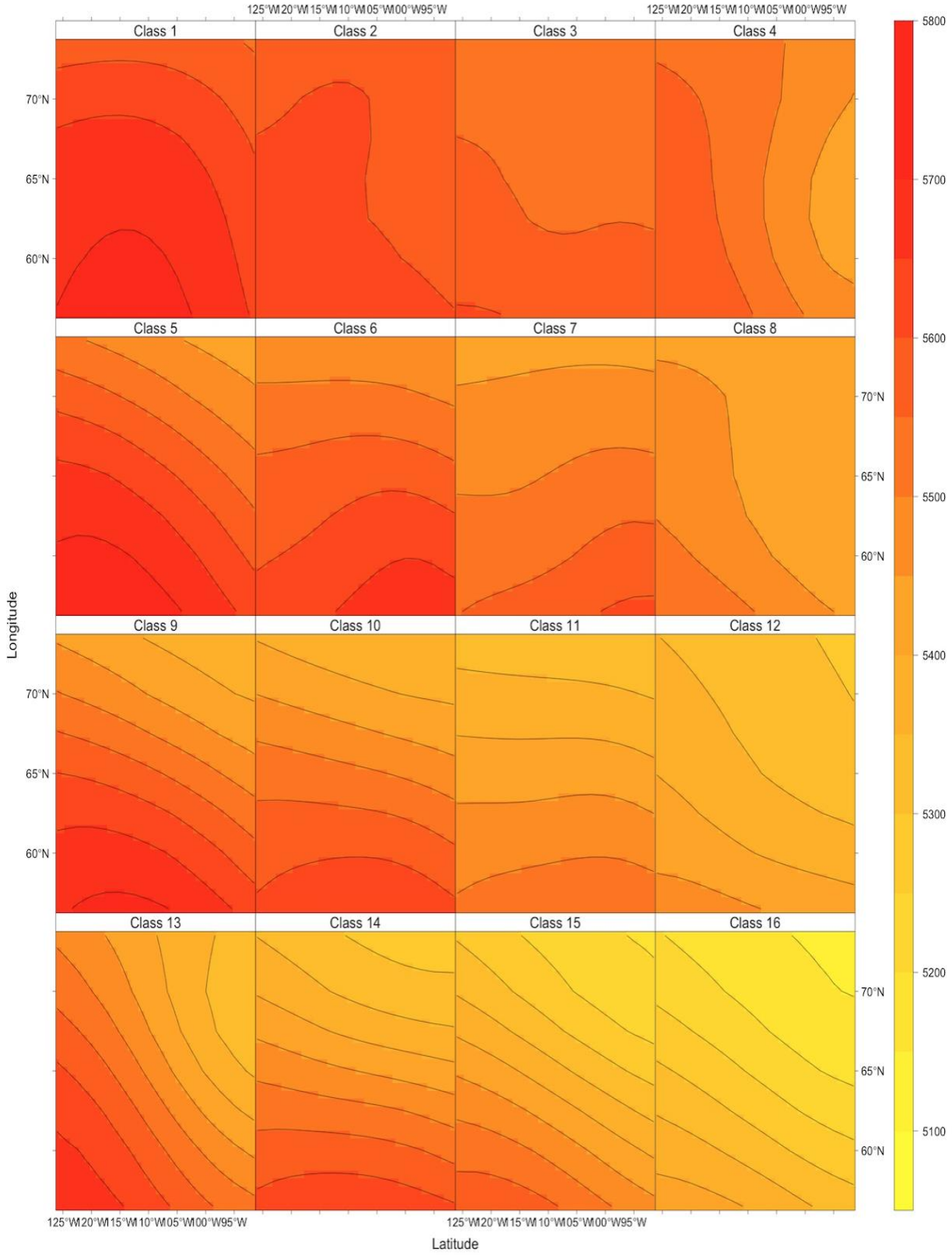

Figure 4. 500 hPa geopotential height of the 16 classified synoptic patterns. Heights are displayed in meters above sea-level.

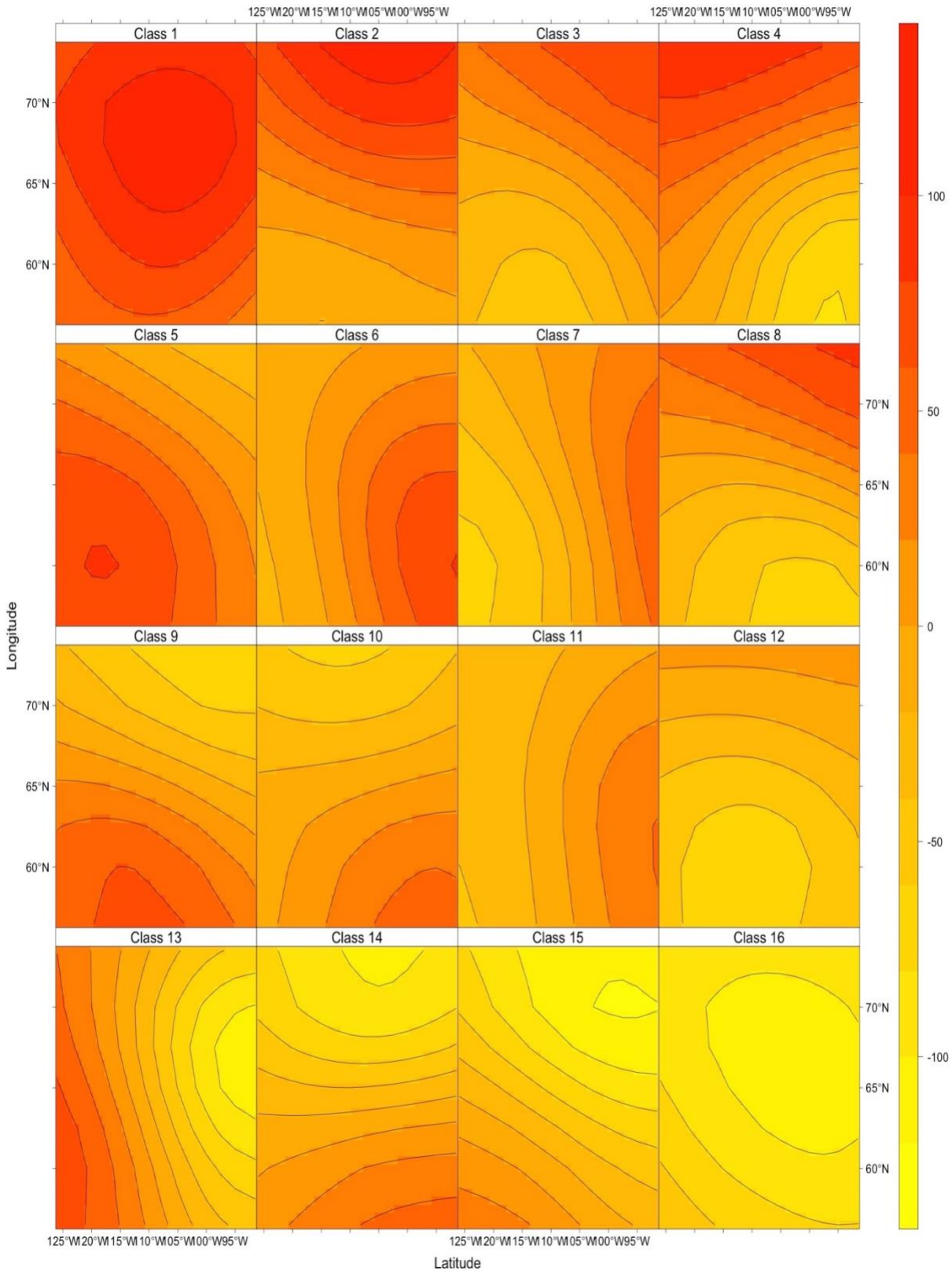

Figure 5. 500 hPa geopotential height anomalies of the 16 classified synoptic patterns. Anomalies are defined as the deviation in meters from average 500 hPa geopotential height.

Pattern occurrence (frequency) was defined as the number of days per period in which a pattern occurred (Figure 6). These days were summed to span the entirety of the study period (2004 – 2018). The average occurrence for all patterns spanning the pre-melt, onset, melt, snow-free and the entire study period (sum of snowmelt and snow-free periods) were 2.9, 1.4, 2.3, 8.8, and 9.8 days, respectively. Total pattern occurrences are presented in Figure 7. Pattern 1 did not occur during in any year during the pre-melt or onset periods, was not dominant during the melt period; however, was dominant during the snow-free season. Similarly, Pattern 2 was not dominant during the pre-melt or onset periods; however, occurred for a higher-than-average number of days during the melt and snow-free periods. Patterns 3, 4, 5, 6, and 7 occurred predominantly during the melt and snow-free periods. Pattern 8 was dominant during the pre-melt, onset, and melt periods and had a low frequency of occurrence during the snow-free season. Patterns 9 and 10 had low occurrences during the pre-melt and onset periods; however, increased occurrence during the melt period and snow-free season. Pattern 11 occurred more than average during the pre-melt and melt periods and was dominant during the onset period; however, did not occur frequently during the snow-free season. Pattern 12 was dominant during pre-melt; however, did not display dominance during the onset, melt, or snow-free periods. Patterns 13 and 14 occurred during each period but were not dominant. Patterns 15 and 16 each occurred for a higher-than-average number of days during the pre-melt period; however, displayed little occurrence during the onset, melt, and snow-free periods. Over the entire study period, patterns 1, 5, and 2 had the highest overall occurrences.

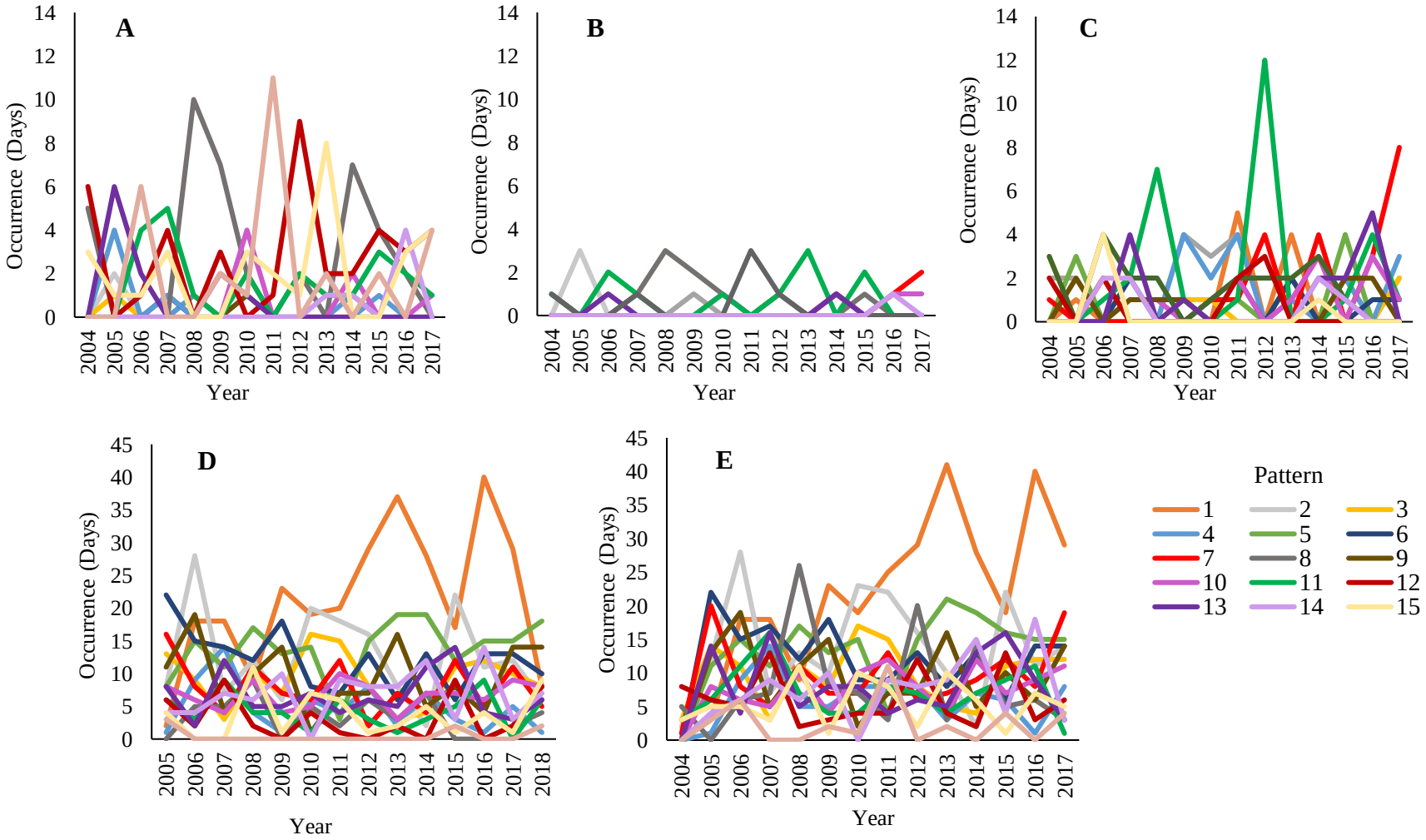

Figure 6. Average pattern occurrence over time in the pre-melt (A), onset (B), melt (C), snow-free (D), and entire study period (E).

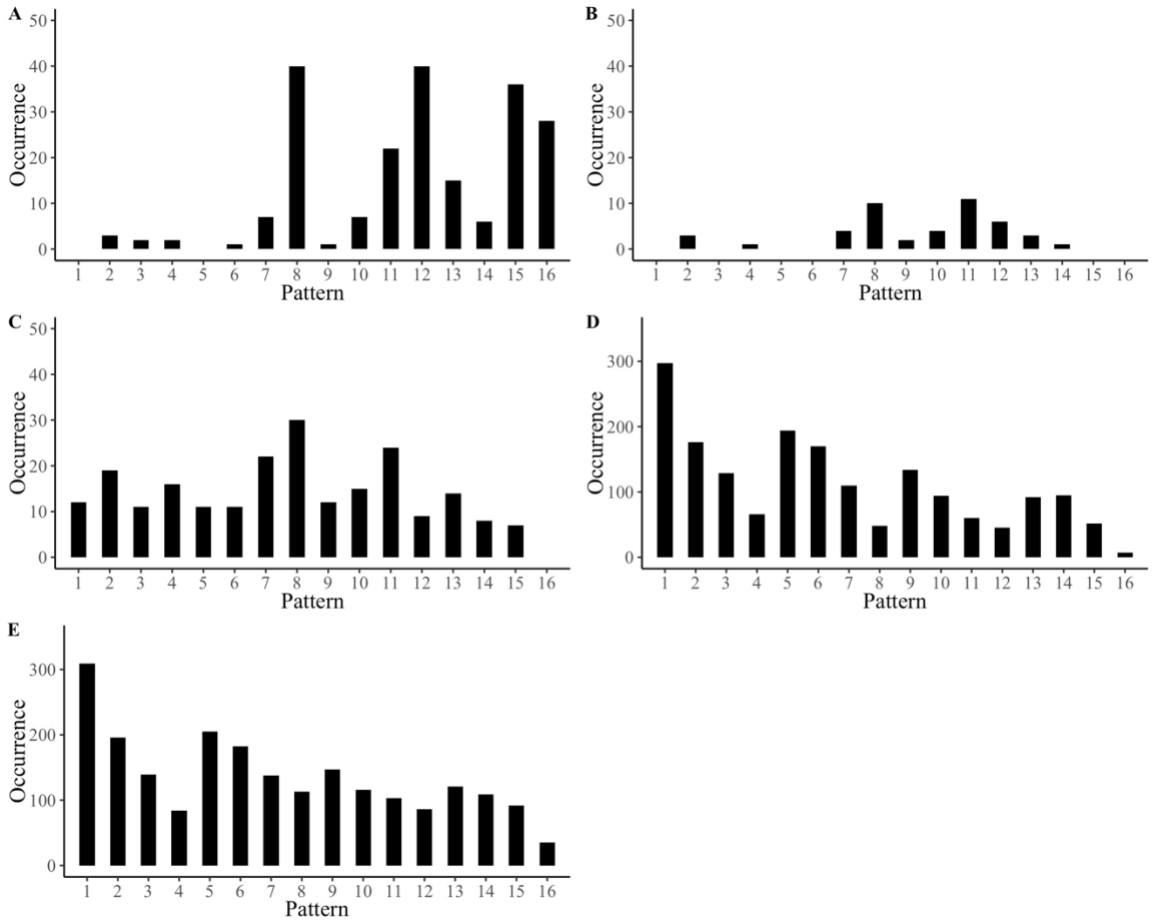

Figure 7. Occurrence (total days) during the pre-melt (A), onset (B), melt (C), snow-free (D) and total study period (E) over the entire study period (2005-2018).

For this study, persistence was defined as the maximum number of successive days a pattern occurred. Like pattern occurrence, persistence was calculated over the entire study period for the pre-melt, onset, melt, snow-free, and total combined periods (Figure 8). During the pre-melt period, patterns 8, 12, 15, and 16 persisted for the longest periods of time. During the onset period, patterns 2, 8, 11, and 12 displayed the longest periods of persistence, while during the melt period, only pattern 8 displayed a dominant length of persistence. Patterns 1, 2, 9, 14, and 15 persisted for the longest periods of time

during the snow-free season. Overall, patterns 1, 2, 8, and 16 persisted for the longest periods of time.

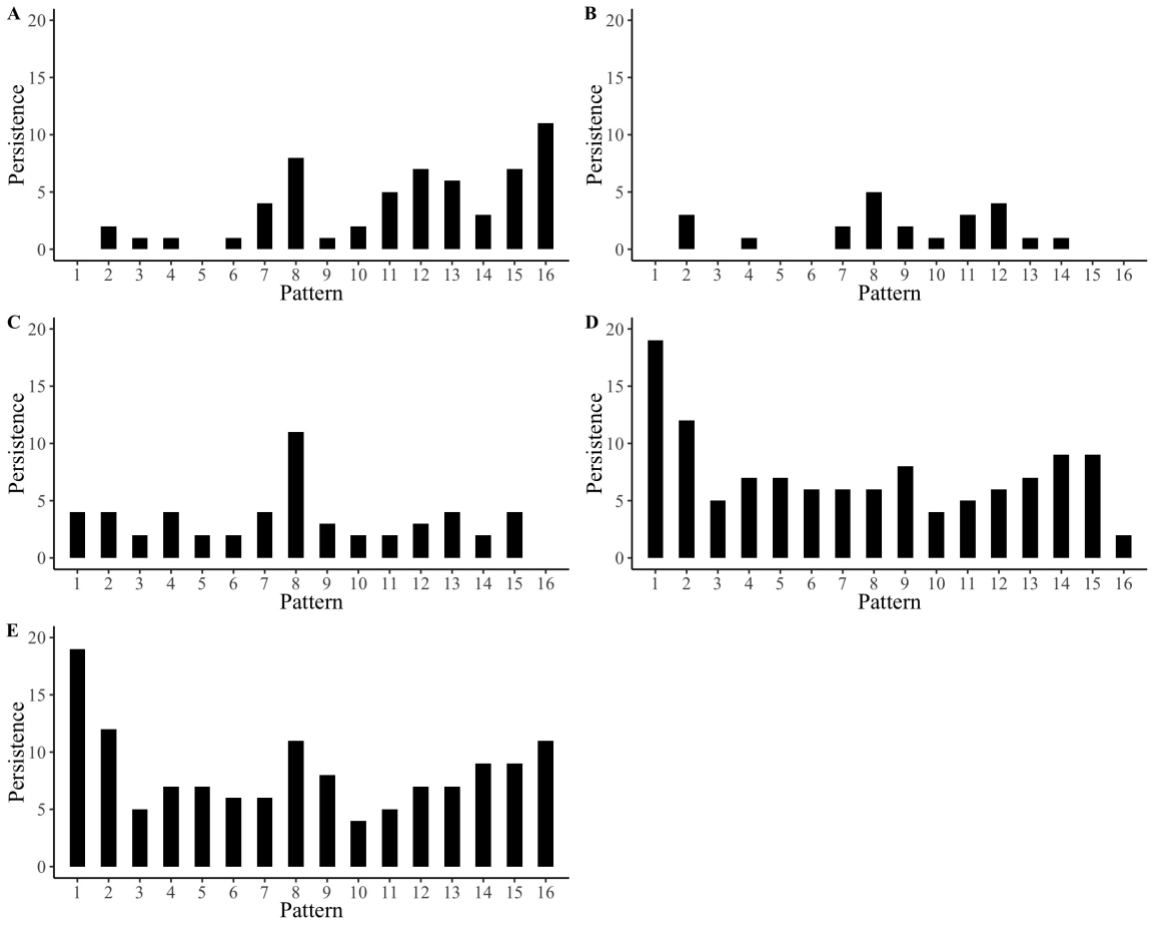

Figure 8. Persistence (maximum number of days a pattern occurred) during the pre-melt (A), onset (B), melt (C), snow-free (d), and total study period (D) over the entire study period (2004-2018).

The meteorological conditions associated with each pattern varied during the pre-melt periods (Figure 9). It should be noted that patterns 1 and 5 did not occur during the melt period, and thus present null meteorological values (Figure 9). Pattern 6 was the only pattern to produce a positive average air temperature, whereas pattern 16 was associated with the coldest average, minimum, and maximum temperatures. Patterns 2, 3,

4, and 6 did not produce precipitation, whereas pattern 14 and 16 produced the largest volume of pre-melt period precipitation. Average surface air pressure was comparable for each pattern. Similarly, average incoming solar radiation was comparable across all patterns, except for patterns 9 and 6 which were associated with the greatest and smallest amounts of solar radiation, respectively. Average surface wind speed was also similar between patterns apart from pattern 6, which was associated with higher wind speeds.

Onset period meteorological conditions varied more than pre-melt conditions; however, it should be noted that patterns 1, 3, 5, 6, 15, and 16 did not occur during the onset period and thus did not contribute to the observed variation in meteorological conditions (Figure 10). Pattern 14 was associated with the coldest average, minimum, and maximum air temperatures, while pattern 9 produced the only positive average and maximum air temperatures during the onset period. Although there was little precipitation during the onset period, pattern 9 was associated with the largest volume. Like the pre-melt period, average surface air pressure and shortwave radiation were comparable across all patterns. Most patterns also produced similar values of average surface wind speed; however, patterns 4 and 7 were associated with slightly higher values.

More variation in meteorological conditions was observed during the melt period (Figure 11). The only pattern that did not occur during melt was pattern 16, which thus did not contribute to the variability in observed meteorological conditions. Pattern 5 was associated with the warmest average, maximum, and minimum air temperatures, whereas pattern 15 was associated with the coldest temperatures. There was some variation in the amount of precipitation associated with each pattern. For example, patterns 1 and 4 did not produce any precipitation, whereas patterns 6, 3, and 7 were associated with the

largest volumes of precipitation. Like the pre-melt period, surface air pressure was fairly consistent across all patterns, apart from pattern 12, which displayed a lower surface air pressure. Additionally, incoming solar radiation was similar between patterns, apart from patterns 2, 4, and 5 which were associated with higher values of solar radiation. Average surface wind speed varied across all patterns. Patterns 4 and 13 displayed the lowest values of wind speed, whereas patterns 11, 15 and 16 were associated with the fastest wind speeds.

Variation in the meteorological conditions associated with each synoptic pattern was also observed during the snow-free season (Figure 12). Pattern 1 was associated with the warmest temperatures, whereas pattern 16 was associated with the coldest temperatures. Patterns 3 and 7 were associated with the highest volumes of average daily precipitation, whereas patterns 4 and 12 were associated with the least. Like the melt periods, surface air pressure was comparable between all patterns. Incoming solar radiation was also similar between patterns, except for patterns 11, 12, 15, and 16, which were associated with lower values of incoming solar radiation. The average surface wind speed associated with each pattern was similar, except for pattern 16 which was associated with the fastest observed wind speeds during the snow-free period.

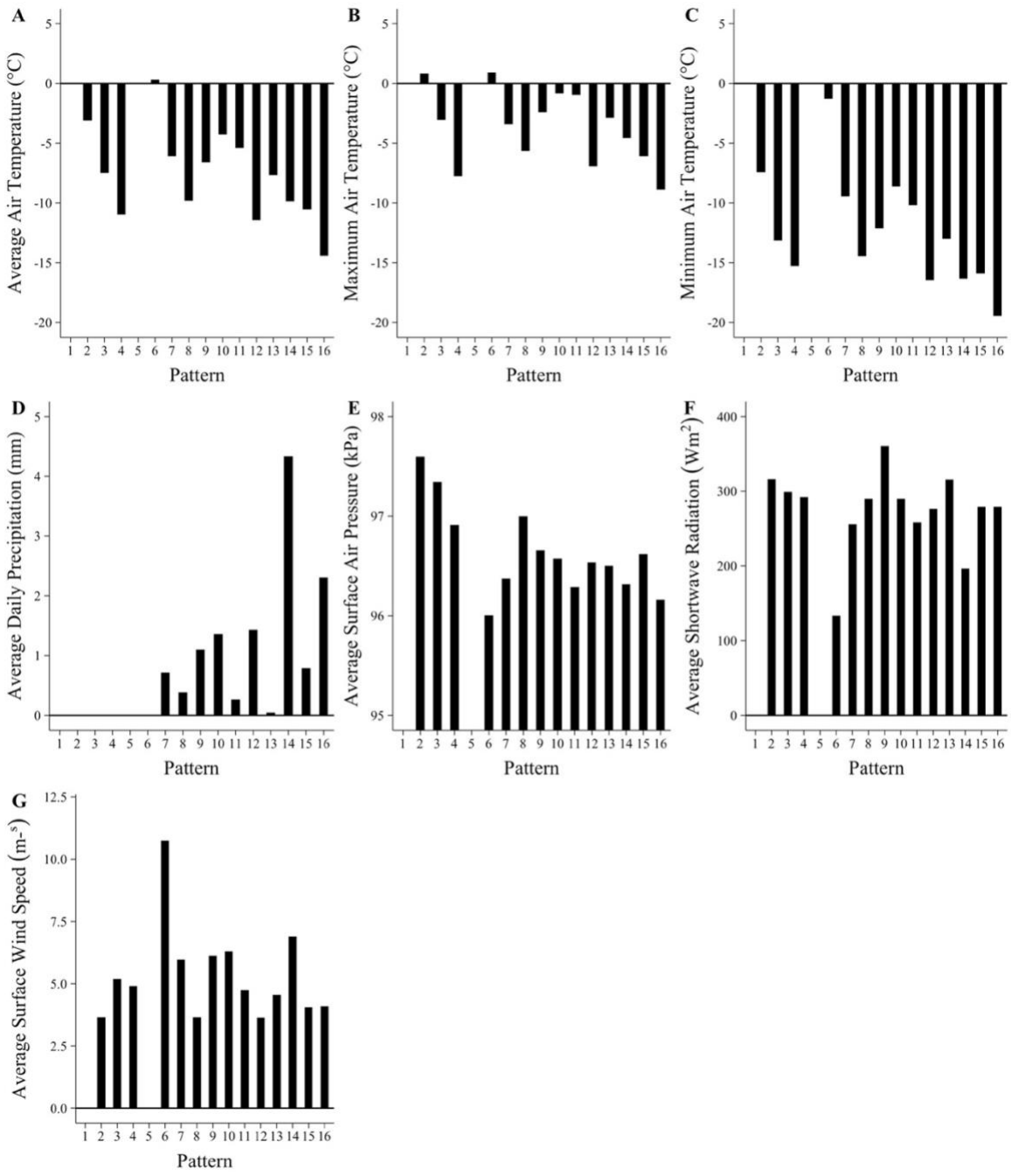

Figure 9. Average daily surface air temperature (A), maximum daily surface air temperature (B), minimum daily surface air temperature (C), average daily precipitation (D), average surface air pressure (E), average shortwave radiation (F), an average surface wind speed (G) for each pattern during the pre-melt period.

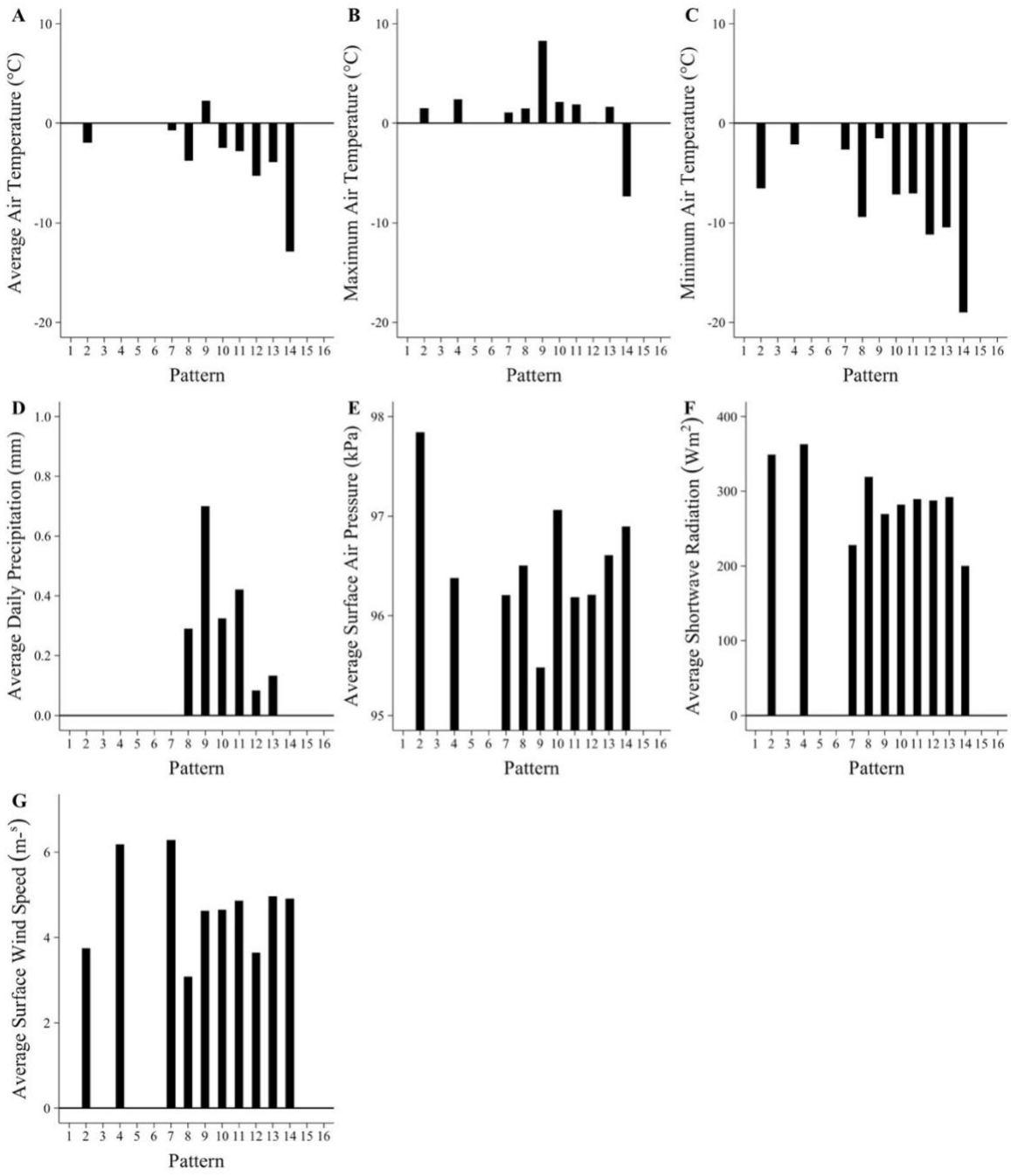

Figure 10. Average daily surface air temperature (A), maximum daily surface air temperature (B), minimum daily surface air temperature (C), average daily precipitation (D), average surface air pressure (E), average shortwave radiation (F), an average surface wind speed (G) for each pattern during the onset period.

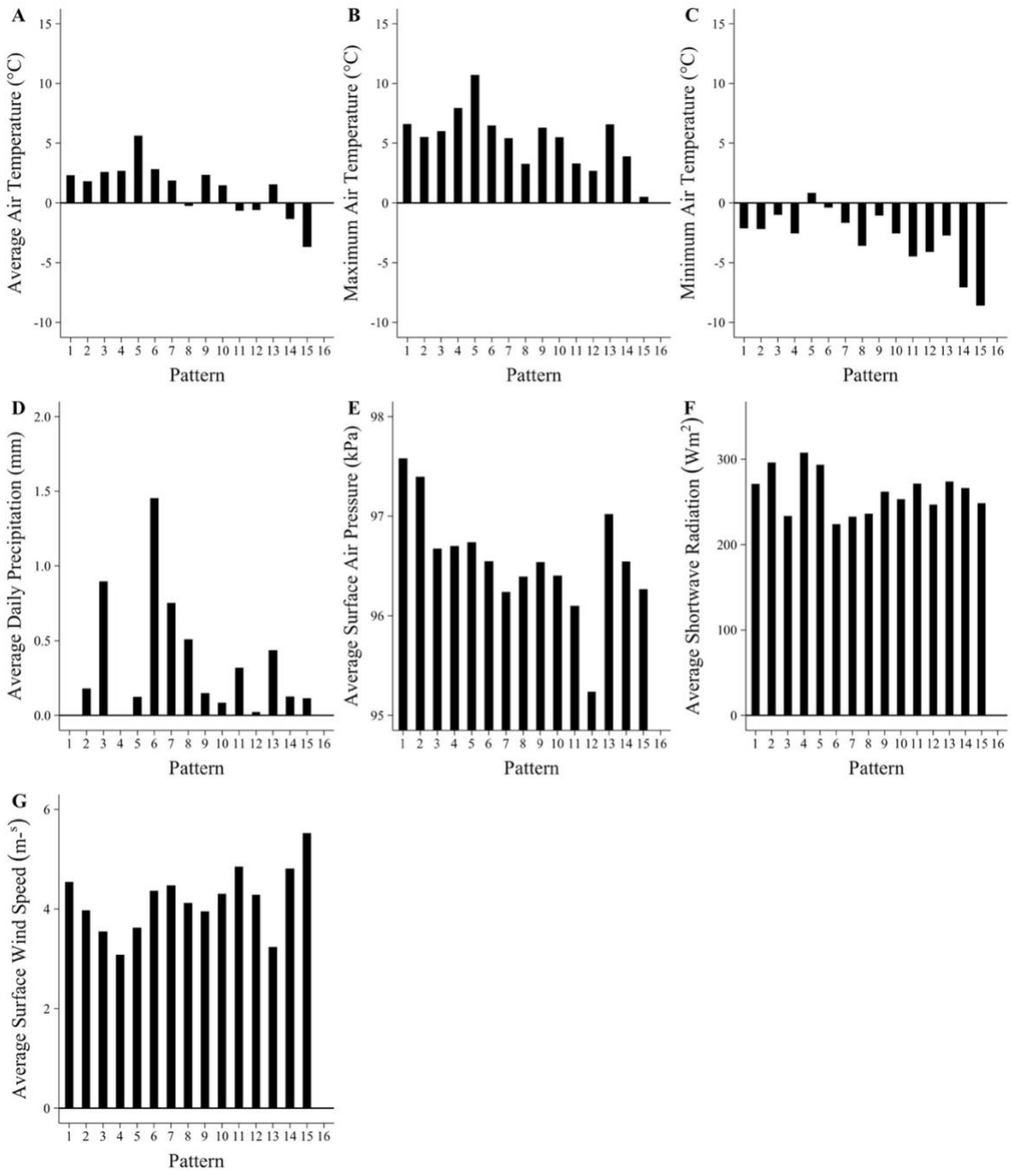

Figure 11. Average daily surface air temperature (A), maximum daily surface air temperature (B), minimum daily surface air temperature (C), average daily precipitation (D), average surface air pressure (E), average shortwave radiation (F), an average surface wind speed (G) for each pattern during the melt period.

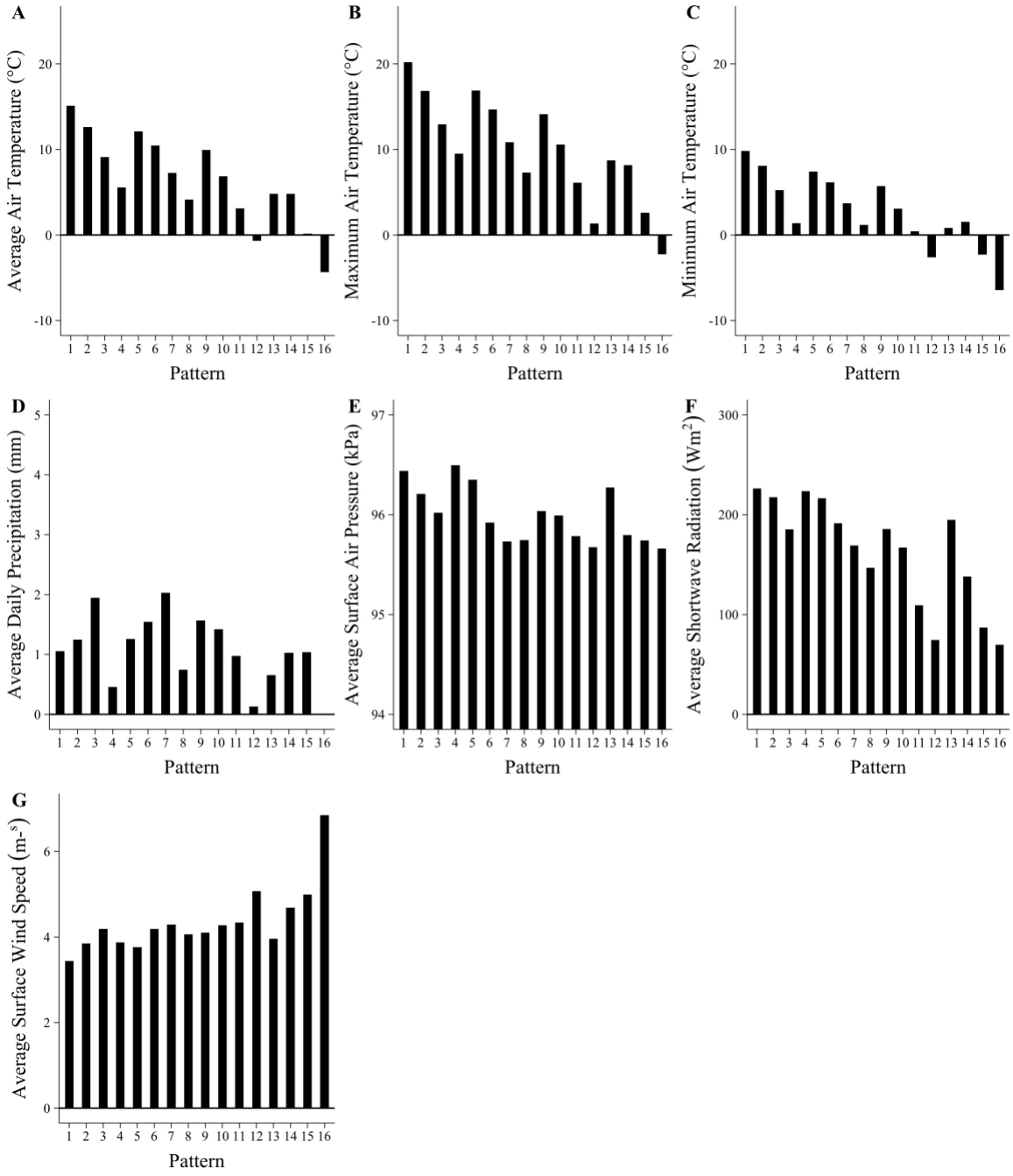

Figure 12. Average daily surface air temperature (A), maximum daily surface air temperature (B), minimum daily surface air temperature (C), average daily precipitation (D), average surface air pressure (E), average shortwave radiation (F), an average surface wind speed (G) for each pattern during snow-free period.

2.4 Synoptic Pattern Clustering

To assist in assessing the relationship between synoptic patterns, snowmelt characteristics, and carbon fluxes, the 16 patterns were subjectively divided into clusters. This reduced redundancy in evaluating similar trends between like patterns. Patterns were sorted based on their synoptic type and were either zonal, meridional, transitional, or gradient in nature, where gradient refers to patterns possessing a steep 500 hPa geopotential height gradient. A visual representation of the subjective division of patterns into clusters is presented in Figure 13.

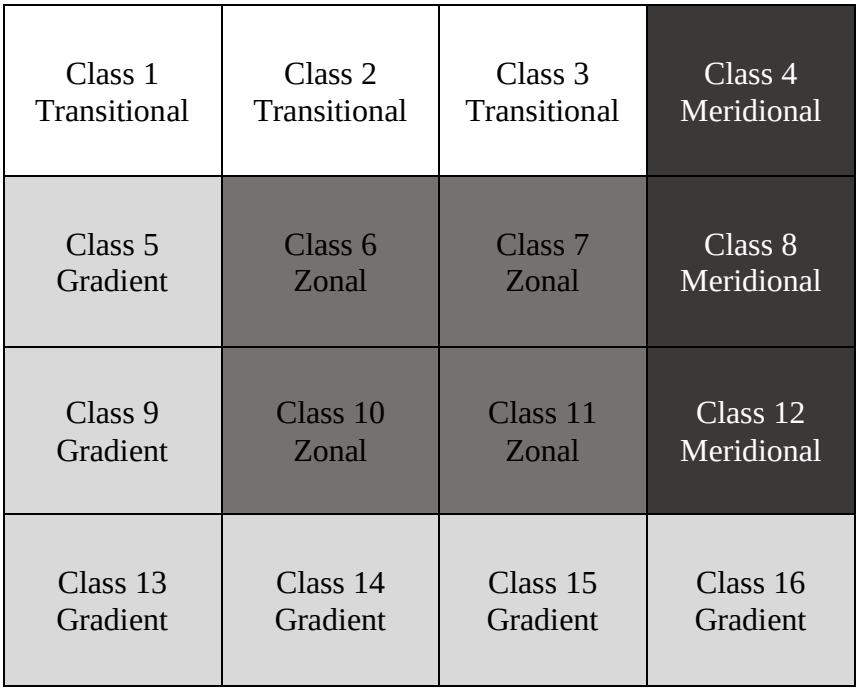

Figure 13. The organization of SOM patterns into the transitional, zonal, gradient, and meridional clusters.

2.5 Statistical Analyses

2.5.1 Assessing the Impacts of Synoptic Patterns on Snowmelt

Relationships between meteorological conditions and snowmelt length were assessed via multiple linear regression where melt period meteorological conditions were the independent variables and snowmelt length was the dependent variable. The meteorological conditions selected for multiple linear regression included heating degree days (HDDs), mean daily incoming solar radiation (W m^2), and mean daily total precipitation (mm) during the length of the melt period. It should be noted that precipitation was not distinguished between snow and rainfall during this period. HDDs were calculated by subtracting the average daily temperature at melt onset from each subsequent day's temperature within the melt period. The sum of these values represented the heating degree days for each melt period. Heating degree calculations were calculated for each year of the study period. The most parsimonious model was selected using Akaike information criterion (AIC). These results were also used to interpret the relative importance of synoptic patterns and the meteorological conditions associated with them on the conditions of snowmelt at the study site.

To assess trends in the state of the atmosphere surrounding snowmelt, pattern and cluster occurrences were calculated as percentages of the total number of occurrences for the pre-melt, onset and melt periods. Snowmelt pattern and cluster occurrences were compared to annual melt onset dates and lengths. Phases of the Arctic Oscillation (AO) and North Atlantic Oscillation (NAO) were compared to snowmelt onset dates to determine if trends between major teleconnection indices and snowmelt existed at the study site via correlation coefficients. Phases, either negative or positive were defined as

the average index for the month or months in which snowmelt occurred. Mann-Kendall tests were performed on pattern occurrences for each of the pre-melt, onset, and melt periods to assess changes in pattern occurrence over time.

2.5.2 Assessing the Impacts of Synoptic Patterns on Carbon Fluxes

Trends in NEE, meteorological conditions, and pattern occurrence over the entire study period (i.e., end of snowmelt to Sept. 30) were evaluated using Mann-Kendall tests. The relationship between average daily NEE and air temperature over the course of the study period was further examined via spearman rank correlation analysis. Additionally, Spearman rank correlation analysis was also used to investigate the potential relationships between the occurrence and persistence of synoptic patterns and NEE. These correlation analyses were performed for the entire study period, on an annual basis, and a monthly basis, which encompassed data from all instances of May, June, July, August, and September throughout the snow-free study period. Furthermore, to assess differences in the corresponding CO_2 fluxes associated with each cluster during different periods of the snow-free season (entire snow-free season and on monthly timescales), Kruskal-Wallis tests were used as data were not normally distributed.

Chapter 3: Snowmelt on the Tundra

3.1 Results

3.1.1 Characteristics of snowmelt

Snowmelt period characteristics are presented in Table 3. Timing of melt onset was variable throughout the study period, ranging from DOY 116 to 149 with a mean onset of DOY 134. The average melt length was 15 days. The longest melt period occurred in 2011 and lasted 24 days, while the shortest melt occurred in 2005 and lasted 8 days. Variations in late-winter snow-depth and average daily temperatures generally did not correspond with increases and decreases in melt period length (Table 3). For example, greater than average snow depth was observed in 2017; however, melt was average in length. Slightly longer melt periods were observed in years in which melt occurred earlier in the year (Figure 14). There was no significant trend in melt onset at Daring Lake between 2004 and 2018 (Figure 15). Similarly, although variable, there was no significant trend in the length of melt period (Figure 16).

Table 3. Annual melt onset, end, and length. Annual mean daily surface air temperature (°C), incoming solar radiation (W m^{-2}), total daily precipitation (mm), heating degree days for the duration of the melt period. Snow depth (cm) at melt onset are also presented.

Year	Onset	End	Length	Temperature	Solar Radiation	Precipitation	HDD	Snow Depth
2004	146	156	11	-0.5	244.5	0.8	19.9	9.0
2005	146	153	8	2.5	304.8	0.1	32.5	23.0
2006	116	130	15	-1.5	242.5	0.1	29.0	35.5
2007	139	152	14	1.0	278.1	0.0	52.5	40.5
2008	133	143	11	0.2	267.2	0.1	41.8	26.3
2009	149	160	12	1.3	310.0	0.3	29.7	17.4
2010	144	154	11	3.2	323.9	0.2	81.9	24.0
2011	126	149	24	1.3	254.1	0.5	131.2	N/A
2012	124	144	21	1.2	228.3	0.4	91.5	7.0
2013	136	151	16	2.7	257.4	0.6	73.5	N/A
2014	132	146	15	0.8	220.3	1.1	53.0	15.5
2015	127	141	15	2.5	293.8	0.0	98.9	19.5
2016	119	136	18	0.2	216.2	0.2	31.2	40.2
2017	127	144	18	2.7	276.0	0.3	54.6	60.3
2018	142	153	12	1.3	266.0	0.7	11.4	29.7

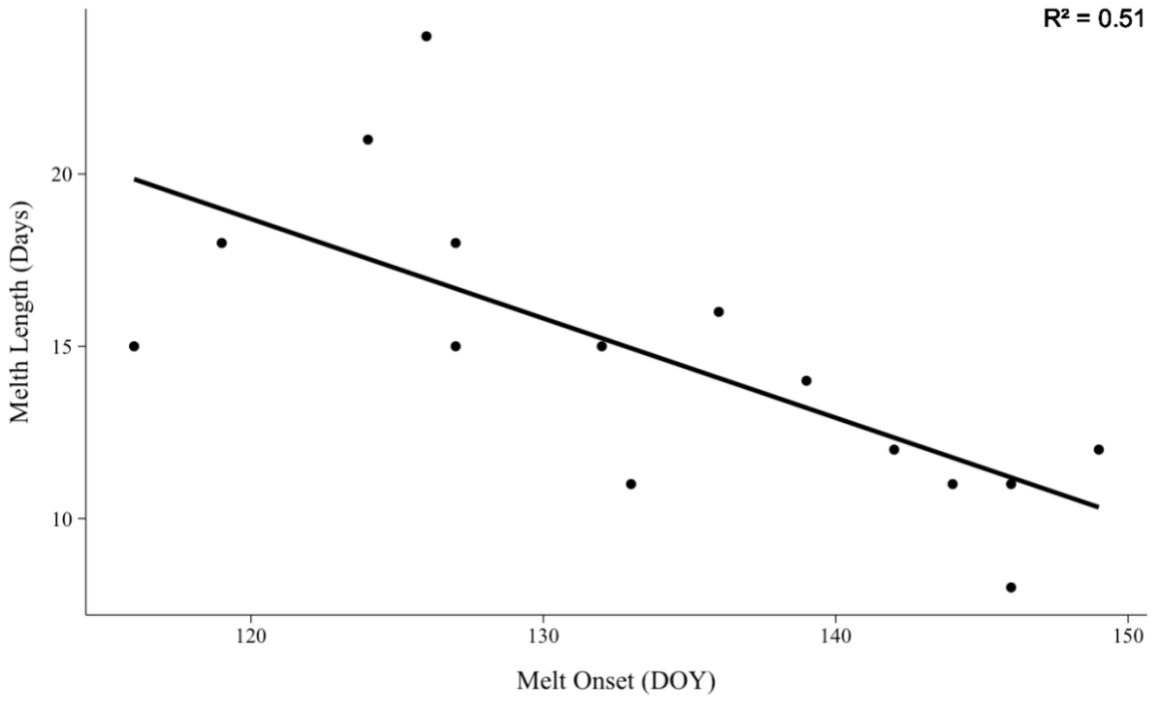

Figure 14. Length of melt and melt onset (DOY) throughout the study period.

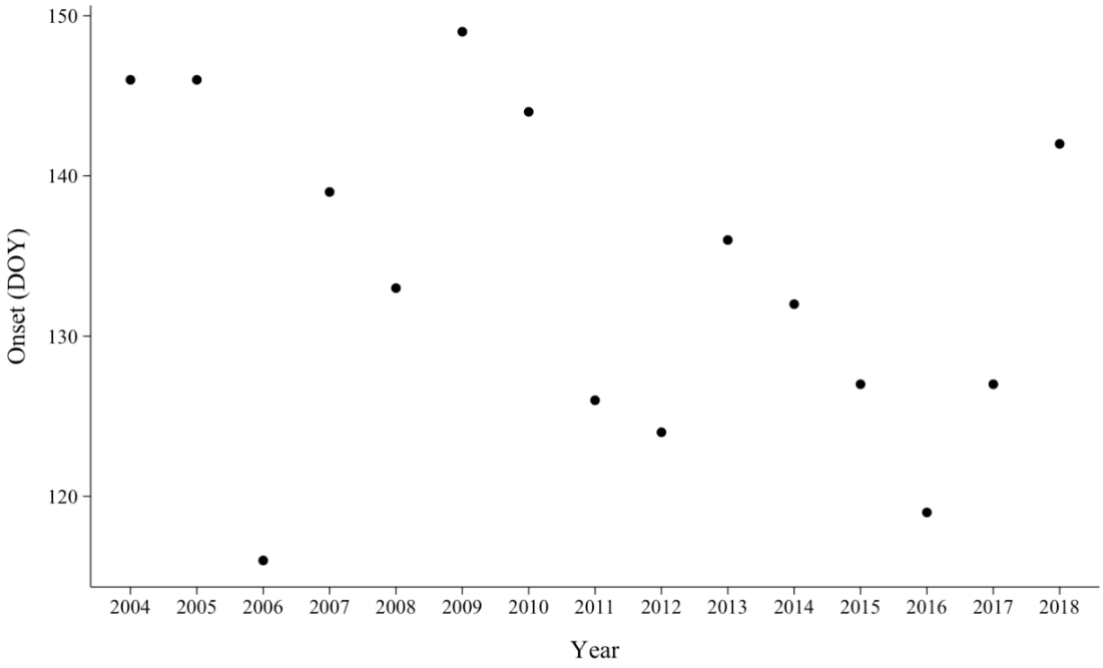

Figure 15. Annual variations in melt onset (DOY).

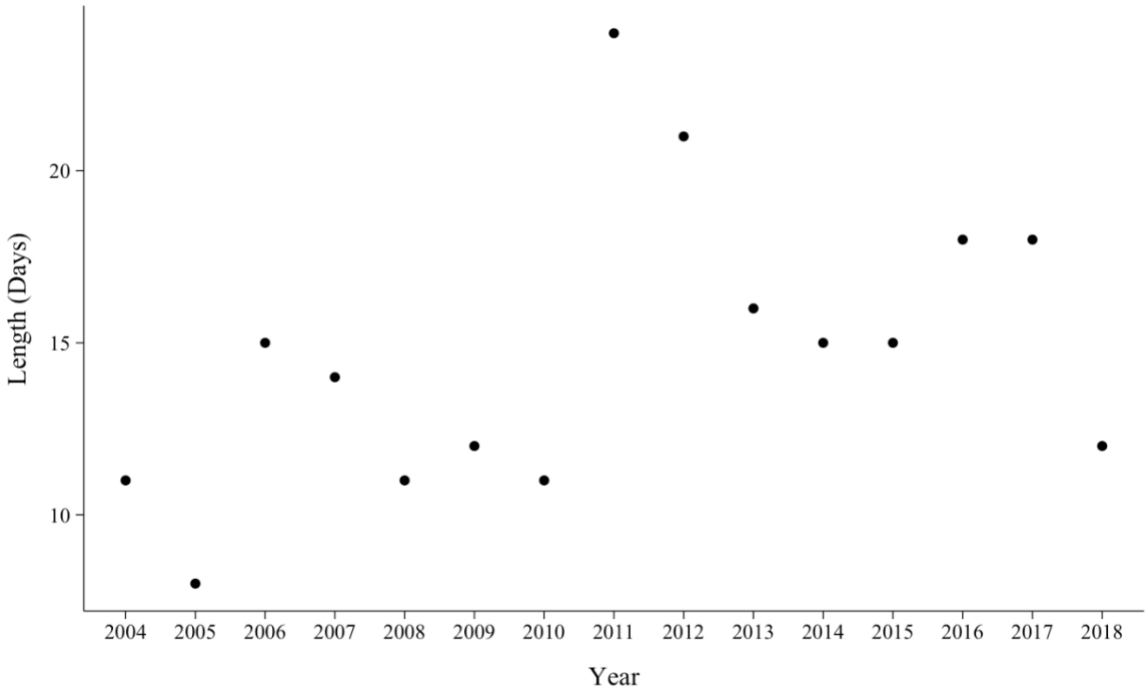

Figure 16. Annual variations in melt length (days).

3.1.2 Analysis of Meteorological Factors Impacting Snowmelt Length

Several linear regression models were tested to evaluate the impact of melt period meteorological conditions on snowmelt length (Appendix 1). Correlation analysis revealed that heating degree days, mean daily incoming solar radiation, and mean daily total precipitation were the most important meteorological variables during snowmelt, while average daily surface wind speed did not correlate significantly with melt length (Table 4). The most parsimonious model did not include precipitation as a significant predictor of melt length (Table 4). The model, which included heating degree days and incoming solar radiation as significant predictors of melt length, had an adjusted R^2 value of 71.5% and P-value of 0.00021 (Table 4). As heating degree days increased melt length increased, while melt length decreased with increasing incoming solar radiation (Figure 17). The counter intuitiveness of the relationship where melt length increases with increasing heating degree days suggests potential issues within the model and raises the question if such a model is capable of adequately capturing tundra melt-meteorological condition relationships.

Table 4. Multiple linear regression variable terms, coefficients, standard errors, and most parsimonious model results where melt length is the dependent variable.

Variable	Term	Coefficient	Standard Error
Intercept	b0	29.56	4.98
Heating degree days	x1	0.087	0.018
Mean daily incoming solar radiation (W m^{-2})	x2	-0.074	0.019
Mean daily total precipitation (mm)	x3	N/A	N/A

Equation	Adjusted R^2	AIC	P-Value
Y = b0 + b1x1 + b2x2	71.47	71.7	0.00021

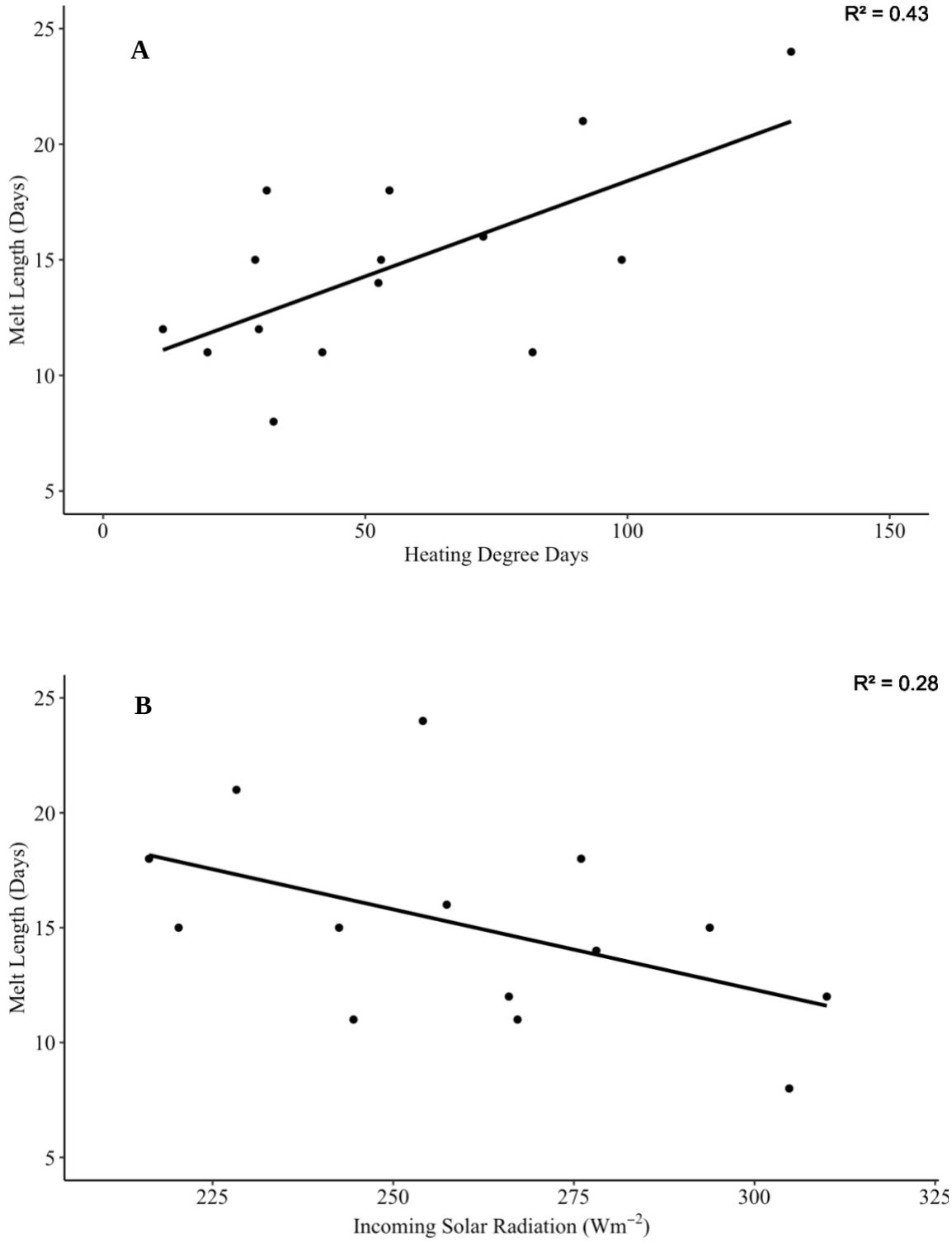

Figure 17. Relationships between melt length, heating degree days (A) and annual average daily incoming solar radiation (B).

3.1.3 The state of the atmosphere during snowmelt

Neither major teleconnection index (AO or NAO) correlated with snowmelt onset (Table 5). During the pre-melt period, the coldest temperatures were associated with the gradient cluster, whereas during the onset and melt periods, the coldest temperatures were associated with the meridional cluster (Figure 18). The transitional cluster produced the warmest temperatures during all three melt periods (Figure 18). Similarly, the transitional cluster was associated with the most incoming solar radiation in all melt periods (Figure 19). The zonal cluster was associated with the least incoming solar radiation in the pre-melt and melt periods, whereas the gradient cluster was associated with the smallest amount of solar radiation during the onset period (Figure 19). Overall, values of incoming solar radiation were greatest during the onset period and smallest during the melt period (Figure 19).

There was little precipitation during snowmelt; however, the pre-melt period was associated with the largest quantities of daily solid precipitation (Figure 20). The gradient cluster produced the largest amount of precipitation during the pre-melt period, whereas the transitional cluster produced none (Figure 20). Little precipitation occurred during the onset and melt periods; however, in each period the zonal cluster was associated with the largest quantity of precipitation (Figure 20).

Table 5. Annual melt onset, Arctic Oscillation (AO) and North Atlantic Oscillation (NAO) phases. Correlation coefficients between teleconnection phases and melt onset are also presented.

Year	Onset	AO	NAO
2004	**146**	-0.09	0.19
2005	**146**	-0.76	-1.25
2006	**116**	0.15	0.05
2007	139	0.89	0.66
2008	133	**-1.21**	**-1.73**
2009	**149**	-0.08	0.24
2010	144	**-0.92**	**-1.49**
2011	126	**1.12**	1.21
2012	124	0.07	-0.22
2013	136	0.49	0.57
2014	132	0.46	-0.92
2015	127	**0.99**	0.44
2016	**119**	-0.54	-0.20
2017	127	-0.41	-0.09
2018	142	0.78	**1.61**
AO Correlation Coefficient	-0.16		
NAO Correlation Coefficient	-0.08		

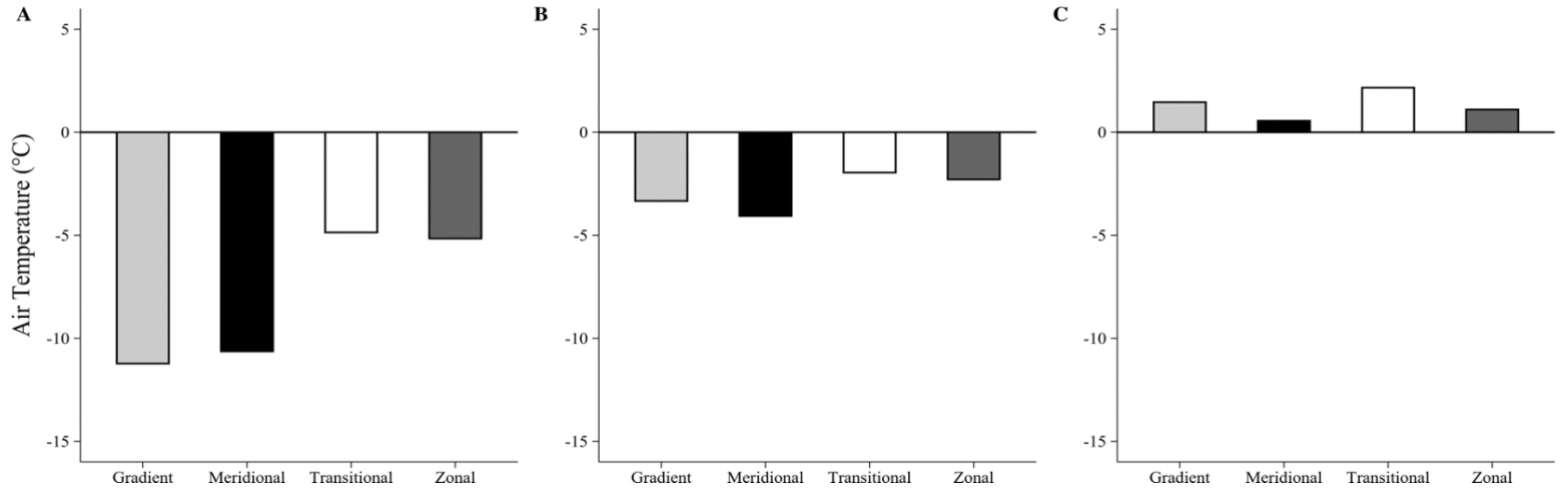

Figure 18. Pre-melt (A), onset (B), and melt (C) period average daily temperatures grouped by cluster.

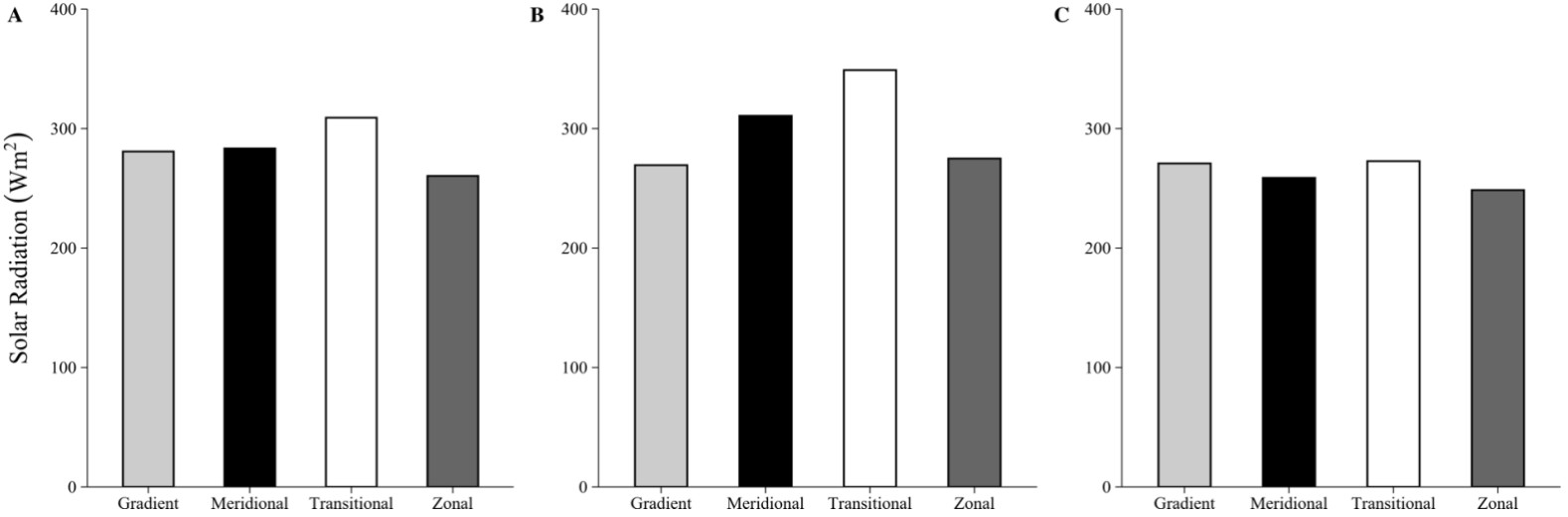

Figure 19. Pre-melt (A), onset (B), and melt (C) period average daily incoming solar radiation grouped by cluster.

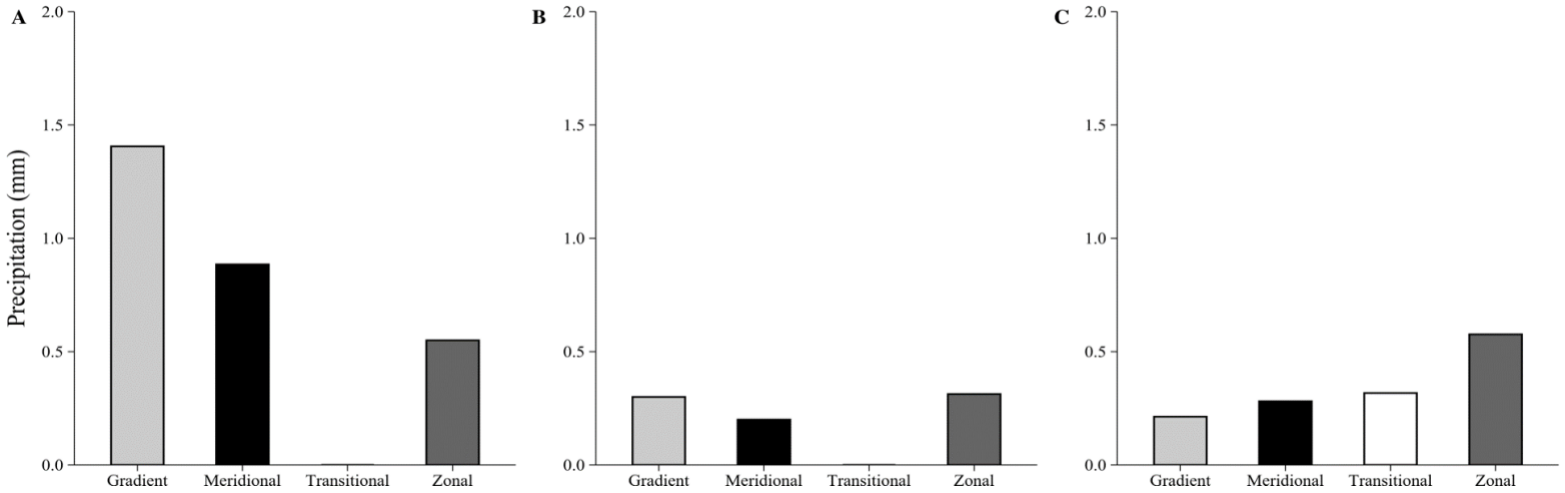

Figure 20. Pre-melt (A), onset (B), and melt (C) period average daily precipitation grouped by cluster.

3.1.4 Synoptic Pattern Variability During the Pre-Melt Period

The pre-melt period was marked by dominant gradient and meridional patterns, where each accounted for ~40% of the total pre-melt time. Zonal patterns were only marginally important (accounting for ~17% of the time) and transitional patterns (P1, P2 and P3) were almost non-existent during pre-melt. Meridional P8 and P12 had the highest mean occurrences throughout the pre-melt period. On Average, each pattern accounted for 19% of the pre-melt period. P16 had the highest pre-melt period one-time occurrence (79% in 2001); however, was only significant in one other year (43% in 2006) (Table 6). There was no clear relationship between pattern or cluster occurrence and snowmelt onset (Table 6). When melt onset occurred earliest (2006), pattern 16 of the gradient cluster was dominant; however, in 2016 when onset was also early, no pattern was dominant (Table 6). When melt onset occurred later in the season, dominant patterns were meridional and gradient in nature. For example, in 2009, when onset occurred latest in the study period pattern 8 of the meridional cluster was dominant. Similarly, in 2004 and 2005, patterns 12 and 13 of the meridional and gradient clusters, respectively, were dominant. It should also be noted that pattern 13 possessed a steep height gradient yet was still meridional in orientation. Additionally, pattern 8 dominated the pre-melt period both in years in which melt was short and average in length (Table 6). Similarly, patterns 16 and 12 were each dominant in years in which melt was long and average in length (Table 6).

3.1.5 Synoptic Pattern Variability During Melt Onset

The onset period was a short 3-day period occurring each year bracketing the first day of melt. Compared to the pre-melt period there was a clear shift in the state of the atmosphere and a distinct trend in cluster occurrence was evident (Table 7). The meridional cluster continued to be of relatively high importance; however, the zonal cluster increased in importance. For example, the meridional cluster accounted for 37.8% of the overall melt periods, whereas the zonal cluster accounted for 42.3% of the overall melt periods (Table 7). Additionally, P11 of the zonal cluster had the highest overall mean onset period occurrence (24.4%) over the entire study period (Table 7). Transitional patterns were only prominent during onset in one year (2005) and the gradient patterns were only important in 2018. As with the pre-melt period, no clear relationship between onset cluster occurrence and snowmelt length was found (Table 7).

3.1.6 Synoptic Pattern Variability During the Melt Period

During the melt period, the zonal cluster continued to dominate. It accounted for 31.3% of overall melt period cluster occurrence (Table 8). The occurrence of transitional patterns also increased substantially compared to previous melt periods (Table 8). A weak, negative correlation was identified between the gradient cluster and snowmelt length; however, cluster occurrence overall did not appear to overtly influence melt length (Table 9). The lack of relationship is especially evident when evaluating certain pattern occurrences, such as P8, which was important during years in which melt occurred over both short and long periods of time (Table 8). Overall, during the melt

period, cluster occurrence was fairly similar between clusters, unlike the pre-melt and melt periods.

Table 6. Annual pre-melt period pattern occurrence (%). Total cluster occurrence and correlation with snowmelt onset dates are presented for each year of the study. Bolded values represent earlier and later than average melt dates (Onset), shorter or longer than average melt durations (Length), and higher than average pattern occurrence.

		Cluster	Transitional				Gradient							Zonal					Meridional			
Year	**Onset**	**Length**	P1	P2	P3	**Total**	P5	P9	P13	P14	P15	P16	**Total**	P6	P7	P10	P11	**Total**	P4	P8	P12	**Total**
2004	**146**	**11**	0	0	0	0	0	0	0	0	21	0	21	0	0	0	0	0	0	**36**	**43**	**79**
2005	**146**	**8**	0	14	7	21	0	0	**43**	0	7	0	**50**	0	29	0	0	29	0	0	0	0
2006	**116**	15	0	0	0	0	0	0	14	0	7	**43**	**64**	0	0	0	29	29	0	0	7	7
2007	139	14	0	0	0	0	0	0	0	0	21	0	21	7	7	0	**36**	**50**	0	0	29	29
2008	133	**11**	0	7	7	14	0	0	0	0	0	0	0	0	0	0	7	7	7	**71**	0	**79**
2009	**149**	12	0	0	0	0	0	0	14	0	0	14	29	0	0	0	0	0	0	**50**	21	**71**
2010	144	**11**	0	0	0	0	0	7	7	0	21	7	43	0	0	29	14	43	0	14	0	14
2011	126	**24**	0	0	0	0	0	0	0	0	14	**79**	**93**	0	0	0	0	0	0	0	7	7
2012	124	**21**	0	0	0	0	0	0	0	0	7	0	7	0	0	0	14	14	0	14	**64**	**79**
2013	136	16	0	0	0	0	0	0	0	7	**57**	14	**79**	0	0	0	7	7	0	0	14	14
2014	132	15	0	0	0	0	0	0	0	7	0	0	7	0	7	14	7	29	0	**50**	14	**64**
2015	127	15	0	0	0	0	0	0	0	0	0	14	14	0	0	0	21	21	7	29	29	**64**
2016	**119**	18	0	0	0	0	0	0	0	29	21	0	**50**	0	0	0	14	14	0	14	21	36
2017	127	18	0	0	0	0	0	0	0	0	29	29	**57**	0	0	7	7	14	0	0	29	29
2018	142	12	0	0	0	0	0	0	29	0	**50**	0	**79**	0	7	0	0	7	0	7	7	14
Mean	134	15	0.0	1.4	0.9	2.4	0.0	0.5	7.1	2.9	17.0	13.3	**41.0**	0.5	3.3	3.3	10.4	17.6	0.9	19.0	19.0	**39.1**
Standard Deviation	10	4.2	0.0	3.9	2.5	6.4	0.0	1.8	13.0	7.6	17.7	22.2	29.4	1.8	7.7	8.1	11.1	15.5	2.5	23.0	17.9	30.1
Onset Date Correlation			0.2				-0.1							0.0					0.1			

Table 7. Annual onset period pattern occurrence (%). Total cluster occurrence and correlation with snowmelt onset dates are presented for each year of the study. Bolded values represent earlier and later than average melt dates (Onset), shorter or longer than average melt durations (Length), and higher than average pattern occurrence.

		Cluster	**Transitional**				**Gradient**							**Zonal**					**Meridional**			
Year	**Onset**	**Length**	P1	P2	P3	**Total**	P5	P9	P13	P14	P15	P16	**Total**	P6	P7	P10	P11	**Total**	P4	P8	P12	**Total**
2004	**146**	**11**	0	0	0	0	0	0	0	0	0	0	0	0	0	0	33	33	0	33	33	**67**
2005	**146**	**8**	0	**100**	0	**100**	0	0	0	0	0	0	0	0	0	0	0	0	0	0	0	0
2006	**116**	15	0	0	0	0	0	0	33	0	0	0	33	0	0	0	**67**	**67**	0	0	0	0
2007	139	14	0	0	0	0	0	0	0	0	0	0	0	0	0	0	33	33	0	33	33	**67**
2008	133	**11**	0	0	0	0	0	0	0	0	0	0	0	0	0	0	0	0	0	**100**	0	**100**
2009	**149**	12	0	0	0	0	0	0	0	0	0	0	0	0	0	0	0	0	33	**67**	0	**100**
2010	144	**11**	0	0	0	0	0	0	0	0	0	0	0	0	0	33	33	**67**	0	33	0	33
2011	126	**24**	0	0	0	0	0	0	0	0	0	0	0	0	0	0	0	0	0	0	**100**	**100**
2012	124	**21**	0	0	0	0	0	0	0	0	0	0	0	0	0	0	33	33	0	33	33	**67**
2013	136	16	0	0	0	0	0	0	0	0	0	0	0	0	0	0	**100**	**100**	0	0	0	0
2014	132	15	0	0	0	0	0	0	33	0	0	0	33	0	33	33	0	**67**	0	0	0	0
2015	127	15	0	0	0	0	0	0	0	0	0	0	0	0	0	0	**67**	**67**	0	33	0	33
2016	**119**	18	0	0	0	0	0	0	0	33	0	0	33	0	33	33	0	**67**	0	0	0	0
2017	127	18	0	0	0	0	0	0	0	0	0	0	0	0	**67**	33	0	**100**	0	0	0	0
2018	142	12	0	0	0	0	0	**67**	33	0	0	0	**100**	0	0	0	0	0	0	0	0	0
Mean	134	14.7	0.0	6.7	0.0	6.7	0.0	4.5	6.6	2.2	0.0	0.0	13.3	0.0	8.9	8.8	24.4	**42.3**	2.2	22.1	13.3	37.8
Standard Deviation	10.4	4.2	0.0	25.8	0.0	25.8	0.0	17.3	13.7	8.5	0.0	0.0	27.6	0.0	19.8	15.1	32.1	36.8	8.5	30.0	27.6	41.6
Melt Length Correlation			NA				-0.1							0.2					0.1			

Table 8. Annual melt period pattern occurrence (%). Total cluster occurrence and correlation with snowmelt onset dates are presented for each year of the study. Bolded values represent earlier and later than average melt dates (Onset), shorter or longer than average melt durations (Length), and higher than average pattern occurrence.

Cluster			**Transitional**				**Gradient**							**Zonal**					**Meridional**			
Year	**Onset**	**Length**	P1	P2	P3	**Total**	P5	P9	P13	P14	P15	P16	**Total**	P6	P7	P10	P11	**Total**	P4	P8	P12	**Total**
2004	**146**	**11**	0	18	27	45	0	0	0	0	0	0	0	0	9	0	27	36	0	0	18	18
2005	**146**	**8**	13	25	0	38	38	25	0	0	0	0	**63**	0	0	0	0	0	0	0	0	0
2006	**116**	15	0	0	13	13	0	0	0	13	27	0	40	0	0	0	27	27	0	7	13	20
2007	139	14	0	0	0	0	0	7	29	14	0	0	**50**	14	0	7	14	36	0	14	0	14
2008	133	**11**	0	0	0	0	0	9	0	0	0	0	9	0	0	9	18	27	0	**64**	0	**64**
2009	**149**	12	0	33	8	42	0	8	8	0	0	0	17	0	0	0	0	0	33	8	0	42
2010	144	**11**	0	27	9	36	9	0	0	0	0	0	9	9	9	9	9	36	18	0	0	18
2011	126	**24**	21	17	0	38	4	0	0	0	0	0	4	8	4	8	8	29	17	4	8	29
2012	124	**21**	0	0	0	0	0	0	0	0	0	0	0	0	19	0	10	29	0	**57**	14	**71**
2013	136	16	25	13	13	**50**	13	0	0	0	0	0	13	13	0	6	13	31	6	0	0	6
2014	132	15	0	0	0	0	0	0	13	13	7	0	33	0	27	20	20	**67**	0	0	0	0
2015	127	15	13	0	0	13	27	13	13	7	0	0	**60**	0	0	0	7	7	13	7	0	20
2016	**119**	18	0	0	0	0	0	11	28	0	0	0	39	6	17	17	0	39	0	22	0	22
2017	127	18	0	11	11	22	0	0	0	0	0	0	0	6	**44**	6	0	**56**	17	6	0	22
2018	142	12	0	0	0	0	0	25	0	8	17	0	**50**	17	0	17	17	**50**	0	0	0	0
Mean	134	14.7	4.8	9.6	5.4	19.8	6.1	6.5	6.1	3.7	3.4	0.0	25.8	4.9	8.6	6.6	**11.3**	**31.3**	6.9	**12.6**	3.5	23.2
Standard Deviation	10.4	4.2	8.7	11.8	8.0	19.6	11.6	8.8	10.3	5.6	8.0	0.0	23.0	6.1	13.0	6.9	9.3	18.8	10.3	20.5	6.4	21.4
Melt Length Correlation			-0.2				-0.4							0.3					0.3			

3.1.7 Energy transport across the SOM grid

As noted above, the pre-melt period was dominated by meridional and gradient synoptic patterns that promoted energy transport from the northwest to southeast. During the pre-melt period, temperatures northwest and west (Paulatuk and Norman Wells, NWT) were warmer than average temperatures at Daring Lake (Figure 21). The onset and melt periods were each dominated by zonal patterns. These zonal patterns carried heat from the west, inducing above-zero temperatures that promote snowmelt (Figure 22, Figure 23). During the onset and melt periods, temperatures west of the study area exceeded those at Daring Lake (Figure 22, Figure 23). As noted above, transitional pattern occurrences, characterized as energy transport from the southwest and west, also increased during the melt period.

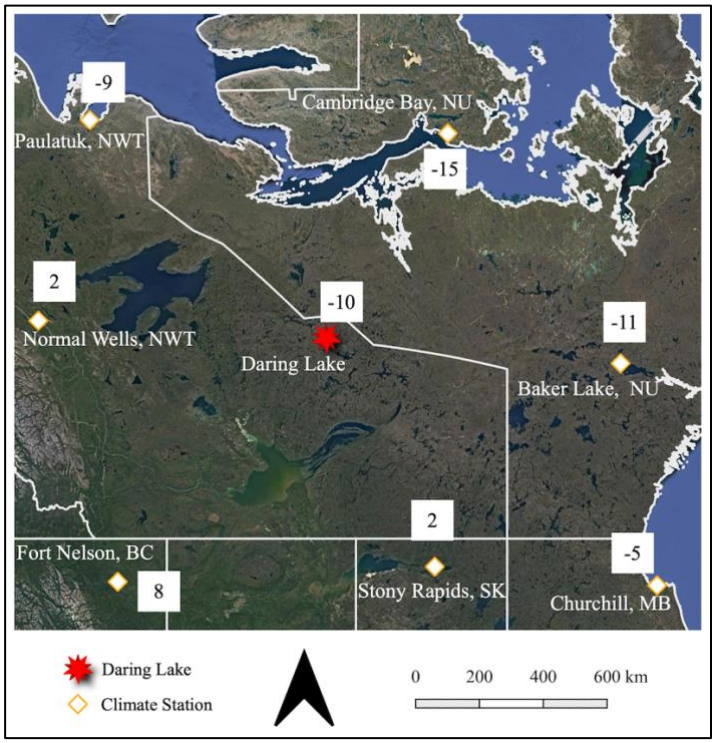

Figure 21. Average pre-melt period surface air temperatures (°C) across the SOM grid over the entire study period.

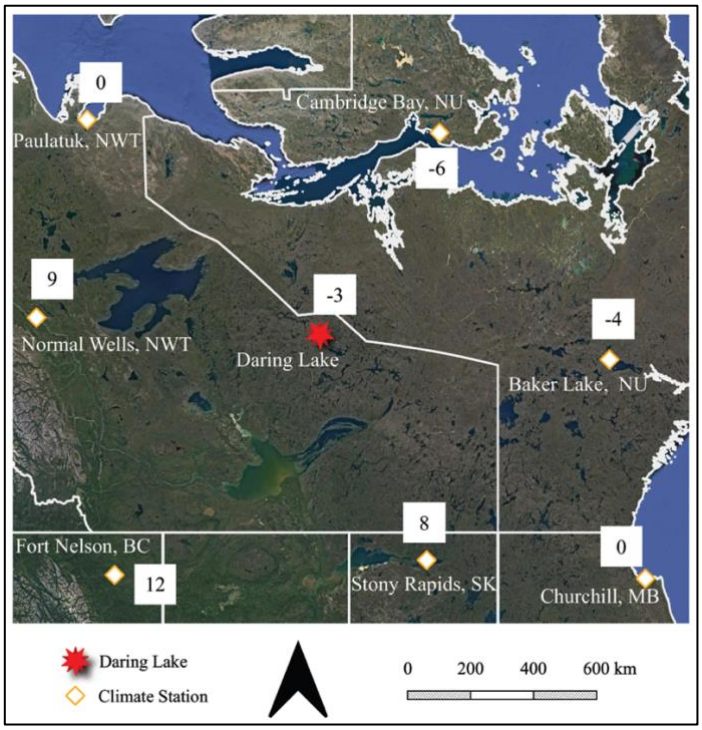

Figure 22. Average onset period surface air temperatures (°C) across the SOM grid over the entire study period.

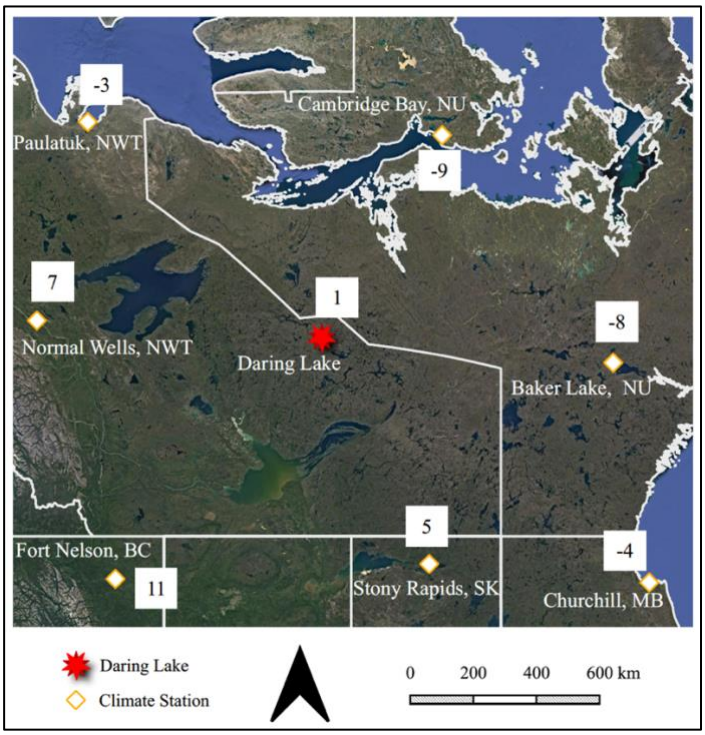

Figure 23. Average melt period surface air temperatures (°C) across the SOM grid over the entire study period.

3.2 Discussion

3.2.1 Snowmelt at Daring Lake

Although some researchers have shown a trend toward earlier onset of snowmelt throughout the Arctic in recent decades (Foster et al., 2008; Wilcox et al., 2019), there was no observed trend in melt onset at Daring Lake between 2004 and 2018. Similarly, although variable, there was no observed trend in melt period length. The trend in snowmelt advancement commonly observed throughout the tundra may not apply at Daring Lake due to the continentality of the region. Daring Lake is in a remote region of the Arctic tundra, at least 300 km from the Arctic coast and 1000 km from Hudson Bay, and as such may not be as easily influence by changes in sea ice cover, such as duration or break up timing, compared to other Arctic regions. Thus, the lack of distinct changes in snowmelt timing and length at Daring Lake may be attributed to its geographic situation and limited relationship to coastal climate dynamics. The large variability in annual snowmelt onset dates and melt length observed at the study site are likely, in part, due to differences in snowpack conditions, meteorological conditions, or site-level characteristics such as vegetation (Bednorz, 2009; Pedersen et al., 2015). There was a tendency for slightly longer melt periods to occur in years where melt occurred earlier in the year, which is likely attributed to depleted sources of radiative energy and lower air temperatures earlier in the late-winter/early-spring (Musselman et al., 2017).

3.2.2 Meteorological Controls on Snowmelt

The most parsimonious multiple linear regression model assessing the relationship between meteorological conditions and snowmelt length identified heating degree days

and incoming solar radiation as the most important predictors of snowmelt. It should be noted that the observed counterintuitive relationship, where melt length increased with greater HDDs, raises questions about the model's capacity to capture the intricacies of tundra snowmelt and meteorological conditions. The observed relationship between HDDs and snowmelt length was contradictory as HDDs were calculated cumulatively over the melt period, and therefore, to some extent, they are dependent on snowmelt length. Thus, the selection of HDDs as an independent variable led to a circular argument, as HDDs themselves are influenced by the phenomenon (snowmelt length) that it is supposed to explain. It might be concluded that this approach did not provide meaningful insights into the meteorological influences on snowmelt length.

Additionally, the model's satisfactory adjusted R^2 value of 71.47%, may also be due to the complexity of snowmelt as an ecosystem scale process. The omission of unavailable meteorological variables such as longwave radiation, or additional variables such as air temperature, which have been found to provide significant energy inputs to melting snowpacks (Zhang et al., 1997), may have improved the model's explanatory power. The relationship between air temperature and snowmelt is well known, as significant melt cannot occur until the air has reached a temperature equal to or greater than 0°C. Several studies have explored the relationship between air temperature and snowmelt in the Arctic and have found that air temperature is a significant determinant of spring snowmelt onset and length (Tan et al., 2011), which can have an impact on spring and summer runoff (Yang and Zhang, 2002) and the distribution of vegetation (Groendahl et al., 2007). It is recommended that future studies incorporate air temperature as an independent variable rather than HDDs.

3.2.3 The atmosphere and snowmelt

The AO and NAO are closely related and have been found to influence the timing of snowmelt in several Arctic regions (Foster et al., 2013; Zheng et al., 2022). It has been found that phases of the AO and NAO correspond with snowmelt timing, in which positive (negative) phases correlate with earlier (later) spring snowmelt (Foster et al., 2013; Zheng et al., 2022). Although the relationship between teleconnection phase and snowmelt is evident in some regions of the Arctic, several factors such as geography and the incorporation of time lag effects in analysis can influence results (Mioduszewski et al., 2014). No significant relationships between the AO or NAO and snowmelt onset or end-of-melt were found for Daring Lake. The AO and NAO were, however, similar in their respective phases throughout the study period. Despite the observed relationships between teleconnection phases in some Arctic areas, the absence of a relationship at Daring Lake may warrant further investigation. However, it should be noted that the relatively short data record used in this study (14 years) may have contributed to the lack of a relationship in these findings.

Similarly, no single synoptic pattern or cluster of patterns was found to directly trigger an early or late snowmelt. This is likely due to the complexity of snowmelt as a process, which depends on several factors acting on different scales. For example, snow redistribution may result in snow-free patches and local energy advection from areas of little snow-cover to areas with snow (Marsh, 1999; Pohl and Marsh 2006). Snowmelt also depends on turbulent energy exchanges between the snowpack, atmosphere, and surrounding vegetation, all of which may vary on an annual basis (Marsh et al., 2010; Prince and Dunne, 1976; Tarboton et al., 1994).

Although no particular pattern or cluster was associated with early or late snowmelt, there was a clear shift in the state of the atmosphere between the pre-melt and melt periods. The pre-melt period was marked by dominance of meridional and steep gradient patterns. Both clusters were associated with cool temperatures and energy transport from the northwest to southwest. The onset and melt periods displayed a clear shift in the state of the atmosphere, with zonal patterns promoting the advection of warm, moist westerly air from the North Pacific (Stone et al., 2002). The shift to zonal patterns likely increased the energy available for snowmelt and is a well-documented synoptic pattern during snowmelt onset across North America (Ballinger et al., 2019; Cline, 1997; Newton, 2018). Additionally, in this region, advective energy has been found to play a more important role in snowmelt than radiative energy, highlighting the role of zonal patterns in snowmelt onset (Mioduszewski et al., 2014).

Chapter 4: Tundra CO_2 Flux

4.1 Results

4.1.1 Interannual variability in snow-free season NEE

Average daily NEE indicated a net uptake of CO_2 in most years; however, NEE was variable throughout the study period (Table 9, Appendix 2). Mean daily snow-free season NEE for the study period was -0.23 g C m^2 day^1 with a standard deviation of 0.16 g C m^2 day^1. Peak carbon uptake typically occurred in July (Appendix 2).

Snow-free season period cluster occurrences for each year are presented in Table 9. Over the course of the study period, gradient cluster occurrence had a range of 23% to 47%, indicating substantial interannual variability. A potential relationship appeared to exist between the frequency of the gradient pattern and the trends in NEE as higher occurrences of gradient patterns appeared to align with more negative annual NEE values, indicating greater CO_2 uptake during these cluster patterns. Occurrences of meridional patterns were least prevalent throughout the study period, ranging from 1% to 23%. The occurrences of these pattern did not appear to align with any trends in annual NEE. Transitional and zonal pattern occurrences displayed a large range in interannual occurrence; however, there were no clear relationships between transitional or zonal pattern occurrences and NEE.

Table 9. Snow-free season average daily NEE (g C m^2 day^1) per year. Total annual snow-free season cluster occurrence (%) is also presented. Negative values indicated an average net CO_2 uptake, while positive values indicate release.

Year	Average Daily NEE	Cluster Occurrence (%)			
		Gradient	Meridional	Transitional	Zonal
2005	-0.012	32	6	19	43
2006	0.013	28	11	38	22
2007	-0.119	28	23	23	26
2008	-0.153	37	11	24	27
2009	-0.298	38	1	32	29
2010	-0.353	24	13	46	17
2011	-0.097	23	6	43	28
2012	-0.007	28	11	41	20
2013	-0.378	41	6	39	14
2014	-0.339	41	11	27	21
2015	-0.276	30	9	38	23
2016	-0.365	30	1	46	24
2017	-0.385	28	7	40	26
2018	-0.447	47	11	18	24
Mean	-0.23	32.50	9.07	33.86	24.57
Standard Deviation	0.16	7.13	5.48	9.87	6.76

Cluster occurrences were also variable among study period months (Appendix 3). During the May/June period, occurrence of each cluster was variable and there was no clear trend between cluster occurrence and NEE. The occurrences of July clusters exhibited variability, except for the meridional cluster, which displayed a negligible frequency of occurrence. Of July occurrences, transitional patterns were dominant and accounted for 54.4% of all pattern occurrences (Appendix 3). Although cluster dominance was fairly consistent, there were no clear trends between cluster occurrence and NEE. Transitional cluster patterns, accompanied by gradient cluster patterns remained fairly dominant in the month of August. Like previous months, there was no clear trend between cluster occurrence and NEE. September cluster occurrences remained variable; however, dominance shifted to the gradient and zonal patterns. As with other months, there were no clear trends between cluster occurrence and NEE.

4.1.2 Atmospheric controls on NEE

Over time, there was a statistically significant decrease in NEE (more uptake over time) (Figure 24). The significant increase in CO_2 uptake over time was not matched by a significant increase in average daily temperature (Figure 23). It should be noted, however, that there was an observed trend of increasing temperatures over time (Figure 25). Additionally, the significant increase in CO_2 uptake was matched by a statistically significant increase in average daily maximum temperature over time (Figure 26). There were no statistically significant differences in pattern occurrence (Appendix 4) or persistence (Appendix 5) over time.

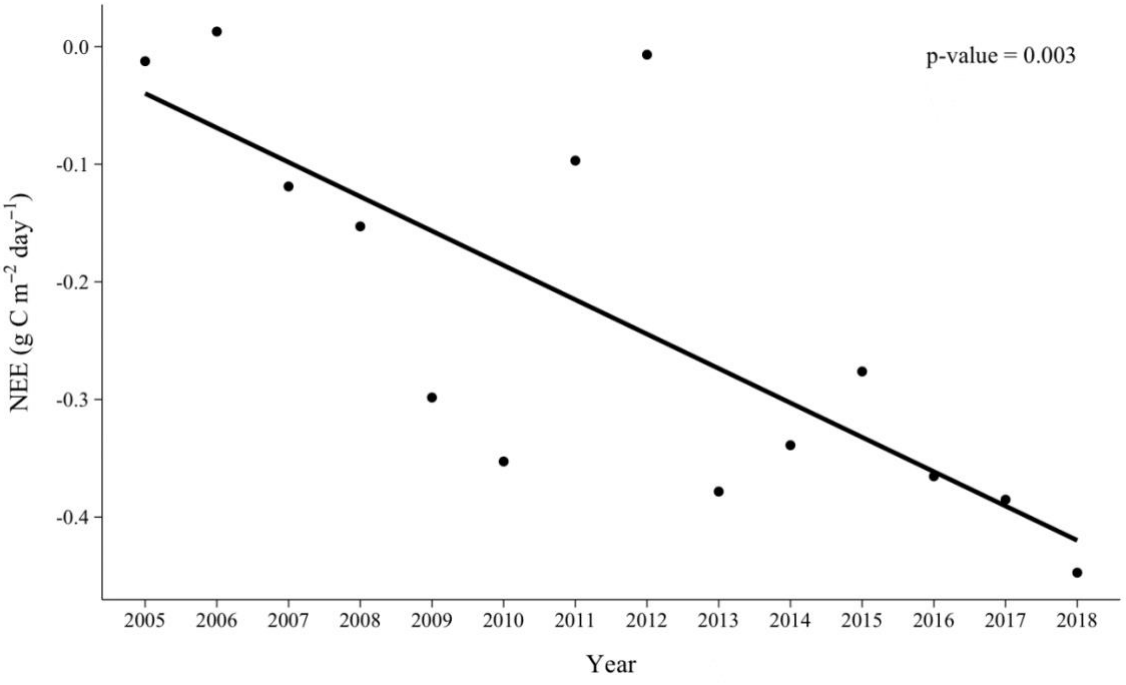

Figure 24. Trend in average daily NEE (g C m^2) over time.

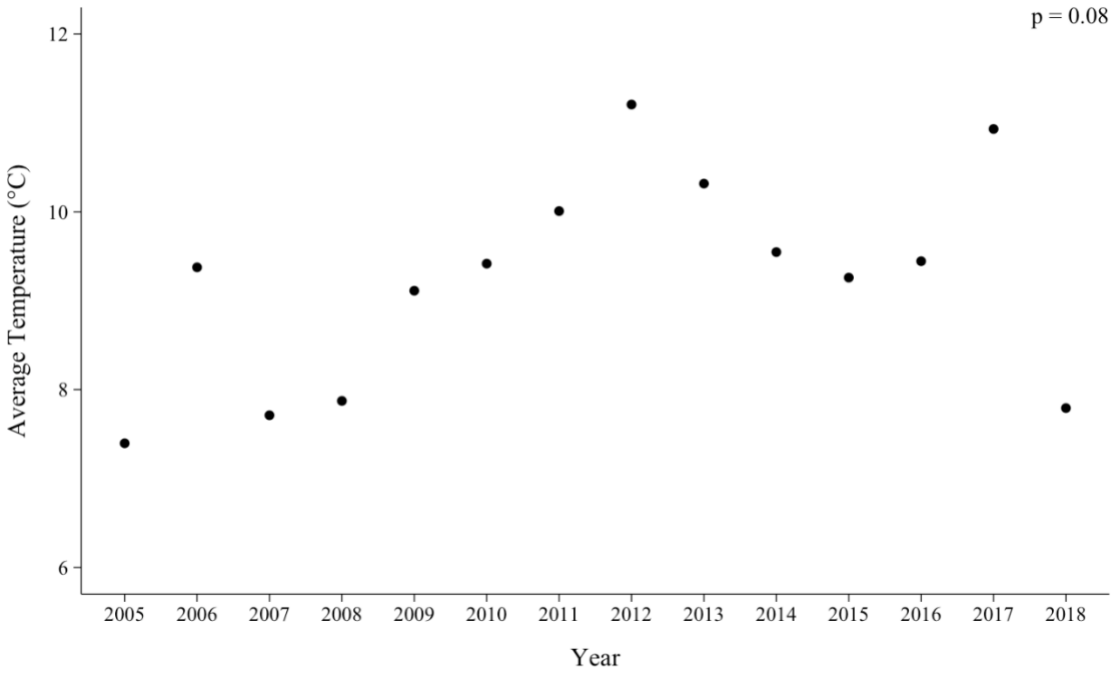

Figure 25. Trend in average daily temperature (°C) over time.

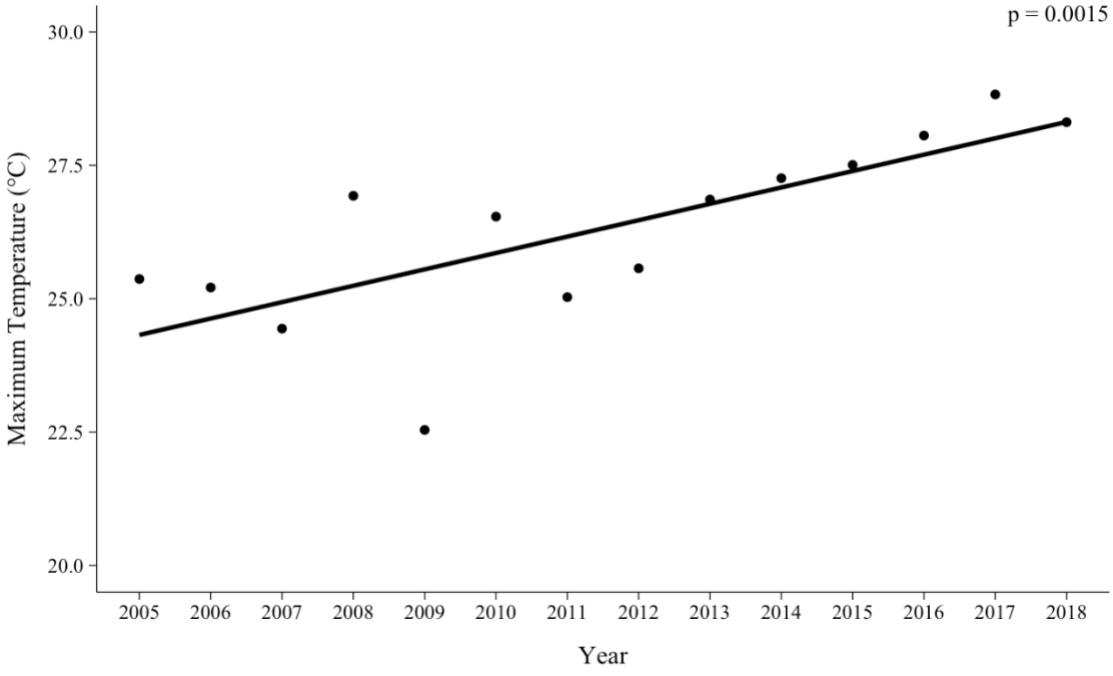

Figure 26. Trend in maximum daily temperature (°C) over time.

Additionally, there was a significant negative correlation between monthly temperature and NEE anomalies ($p < 0.0001$, $R^2 = -0.74$, Figure 27). A positive trend in temperature anomalies was accompanied by a negative trend in NEE anomalies (Figure 28). This indicated that more positive temperature anomalies (warmer temperatures) were associated with increased carbon uptake (more negative NEE anomalies).

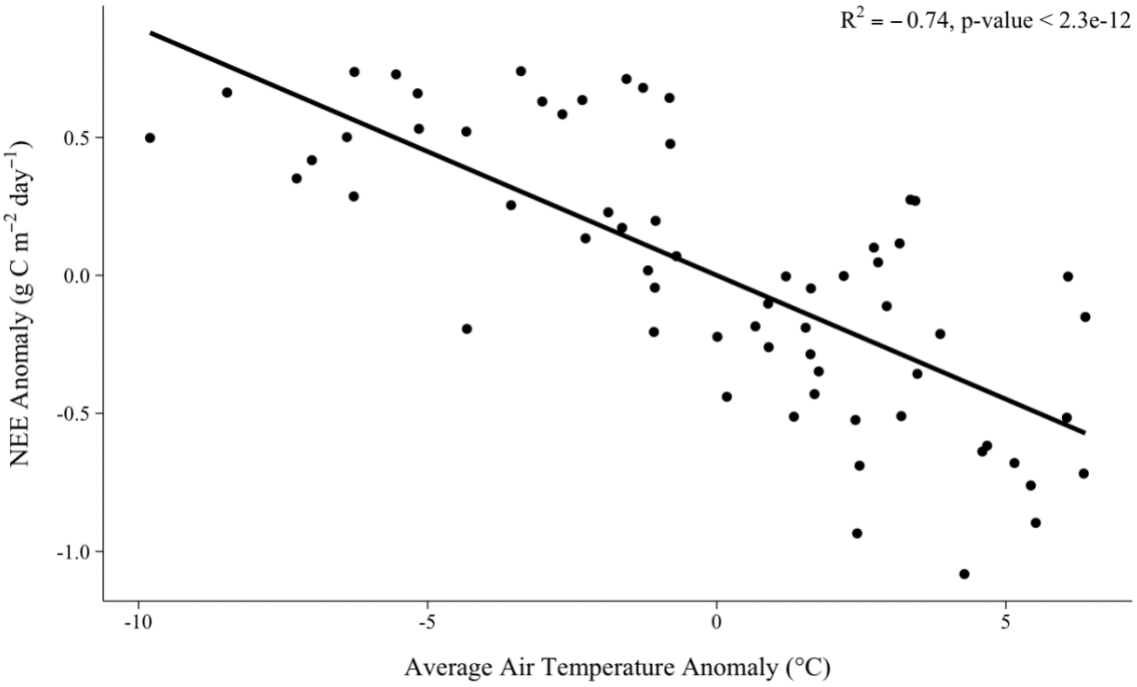

Figure 27. The relationship between average daily NEE and air temperature anomalies for each month of the study period.

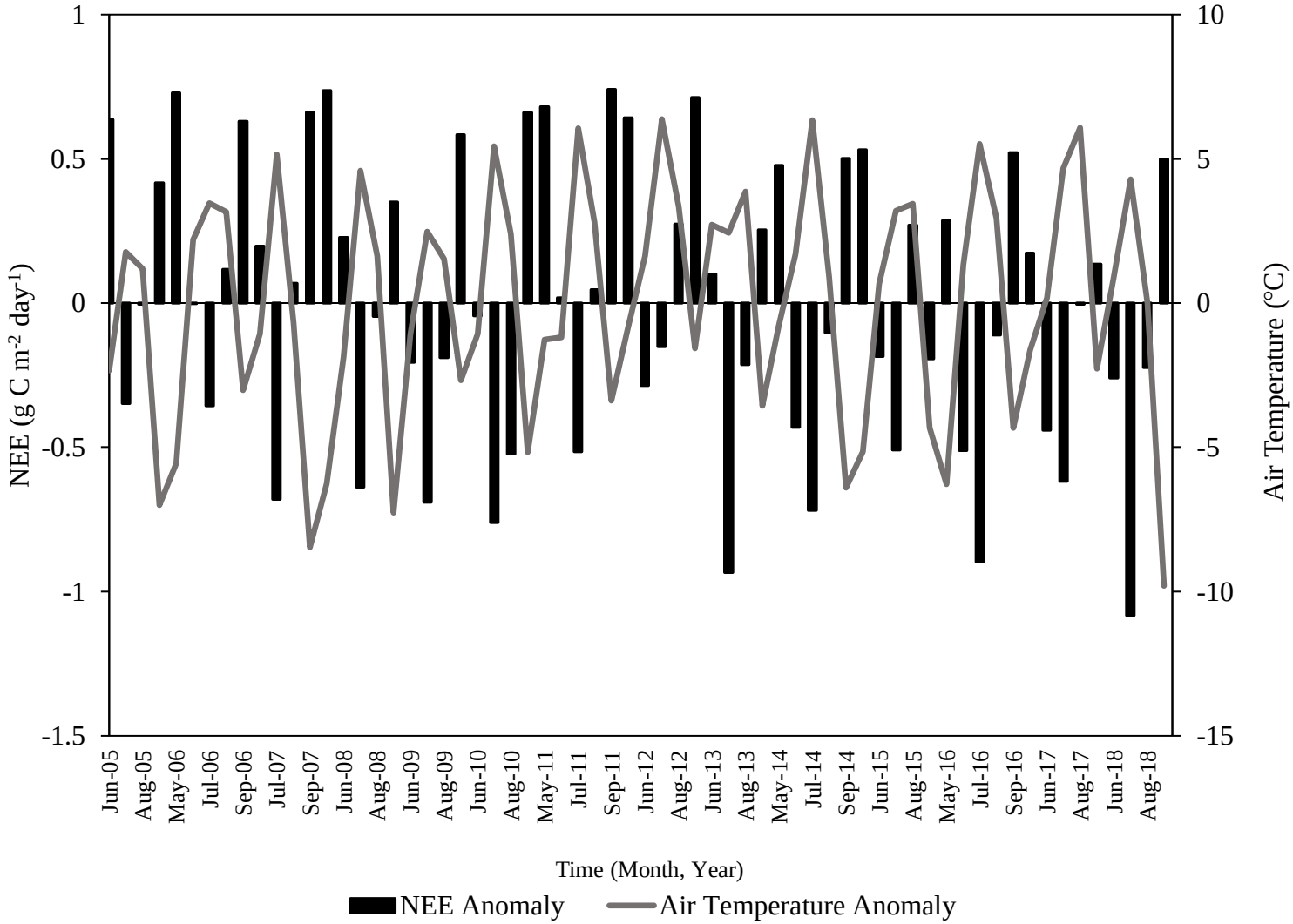

Figure 28. Monthly average daily NEE (g C m^2) and average air temperature (°C) anomalies over time.

Throughout the study period, there were few significant spearman rank correlations (r_s) between cluster occurrence, persistence, and NEE (Table 10). On a monthly timescale (encompasses each month occurring over the entire study period), there was a significant negative correlation between transitional cluster occurrence and NEE ($r_s = -0.62$, $p < 0.05$). Moreover, a significant negative correlation between gradient cluster occurrence and NEE was found specifically during the month of August ($r_s = -0.62$, $p < 0.05$).

Relationships between cluster persistence occurred at a higher frequency (Table 10). On a monthly timescale, there was a negative correlation between transitional cluster persistence and NEE ($r_s = -0.57$, $p < 0.05$). Positive correlations between meridional cluster persistence ($r_s = 0.46$, $p < 0.05$) and zonal cluster persistence ($r_s = 0.27$, $p < 0.05$) were also observed. It should be noted that there was also a positive correlation between meridional cluster persistence and NEE ($r_s = 0.64$, $p < 0.05$).

Table 10. Significant ($p < 0.05$) Spearman correlation coefficients (r_s) showing the relationship between total cluster occurrence (days), average cluster persistence (days), and NEE (g C m^{-2} day^{-1}). Correlation coefficients are presented for the entire study period on a monthly basis (each month occurring over the entire study period), annually, and for specific monthly periods (May/June, July, August, and September). Negative correlation values signify that greater cluster occurrence and persistence are associated with more negative values of NEE, whereas positive correlation values indicate that cluster occurrence and persistence correlate with more positive values of NEE.

NEE	Transitional	Gradient	Meridional	Zonal
		Occurrence		
Monthly	-0.62			
Annual				
May/June				
July				
August		-0.62		
September				
		Persistence		
Monthly	-0.57		0.46	0.27
Annual				
May/June			0.64	
July				
August				
September				

Kruskal-Wallis analysis identified a significant difference in average daily temperatures between clusters over the entire study period ($H = 541.68$, $p < 0.05$, Figure 29). Over the study period, the transitional cluster was associated with the highest air temperatures, while the meridional cluster was associated with the coldest temperatures (Figure 29). Overall, the range in temperatures among clusters was fairly consistent, although both the transitional and gradient clusters exhibited temperature outliers. (Figure 29). Similarly, during each month of the study period the transitional cluster was associated with the warmest temperatures while the meridional cluster was associated with the coldest temperatures (Figure 30). Temperatures between clusters during each month were significantly different from one another (Figure 30).

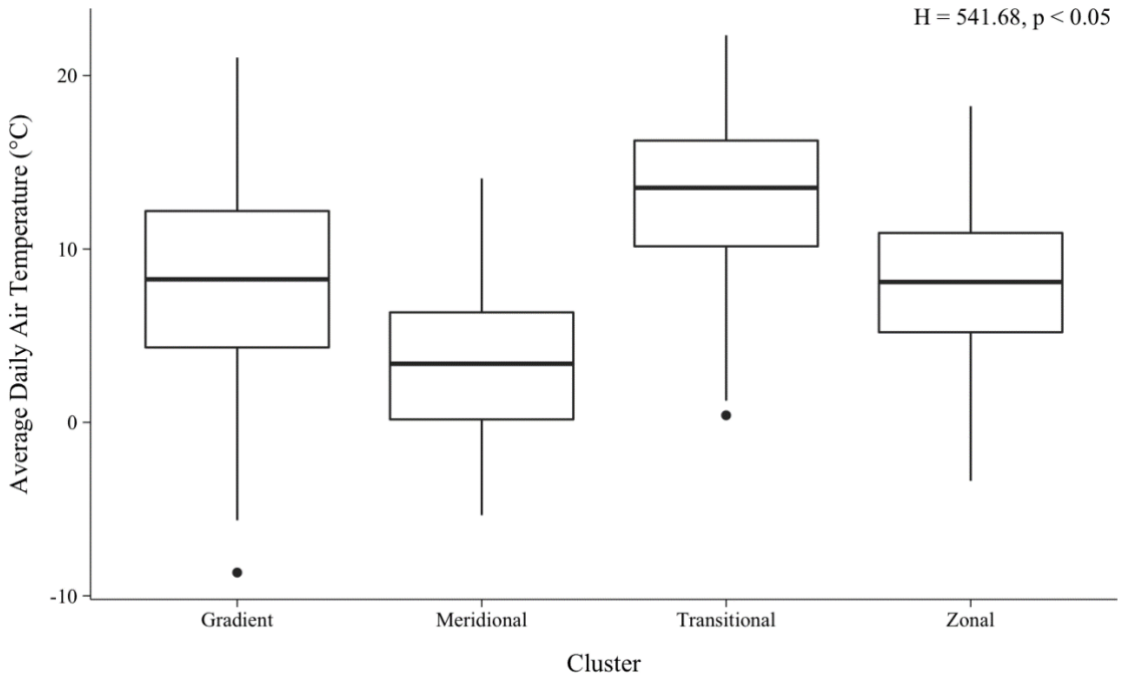

Figure 29. Average daily snow-free season air temperatures (°C) associated with each pattern cluster over the entire study period.

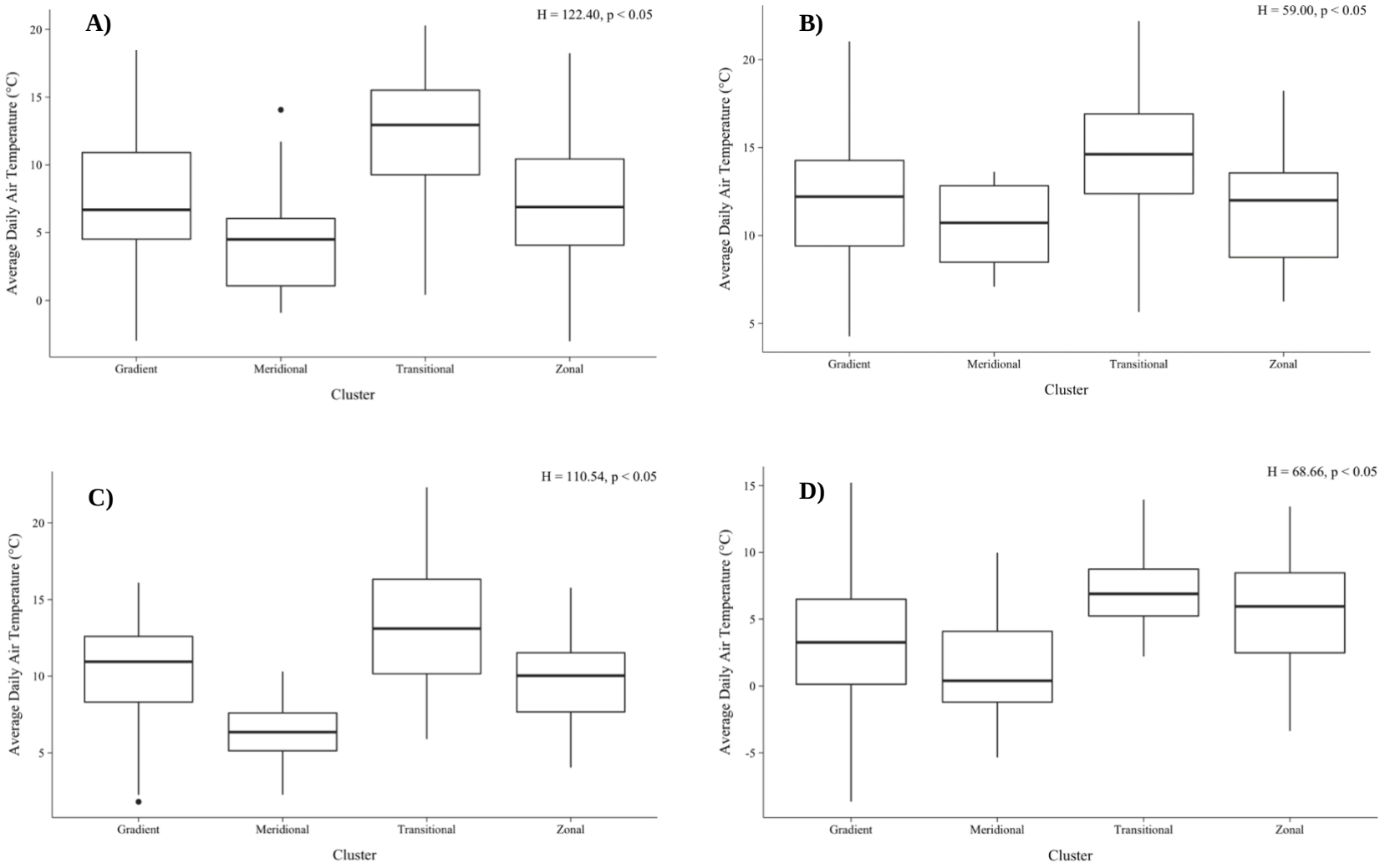

Figure 30. Average daily snow-free season air temperatures (°C) associated with each pattern cluster in the May/June (A), July (B), August (C), and September (D) periods.

Over the entire study period, there was a statistically significant difference in NEE between clusters ($H = 175.36$, $p < 0.05$, Figure 31). Days in which the transitional cluster occurred were associated with the greatest average daily CO_2 uptake (Figure 31). Days in which the meridional cluster occurred were associated with the least amount of CO_2 uptake (i.e., positive NEE, Figure 31). Over the entire study period, the meridional and zonal clusters were the only clusters to display a positive median NEE. Although the transitional cluster was associated with greatest average CO_2 uptake, it also exhibited the most extensive variation in NEE (Figure 31).

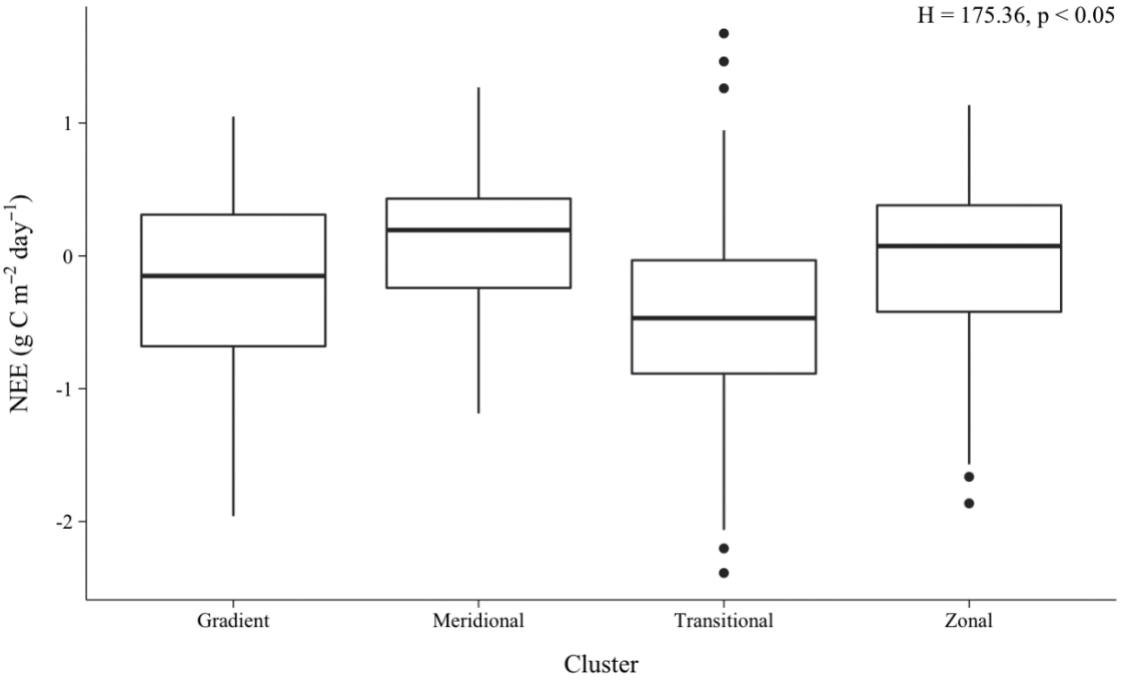

Figure 31. Average daily snow-free season NEE (g C m^{-2}) associated with each pattern cluster over the entire study period.

Across individual monthly periods, there were also significant differences in NEE between clusters during the May/June period ($H = 35.59$, $p < 0.05$) and during the August

period ($H= 29$, $p < 0.05$). During the May/June period, the transitional cluster was associated with the most negative NEE and the meridional cluster was associated with the most positive NEE (Figure 32, A). During the July period, NEE was comparable across all cluster occurrences, while the greatest range in NEE was observed on days in which the transitional and gradient clusters occurred (Figure 32, B). The zonal cluster was the only cluster associated with positive NEE during the August period, and there was a large range in NEE associated with days in which the transitional cluster occurred (Figure 32, C). NEE was similar across the occurrences of each cluster during the September period (Figure 32, D).

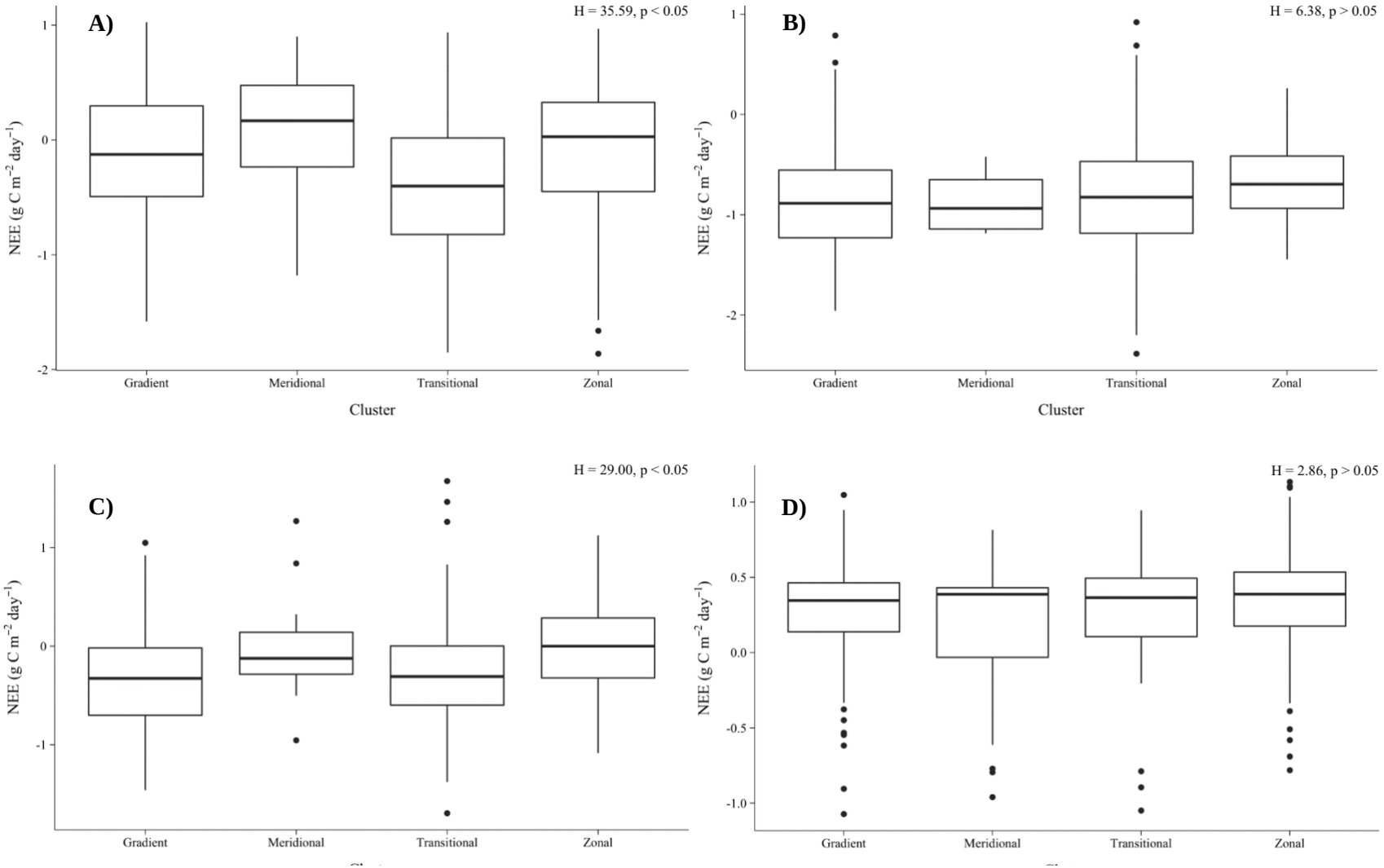

Figure 32. Average daily snow-free season NEE (g C m^{-2}) associated with each pattern cluster in the May/June (A), July (B), August (C), and September (D) periods.

4.2 Discussion

Developing an understanding of the role that atmospheric circulation plays in carbon fluxes on the Arctic tundra is crucial for comprehending future and current trends in the Arctic carbon cycle. In this study, the relationships between CO_2 fluxes (NEE) and synoptic patterns were assessed. Although relationships between synoptic patterns cand CO_2 fluxes have been observed elsewhere (Randazzo et al., 2020), the analysis of synoptic cluster occurrence and NEE at Daring Lake did not indicate any consistent relationships. This is likely due to the complexity of the ecosystem-scale processes and characteristics that drive NEE such as soil moisture, soil temperature, and permafrost dynamics which likely cannot linearly be explained by synoptic patterns (Mu et al., 2017; Neff and Hooper, 2002).

Trends in NEE and maximum air temperature were observed over time at the study site. The statistically significant increase in the negativity of NEE indicated an increase in carbon uptake over time. There is evidence of increases in carbon uptake at other sites throughout the Arctic due to factors such as increased vegetation productivity or changes in temperature and snow dynamics (McGuire et al., 2009). The findings of this study emphasize the importance of long-term studies on carbon cycles on the Arctic tundra due to their sensitivity to change over time. Although a trend in daily maximum air temperature was observed, there were no significant trends in average daily air temperatures or synoptic cluster occurrences. This suggested that factors beyond synoptic patterns, such as permafrost dynamics, or nutrient availability may exert a greater influence over the observed changes in NEE over time (Mack et al., 2004; Schneider von Deimling 2015). Due to the complexity of the interplay of the factors contributing to the

variability in NEE, including synoptic patterns, future studies should extend the ground measurement of variables such as soil characteristics to gain a more robust understanding of carbon dynamics on the Tundra.

Maximum daily temperatures increased significantly over the study period along with increases in the negativity of NEE over time. The relationship between temperature and NEE was also observed in the significant correlation between temperature and NEE anomalies, indicating that increased carbon uptake was associated with higher temperatures. This correlation was likely due to the temperature dependence of photosynthesis and ecosystem respiration, as warmer temperatures generally enhance plant growth and photosynthetic rates, thus influencing NEE (Zhou et al., 2019). Similar trends have been observed elsewhere on the tundra (Welker et al., 2004); however, it should be noted that the dynamics and magnitude of NEE in the Arctic tundra under warmer conditions are still uncertain and likely influenced by an array of factors such as changes in nutrient availability, active layer depth, or microbial activity (Natali et al., 2012; Schuur et al., 2009). The observed interactions between temperature and NEE at the study site further highlight the importance of ongoing investigations of carbon dynamics and their changes over time on the tundra.

Over the entire study period, there was a significant negative correlation between the occurrence of the transitional cluster and NEE. Interestingly, the transitional cluster was characterized by warmer temperatures compared to other clusters. These findings indicated that the transitional cluster may have created favourable conditions for CO_2 uptake; however, the mechanisms in which this correlation occurred warrants further investigation. In contrast, the occurrence of the gradient cluster also exhibited a negative correlation with NEE during the August periods. The gradient cluster, unlike the

transitional cluster, was characterized by average temperatures. This difference in relationship between clusters and their associated temperatures indicated that factors beyond atmospheric circulation interact to influence carbon dynamics at different timescales and that synoptic patterns alone likely cannot linearly describe the variability in NEE at the study site.

To assess the importance of the consecutive occurrence of a synoptic cluster, the relationship between NEE and cluster persistence was also investigated. Over the entire study period, the persistence of the transitional cluster possessed a significant negative correlation with NEE. The negative correlation suggested that the longer persistence of this cluster created a longer period in which conditions for CO_2 uptake were favourable. These conditions may have included factors such as optimal growing or photosynthetic conditions; however, must be studied further. Additionally, over the entire study period, the persistence of the meridional and zonal clusters exhibited weak positive correlations with NEE. Over the entire study period, the meridional cluster was characterized by the coldest temperatures and the zonal cluster was associated with average temperatures; however, both clusters were associated with slightly positive NEE. The lack of consistent correlation between the conditions associated with these clusters again indicated that the complex interactions of factors such as active layer depth or microbial activity may be more dominant than the suggested linear correlation between NEE and atmospheric circulation (Law et al., 2002; Verburg et al., 2004). The contrasting conditions and correlations between cluster persistence and NEE further emphasize the importance of further investigation of the non-linear interaction of factors at play in Arctic tundra carbon exchanges.

Although this study did not highlight strong relationships between atmospheric circulation and NEE, it must be acknowledged that non-linear relationships between NEE and atmospheric circulation may exist. For example, the complex interactions of the driving factors of NEE may contribute to a non-linear response in carbon exchange at the study site (Reyes et al., 2017; Sun et al., 2020). Additionally, lag effects may contribute significantly to carbon fluxes over time due to the varying and staggered impacts that atmospheric circulation has on ecosystem-scale processes (Zhang et al., 2015). Future studies should include broader temporal and spatial scales that comprise of multiple ecosystem processes and their interactions to encompass the full extent of the non-linear relationships between the atmosphere and Arctic tundra NEE.

This study sought to highlight the complex relationships between synoptic patterns and NEE in the Arctic tundra. While no consistent relationships between atmospheric circulation and NEE were found, long-term analysis revealed changes in NEE and maximum daily temperature over time. This finding highlighted the relationship between temperature and NEE on the Arctic tundra. The analysis of the impacts of synoptic cluster occurrence and persistence on NEE indicated that synoptic patterns alone cannot linearly explain the variability in NEE at the study site. It is suggested that the possibility of non-linear relationships between atmospheric circulation and NEE be investigated further on the Arctic tundra. These studies should possess a broader spatial scale and consider various ecosystem processes and interactions. By broadening the scope of this investigation, current and future trends in carbon exchanges in the region may be identified, providing valuable insight into the potential for change over time in a highly important, but vulnerable ecosystem.

Chapter 5: General Conclusions and Future Research

5.1 General conclusions

5.1.1 Synoptic controls on snowmelt

Large interannual variability in melt onset and length was observed throughout the study period, however there was no significant advancement in snowmelt onset or differences in the length of melt throughout the study period. Typically, melt length corresponded with recorded snow depths, where melt occurred over longer periods of time when snow depth was greater and vice versa. Longer melt periods also occurred in years where melt occurred earlier in the year. The increase in melt length in these cases was likely a result of lower air temperatures and depleted sources of radiative energy earlier in the spring.

Heating degree days and incoming solar radiation were identified as important predictors of melt length through multiple linear regression. However, the use of heating degree days as an independent variable to the model was questioned due to its dependence on melt length. The model produced satisfactory results that may have been improved with the inclusion of additional variables such as downwelling longwave radiation, or air temperature in place of heating degree days.

Large-scale teleconnection indices and locally derived synoptic patterns were not associated with early or late melts. This is likely due to the continentality of the region. Daring Lake is situated in a remote region of the Arctic and as such may not be as closely impacted by factors such as changes in sea ice cover and coastal climate dynamics compared to other Arctic regions. During the transition from pre-melt to melt period, the atmosphere shifted from dominant meridional patterns to zonal patterns. This indicated

that the advection of warm westerly air triggering above-zero temperatures was an important factor in snowmelt onset at Daring Lake.

Snowmelt is a profound annual event on the tundra that influences many ecosystem-scale processes and characteristics (Wipf, 2010) such as carbon cycling (Aurela et al., 2004; Winchell et al., 2016) and the distribution of flora and fauna (Kankaanpää et al., 2018). Due to the variability of snowmelt timing in the tundra, it is crucial to develop an understanding of the controls on snowmelt to better understand the impacts that changing climates and snowmelt characteristics may have in the Arctic and globally. Although melt onset and length were not well correlated with specific synoptic patterns, the suggestion that a switch to zonal patterns was important for melt onset was notable. This finding requires further investigation as to what initiates these zonal patterns, and if this same association is present in other areas of the Arctic. Furthermore, the incidence of these patterns under conditions of climate change should also be investigated.

5.1.2 Synoptic Controls on CO_2 Flux

Studying the relationship between atmospheric circulation and Arctic tundra carbon fluxes is essential for understanding both current and future trends in Arctic tundra NEE. This study employed the use of a synoptic climatology approach to assess these potential relationships. Annual synoptic cluster occurrences were not significantly related to annual NEE at Daring Lake. This lack of observed relationship is likely due to the complexity of the controls on NEE, such as soil moisture, permafrost dynamics, and vegetation composition, (Mu et al., 2017; Neff and Hooper, 2002).

Mann-Kendall tests revealed a significant increase in the negativity of NEE, and an increase in maximum air temperature over time. No significant trend in average daily temperature was observed. The increase in the negativity of NEE indicated that CO_2 sequestration has increased over time, which has been observed at other Arctic sites (McGuire et al., 2009). This change over time highlights the importance of prolonged carbon flux studies in the Arctic tundra to capture temporal changes and underscores a need to understand these changes further.

Although there was no significant change in average daily temperature, there was a strong correlation between temperature and NEE anomalies throughout the study period. This is likely due to the complex role of temperature in processes such as plant growth and photosynthesis. It must be noted that current and future NEE dynamics under warmer conditions in the tundra are not well understood and are likely to be influenced by several factors such as nutrient availability, active layer depth, or microbial activity (Natali et al., 2012; Schuur et al., 2009).

Over the entire snow-free period, a negative correlation between the occurrence of the transitional cluster and NEE was observed. Similarly, a negative correlation between August gradient cluster occurrence and NEE was also observed. Although both clusters were associated with warmer than average temperatures, consistent trends between clusters, their associated temperatures, and NEE were not observed. The lack of consistency in these relationships is likely due to the complex interplay of factors controlling NEE such as soil moisture, permafrost dynamics, and vegetation cover (Mu et al., 2017; Neff and Hooper, 2002).

Similarly, a significant negative correlation was observed between the entire study period transitional cluster persistence and NEE, indicating that the increased persistence

of patterns in this cluster may have provided favourable conditions for CO_2 uptake. A slight positive correlation between the persistence of the meridional and zonal clusters and NEE was also observed. Like the correlations among cluster occurrence and NEE, there were no clear or consistent patterns in these relationships. This potential relationship could be a focus of further investigation of the impacts of synoptic pattern persistence and their impacts on ecosystem-scale processes.

Although clear relationships between atmospheric circulation and NEE were not consistently evident, the potential for the existence of non-linear relationships between the two must be acknowledged. The complex interconnectedness of the factors contributing to NEE may potentially be impacted by the lag effects of past synoptic patterns (Zhang et al., 2015). Overall, this study has highlighted the complexity of NEE at the Arctic tundra, and the need to broaden the scope of our knowledge over time and space.

5.2 Summary of Findings and Research Questions

Research Question 1: Does the state of the atmosphere change leading up to and during snowmelt?

Meridional and steep gradient patterns dominate the pre-melt period. Although the steep gradient and meridional patterns belong to two separate clusters, they are all meridional in shape. These patterns are associated with cool temperatures and energy transport from the west and northwest to the southwest of the SOM grid. The atmosphere undergoes a shift from meridional patterns during the pre-melt period to zonal patterns during the onset and melt periods. These patterns are associated with the transfer of warm, moist

North Pacific air from the west of the SOM grid. Zonal patterns are commonly observed during snowmelt across North America.

Research Question 2: Do certain synoptic patterns exert greater control over snowmelt timing and length than others?

There were no patterns associated with early (late) snowmelt or short (long) melt periods. This is likely due to the complex nature of snowmelt in the Daring Lake region, which depends on several factors such as geographical location, meteorological conditions, and energy transport. Similarly, large teleconnection indices were not found to influence the timing of snowmelt. The lack of relationship between small scale synoptic patterns, large-scale teleconnection, and snowmelt may warrant further investigation into the geographical impacts on ecosystem-scale processes such as snowmelt in the region.

Research Question 3: Is more positive or negative NEE associated with certain synoptic patterns?

Over the course of the study period, the occurrence and persistence of the transitional cluster correlated with more negative NEE. Furthermore, the August occurrence of the gradient cluster also possessed a negative correlation with NEE; however, this relationship was not observed across any other months. Additionally, several positive correlations between the monthly persistence of the meridional and zonal clusters were also observed; however, there were no clear patterns in these correlations. These findings suggest that synoptic patterns alone may not be able to explain the variability in NEE as the study site.

Research Question 4: Does the state of the atmosphere influence the interannual variability in CO_2 flux?

During the study period an increase in the negativity of NEE was observed over time. The variability in NEE over time was not matched by any changes in cluster occurrence or persistence. Additionally, no consistent correlations were found between NEE and pattern occurrence or persistence. While no consistent relationships were found, this study highlighted the importance of the ongoing investigation of surface-atmosphere relationships and their potential to change over time.

5.3 Recommendations for Future Research

5.3.1 Snowmelt at Daring Lake

To better capture the intricacies of snowmelt at Daring Lake, several recommendations for future research are listed below. A broader range of meteorological variables, such as longwave radiation, should be included in snowmelt models. The possibility of including data on vegetation cover and snowpack conditions should also be explored. Increasing the length of the snowmelt record and calculating the odds ratios of pattern occurrence (probability of pattern occurrence vs. probability of non-occurrence) may provide further insights into potential relationships between melt timing and characteristics and synoptic patterns or large-scale teleconnection indices. Furthermore, the exploration of lag effects of synoptic patterns is recommended for future research, as past synoptic patterns may influence future snowmelt conditions. Finally, increasing the spatial scale of this study, either encompassing a greater area of the Daring Lake region,

or by including several Arctic regions, may highlight the potential differences in the influence of synoptic patterns on snowmelt depending on geographic location.

5.3.2 NEE at Daring Lake

As mentioned in Chapter 4, there are several recommendations for further research studying the impacts of atmospheric circulation on carbon fluxes. Future research should expand the spatial scale at which the study is conducted by including a broader range of data on carbon fluxes throughout the Arctic tundra. Additionally, to examine the full extent to which synoptic patterns may influence carbon fluxes non-linearly, the impacts of lag effects should be explored. These recommendations aim to broaden our understanding of the large-scale driving forces on carbon fluxes in the Arctic tundra and may help shed light on their potential to change over time.

Appendices

Appendix 1. Melt period multiple linear regression models, adjusted R^2, AIC and P-values.

Equation	Adjusted R^2	AIC	P-Value
Y = b0 + b1x1	38.48	82.43	0.00807
Y = b0 + b2x2	22.55	85.88	0.04216
Y = b0 + b3x3	-0.06	90.60	0.6638
Y = b0 + b1x1 + b2x2 + b3x3	70.38	72.96	0.00083
Y = b0 + b1x1 + b2x2	**71.47**	**71.70**	**0.00021**
Y = b0 + b1x1 + b4x3	37.14	83.55	0.02446
Y = b0 + b2x2 + b3x3	18.86	87.38	0.11320

Appendix 2: 5-day running means of daily values of average daily NEE (g C m^{-2} day^{-1}) over the entire study period.

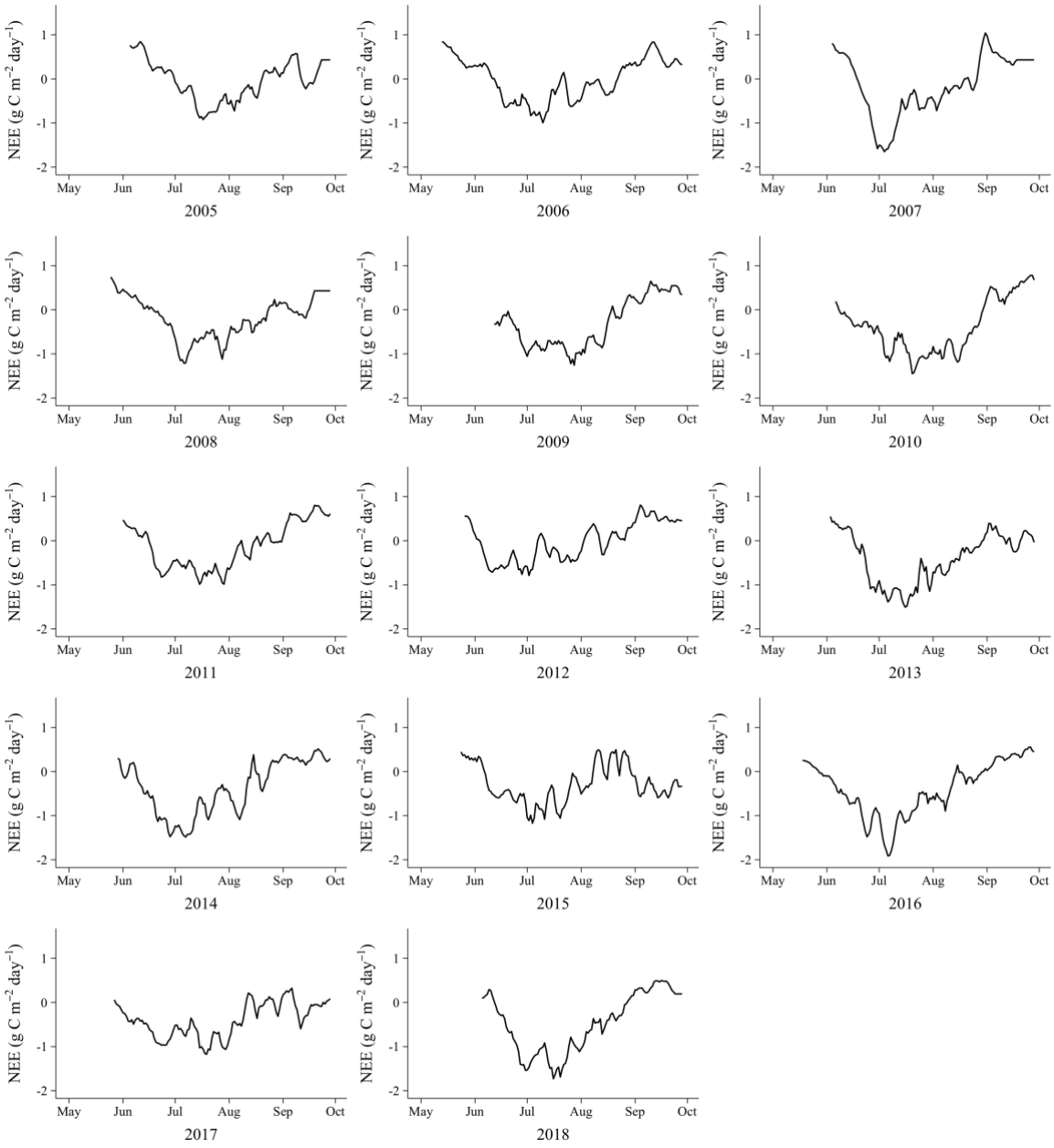

Appendix 3. Pattern occurrence, organized by cluster and by annual average daily NEE (g C m^{-2} day^{-1}) where A) represents May/June pattern occurrence, B) represents July pattern occurrence, C) represents August pattern occurrence, and D) represents September pattern occurrence. Bolded occurrences represent patterns or clusters displaying dominance.

A)

Year	Mean Daily NEE	Cluster																			
		Transitional				Gradient							Zonal					Meridional			
		P1	P2	P3	**Total**	P5	P9	P13	P14	P15	P16	**Total**	P6	P7	P10	P11	**Total**	P4	P8	P12	**Total**
2005	0.46	0	0	14	14	0	14	11	7	0	0	32	25	21	4	4	**54**	0	0	0	0
2006	0.12	16	10	2	27	14	8	2	6	0	0	29	2	14	8	6	29	14	0	0	14
2007	0.02	17	3	3	24	7	3	10	3	0	0	24	10	7	3	3	24	10	17	0	28
2008	0.17	0	3	5	8	13	13	0	0	5	0	31	15	21	8	5	**49**	5	5	3	13
2009	-0.38	0	10	10	19	0	0	19	10	0	0	29	19	29	5	0	**52**	0	0	0	0
2010	-0.21	11	15	4	30	4	0	26	0	0	0	30	7	11	15	0	33	7	0	0	7
2011	-0.12	28	3	0	31	0	3	9	6	9	0	28	3	9	9	6	28	6	6	0	13
2012	-0.26	18	16	8	**42**	0	3	3	0	0	0	5	5	5	8	0	18	21	13	0	34
2013	-0.07	**50**	3	7	**60**	23	0	0	0	0	0	23	13	3	0	0	17	0	0	0	0
2014	-0.47	26	3	9	**37**	3	0	6	6	0	0	14	17	0	9	0	26	20	3	0	23
2015	-0.18	8	3	3	13	15	5	**33**	3	0	0	**55**	5	13	5	5	28	5	0	0	5
2016	-0.41	11	11	20	**41**	9	4	7	4	0	0	24	17	7	7	2	33	2	0	0	2
2017	-0.50	5	8	8	22	14	11	3	3	3	0	32	16	8	8	0	32	8	0	5	14
2018	-0.43	0	7	21	29	25	7	0	0	0	0	32	29	4	0	0	32	0	7	0	7
Mean	-0.161	**13.6**	6.7	8.1	28.3	9.0	5.1	9.1	3.4	1.2	0.0	27.8	**13.2**	10.8	6.3	2.2	**32.5**	7.1	3.7	0.6	11.4
Standard Deviation	0.280	14.1	4.9	6.4	13.8	8.5	4.8	10.1	3.2	2.8	0.0	10.9	8.1	8.0	3.9	2.5	11.5	7.1	5.6	1.6	10.7

B)

Year	Mean Daily NEE	Cluster																		
		Transitional				Gradient							Zonal					Meridional			
		P1	P2	P3	**Total**	P5	P9	P13	P14	P15	P16	**Total**	P6	P7	P10	P11	**Total**	P4	P8	P12	**Total**
2005	-0.52	6	3	16	26	6	10	16	0	0	0	32	16	10	16	0	**42**	0	0	0	0
2006	-0.53	0	29	13	**42**	16	**35**	0	0	0	0	**52**	3	0	0	0	3	3	0	0	3
2007	-0.85	**39**	16	0	**55**	26	0	0	0	0	0	26	19	0	0	0	19	0	0	0	0
2008	-0.81	10	19	19	**48**	23	6	0	0	0	0	29	16	0	3	0	19	3	0	0	3
2009	-0.86	**42**	0	3	**45**	13	10	0	6	0	0	29	23	0	3	0	26	0	0	0	0
2010	-0.94	**35**	23	19	**77**	16	3	0	0	0	0	19	3	0	0	0	3	0	0	0	0
2011	-0.69	23	29	23	**74**	6	6	0	0	0	0	13	13	0	0	0	13	0	0	0	0
2012	-0.32	**42**	29	0	**71**	19	6	0	0	0	0	26	3	0	0	0	3	0	0	0	0
2013	-1.11	29	23	0	**52**	23	0	13	0	0	0	**35**	3	3	3	0	10	3	0	0	3
2014	-0.89	**55**	3	3	**61**	16	3	6	0	0	0	26	6	3	3	0	13	0	0	0	0
2015	-0.68	19	**39**	6	**65**	13	10	3	0	0	0	26	0	0	6	0	6	3	0	0	3
2016	-1.07	**55**	3	0	**58**	16	6	0	16	0	0	**39**	0	0	3	0	3	0	0	0	0
2017	-0.79	29	13	0	**42**	16	16	6	3	0	0	**42**	10	0	3	0	13	3	0	0	3
2018	-1.26	26	13	6	**45**	**32**	10	3	0	0	0	**45**	6	0	3	0	10	0	0	0	0
Mean	-0.81	**29.3**	17.3	7.8	**54.4**	17.3	8.8	3.5	1.8	0.0	0.0	31.3	8.8	1.2	3.2	0.0	13.1	1.2	0.0	0.0	1.2
Standard Deviation	0.250	16.8	12.0	8.5	14.4	7.0	8.8	5.3	4.5	0.0	0.0	10.4	7.4	2.7	4.2	0.0	10.8	1.6	0.0	0.0	1.6

C)

Year	Mean Daily NEE	Cluster																			
		Transitional				Gradient							Zonal					Meridional			
		P1	P2	P3	**Total**	P5	P9	P13	P14	P15	P16	**Total**	P6	P7	P10	P11	**Total**	P4	P8	P12	**Total**
2005	-0.18	0	23	6	29	19	10	0	3	0	0	**32**	26	6	3	0	**35**	3	0	0	3
2006	0.06	10	**39**	6	**55**	3	6	0	0	0	0	10	29	0	6	0	**35**	0	0	0	0
2007	-0.10	3	3	6	13	3	10	6	10	0	0	29	16	0	3	3	23	**35**	0	0	**35**
2008	-0.22	19	16	0	**35**	16	10	0	10	0	0	**35**	0	3	10	0	13	0	16	0	16
2009	-0.36	19	13	10	**42**	13	26	0	0	0	0	**39**	16	0	0	0	16	3	0	0	3
2010	-0.70	16	23	19	**58**	23	0	0	0	0	0	23	3	6	0	0	10	10	0	0	10
2011	-0.13	13	26	26	**65**	0	0	0	0	0	0	0	6	23	6	0	**35**	0	0	0	0
2012	0.1	23	3	6	**32**	23	10	6	0	0	0	**39**	23	0	6	0	29	0	0	0	0
2013	-0.39	**42**	0	0	**42**	13	16	0	10	6	0	**45**	3	3	3	0	10	0	3	0	3
2014	-0.28	6	0	0	6	**42**	13	0	0	0	0	**55**	16	10	10	0	**35**	0	3	0	3
2015	0.10	26	19	19	**65**	6	6	0	0	0	0	13	10	13	0	0	23	0	0	0	0
2016	-0.29	**55**	16	6	**77**	13	0	0	0	0	0	13	10	0	0	0	10	0	0	0	0
2017	-0.18	**58**	16	6	**81**	3	3	0	0	0	0	6	10	0	3	0	13	0	0	0	0
2018	-0.40	0	0	0	0	3	29	13	13	0	0	**58**	0	13	16	6	**35**	3	3	0	6
Mean	-0.220	**20.7**	14.1	8.1	**42.9**	12.9	9.9	1.8	3.2	0.5	0.0	28.3	12.0	5.5	4.8	0.7	23.0	3.9	1.8	0.0	5.8
Standard Deviation	0.209	18.8	11.6	8.1	25.4	11.3	8.9	3.9	4.9	1.7	0.0	18.2	9.3	6.9	4.7	1.9	11.1	9.5	4.3	0.0	9.7

D)

Year	Mean Daily NEE	Cluster																			
		Transitional				Gradient							Zonal					Meridional			
		P1	P2	P3	**Total**	P5	P9	P13	P14	P15	P16	**Total**	P6	P7	P10	P11	**Total**	P4	P8	P12	**Total**
2005	0.24	0	0	7	7	0	3	0	3	13	10	**30**	7	17	3	17	**43**	0	0	20	20
2006	0.46	23	7	7	**37**	7	7	3	3	0	0	20	13	3	0	0	17	3	17	7	27
2007	0.49	0	0	0	0	0	0	23	10	0	0	**33**	0	7	7	23	**37**	0	0	**30**	**30**
2008	0.18	0	0	7	7	0	0	17	10	**30**	0	**57**	3	7	7	7	23	3	7	3	13
2009	0.41	13	0	3	17	17	10	3	20	3	0	**53**	7	3	7	13	**30**	0	0	0	0
2010	0.49	0	7	10	17	3	0	0	0	23	0	27	13	3	3	3	23	3	17	13	**33**
2011	0.57	0	0	0	0	3	13	3	23	10	0	**53**	0	7	17	13	**37**	7	0	3	10
2012	0.54	7	0	10	17	7	3	10	27	3	0	**50**	10	0	10	10	**30**	0	3	0	3
2013	0.08	0	0	3	3	3	**37**	3	17	0	0	**60**	0	13	3	3	20	3	7	7	17
2014	0.33	0	0	0	0	0	0	23	**33**	17	0	**73**	0	0	0	10	10	0	17	0	17
2015	-0.37	0	10	7	17	0	3	0	7	3	7	20	3	10	10	10	**33**	0	0	**30**	**30**
2016	0.35	3	0	3	7	7	0	3	23	13	0	**47**	7	7	7	27	**47**	0	0	0	0
2017	-0.04	0	0	17	17	13	13	0	3	0	0	**30**	3	27	13	0	**43**	3	7	0	10
2018	0.32	0	0	0	0	0	0	3	10	**30**	7	**50**	0	0	7	13	20	0	3	27	**30**
Mean	0.288	3.3	1.7	5.2	10.2	4.3	6.4	6.7	13.6	10.5	1.7	**43.1**	4.8	7.4	6.7	10.7	29.5	1.7	5.5	10.0	17.1
Standard Deviation	0.258	6.9	3.4	4.8	10.4	5.3	10.0	8.4	10.3	11.0	3.4	16.4	4.8	7.4	4.7	8.0	11.1	2.2	6.6	11.8	11.6

Appendix 4: Average annual transitional (A), gradient (B), meridional (C), and zonal (D) cluster occurrence (%) over the entire study period.

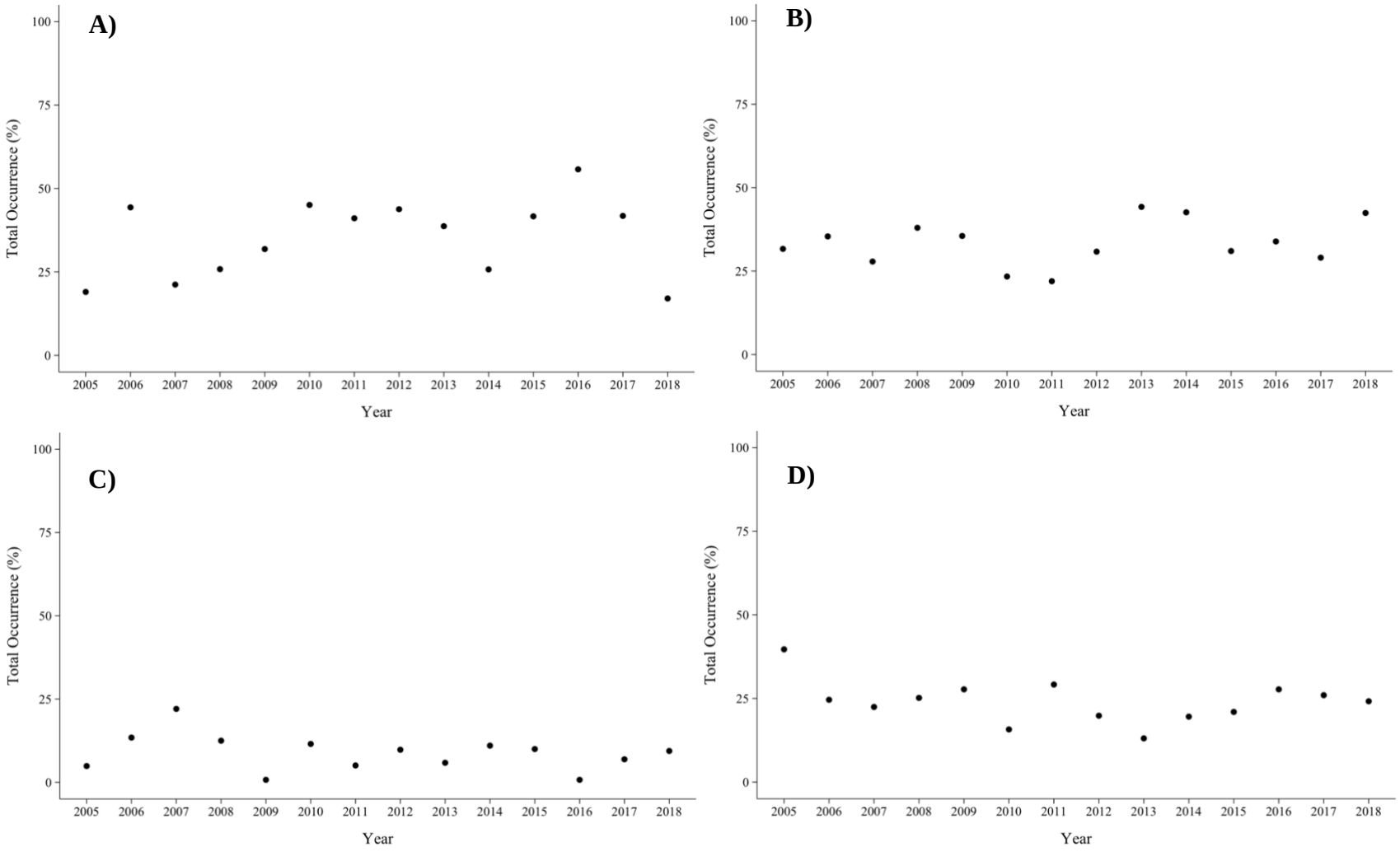

Appendix 5: Average annual transitional (A), gradient (B), meridional (C), and zonal (D) cluster persistence (days) over the entire study period

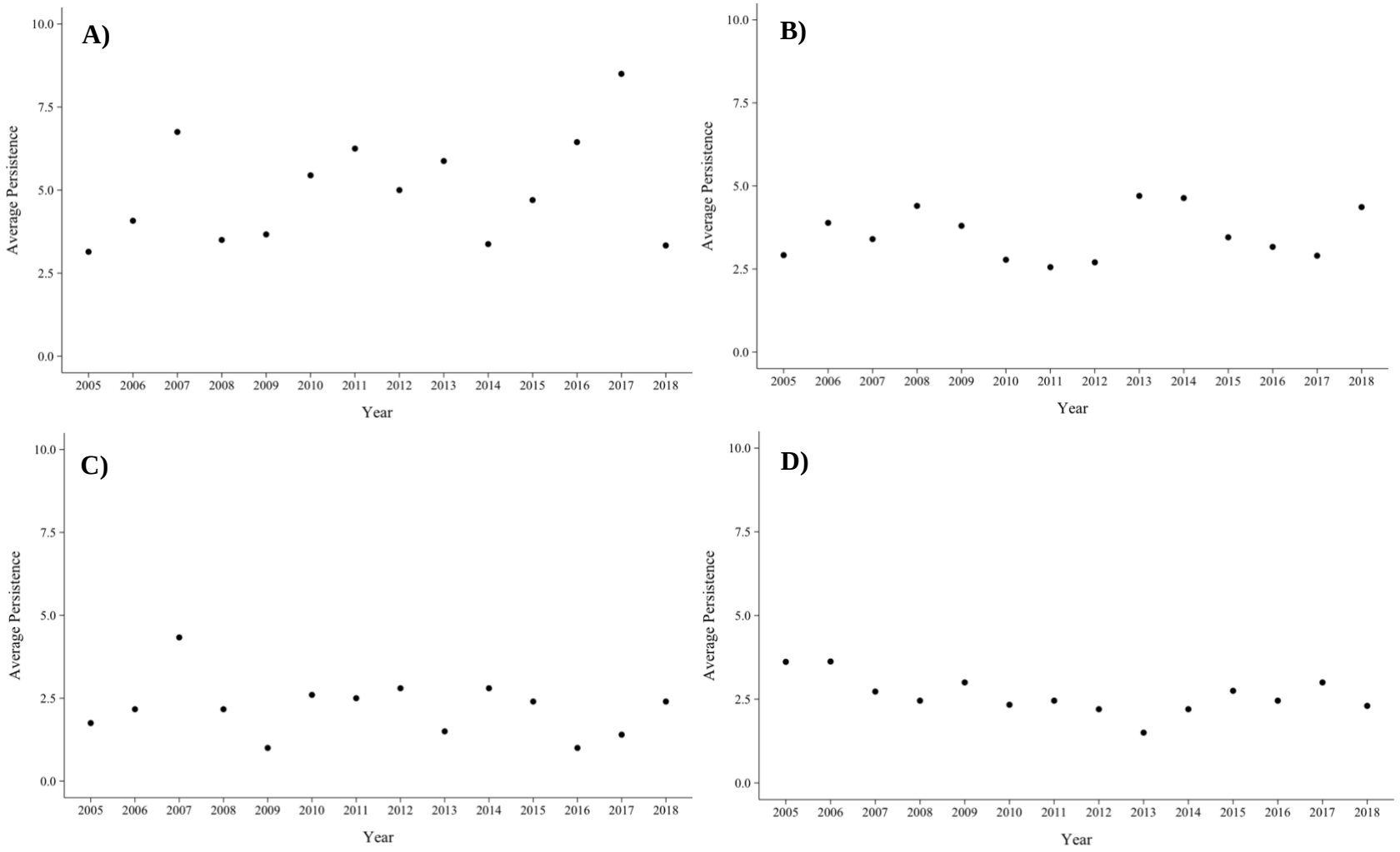

References

Assini, J., & Young, K. L. (2012). Snow cover and snowmelt of an extensive High Arctic wetland: spatial and temporal seasonal patterns. Hydrological Sciences Journal, 57(4), 738-755.

Aurela, M., Laurila, T., & Tuovinen, J. P. (2004). The timing of snow melt controls the annual CO_2 balance in a subarctic fen. Geophysical Research Letters, 31(16).

Ballinger, T. J., Lee, C. C., Sheridan, S. C., Crawford, A. D., Overland, J. E., & Wang, M. (2019). Subseasonal atmospheric regimes and ocean background forcing of Pacific Arctic sea ice melt onset. Climate Dynamics, 52(9), 5657-5672.

Bednorz, E. (2009). Synoptic conditions for rapid snowmelt in the Polish-German lowlands. Theoretical and Applied Climatology, 97(3-4), 279-286.

Boelaert, J., Ollion E., Sodoge J., Megdoud M., Naji O., Lemba Kote A., Renoud T., Hym S. 2021. aweSOM: Interactive Self-Organizing Maps. R package version 1.2. https://cran.r-project.org/web/packages/aweSOM/index.html

Bonfils, C. J. W., Phillips, T. J., Lawrence, D. M., Cameron-Smith, P., Riley, W. J., & Subin, Z. M. (2012). On the influence of shrub height and expansion on northern high latitude climate. Environmental Research Letters, 7(1), 015503.

Box, J. E., Colgan, W. T., Christensen, T. R., Schmidt, N. M., Lund, M., Parmentier, F. J. W., Brown, R., Bhatt, U. S., Euskirchen, E. S., Romanovsky, V. E., & Walsh, J. E. (2019). Key indicators of Arctic climate change: 1971–2017. Environmental Research Letters, 14(4), 045010.

Chen, Y., Ashizawa, N., Yeo, C. K., Yanai, N., & Yean, S. (2021). Multi-scale Self-Organizing Map assisted Deep Autoencoding Gaussian Mixture Model for unsupervised intrusion detection. Knowledge-Based Systems, 224, 107086.

Christensen, T. R., Jonasson, S., Callaghan, T. V., & Havström, M. (1999). On the potential CO_2 release from tundra soils in a changing climate. Applied Soil Ecology, 11(2-3), 127-134.

Cline, D. W. (1997). Snow surface energy exchanges and snowmelt at a continental, midlatitude Alpine site. Water Resources Research, 33(4), 689-701.

Dagg, J., & Lafleur, P. (2011). Vegetation Community, Foliar Nitrogen, and Temperature Effects on Tundra CO_2 Exchange across a Soil Moisture Gradient. Arctic, Antarctic, and Alpine Research, 43(2), 189-197.

Dayan, U., Tubi, A., & Levy, I. (2012). On the importance of synoptic classification methods with respect to environmental phenomena. International Journal of Climatology, 32(5), 681-694.

Dredge, L. A., Kerr, D. E., & Wolfe, S. A. (1999). Surficial materials and related ground ice conditions, Slave Province, NWT, Canada. Canadian Journal of Earth Sciences, 36(7), 1227-1238.

Derksen, C., Brown, R., Mudryk, L., Luojus, K. (2015). Terrestrial Snow Cover. Arctic Report Card 2015.

Euskirchen, E. S., Bret-Harte, M. S., Scott, G. J., Edgar, C., & Shaver, G. R. (2012). Seasonal patterns of carbon dioxide and water fluxes in three representative tundra ecosystems in northern Alaska. Ecosphere, 3(1), 1-19.

Forest, F., Lebbah, M., Azzag, H., & Lacaille, J. (2020). A survey and implementation of performance metrics for self-organized maps. arXiv preprint arXiv:2011.05847.

Foster, J. L., Robinson, D. A., Hall, D. K., & Estilow, T. W. (2008). Spring snow melt timing and changes over Arctic lands. Polar Geography, 31(3-4), 145-157.

Foster, J. L., Cohen, J., Robinson, D. A., & Estilow, T. W. (2013). A look at the date of snowmelt and correlations with the Arctic Oscillation. Annals of Glaciology, 54(62), 196-204.

Gibson, P. B., Perkins-Kirkpatrick, S. E., Uotila, P., Pepler, A. S., & Alexander, L. V. (2017). On the use of self-organizing maps for studying climate extremes. Journal of Geophysical Research: Atmospheres, 122(7), 3891-3903.

Grant, R. F., E. R. Humphreys, and P. M. Lafleur (2015), Ecosystem CO_2 and CH_4 exchange in a mixed tundra and a fen within a hydrologically diverse Arctic landscape: 1. Modeling versus measurements, Journal of Geophysical Research: Biogeosciences, 120, doi:10.1002/ 2014JG002888.

Groendahl, L., Friborg, T., & Soegaard, H. (2007). Temperature and snow-melt controls on interannual variability in carbon exchange in the high Arctic. Theoretical and Applied Climatology, 88(1), 111-125.

Grosse, G., Goetz, S., McGuire, A. D., Romanovsky, V. E., & Schuur, E. A. (2016). Changing permafrost in a warming world and feedbacks to the Earth system. Environmental Research Letters, 11(4), 040201.

Grote, T. (2020). A synoptic climatology of rain-on-snow flooding in Mid-Atlantic region using NCEP/NCAR Re-Analysis. Physical Geography, 1-20.

Hewitson, B. C., & Crane, R. G. (2002). Self-organizing maps: applications to synoptic climatology. Climate Research, 22(1), 13-26.

Humphreys, E. R., and Lafleur, P. M. (2011), Does earlier snowmelt lead to greater CO_2 sequestration in two low Arctic tundra ecosystems? Geophysical Research Letters, 38, L09703, doi:10.1029/2011GL047339.

Huth R, Beck C, Philipp A, Demuzere M, Ustrnul Z, Cahynov' M, Kysel'y J, Einar Tveitof O. (2008). Classifications of atmospheric circulation patterns. Trends and Directions in Climate Research 1146: 105–152.

Intergovernmental Panel on Climate Change (IPCC). (2001), Climate Change 2001: The Scientific Basis; Contribution of Working Group I to the Third Assessment Report of the IPCC, edited by J. C. Houghton et al., 881 pp., Cambridge University Press, New York.

Jagric, T., & Zunko, M. (2013). Neural Network World: Optimized Spiral Spherical SOM (OSS-SOM). Neural Network World, 23(5), 411.

Jiang, Y., Rastetter, E. B., Shaver, G. R., Rocha, A. V., Zhuang, Q., & Kwiatkowski, B. L. (2017). Modeling long-term changes in tundra carbon balance following wildfire, climate change, and potential nutrient addition. Ecological Applications, 27(1), 105-117.

Kanamitsu, W. Ebisuzaki, J. Woollen, S-K Yang, J.J. Hnilo, M. Fiorino, and G. L. Potter. (2002). NCEP-DOE AMIP-II Reanalysis (R-2). Bulletin of the American Meteorological Society.

Kankaanpää, T., Skov, K., Abrego, N., Lund, M., Schmidt, N. M., & Roslin, T. (2018). Spatiotemporal snowmelt patterns within a high Arctic landscape, with implications for flora and fauna. Arctic, Antarctic, and Alpine Research, 50(1), e1415624.

Kaski, S., & Lagus, K. (1996, July). Comparing self-organizing maps. In International conference on artificial neural networks (pp. 809-814). Springer, Berlin, Heidelberg.

Kohonen, T. (1990). The self-organizing map. Proceedings of the IEEE, 78(9), 1464-1480.

Kohonen, T. (2013). Essentials of the self-organizing map. Neural networks, 37, 52-65.

Kudo, G., Nordenhäll, U., & Molau, U. (1999). Effects of snowmelt timing on leaf traits, leaf production, and shoot growth of alpine plants: comparisons along a snowmelt gradient in northern Sweden. Ecoscience, 6(3), 439-450.

Lafleur, P. M., & Humphreys, E. R. (2008). Spring warming and carbon dioxide exchange over low Arctic tundra in central Canada. Global Change Biology, 14(4), 740-756.

Lafleur, P. M., & Humphreys, E. R. (2018). Tundra shrub effects on growing season energy and carbon dioxide exchange. Environmental Research Letters, 13(5), 055001.

Law, B.E., Falge, E., Gu, L., Baldocchi, D.D., Bakwin, P., Berbigier, P., Davis, K., Dolman, A.J., Falk, M., Fuentes, J.D. and Goldstein, A. (2002). Environmental controls over carbon dioxide and water vapor exchange of terrestrial vegetation. Agricultural and Forest Meteorology, 113(1-4), 97-120.

Lawrence, D. M., & Swenson, S. C. (2011). Permafrost response to increasing Arctic shrub abundance depends on the relative influence of shrubs on local soil cooling versus large-scale climate warming. Environmental Research Letters, 6(4), 045504.

Lemus-Canovas, M., Lopez-Bustins, J.A., Martin-Vide, J., Royé, D. 2019. synoptReg: An R package for computing a synoptic climate classification and a spatial

regionalization of environmental data. Environmental Modelling & Software, Vol. 118,114-119pp, ISSN 1364-8152, https://doi.org/10.1016/j.envsoft.2019.04.006

Le Thi, H. A., & Nguyen, M. C. (2014). Self-organizing maps by difference of convex functions optimization. Data Mining and Knowledge Discovery, 28, 1336-1365.

Li, Q., Ma, M., Wu, X., & Yang, H. (2018). Snow cover and vegetation-induced decrease in global albedo from 2002 to 2016. Journal of Geophysical Research: Atmospheres, 123(1), 124-138.

Liu, H., Zhang, Q., Katul, G. G., Cole, J. J., Chapin III, F. S., & MacIntyre, S. (2016). Large CO_2 effluxes at night and during synoptic weather events significantly contribute to CO_2 emissions from a reservoir. Environmental Research Letters, 11(6), 064001.

Loranty, M. M., Abbott, B. W., Blok, D., Douglas, T. A., Epstein, H. E., Forbes, B. C., Jones, B.M., Kholodov, A. L., Kropp, H., Malhotra, A., & Mamet, S. D. (2018). Reviews and syntheses: Changing ecosystem influences on soil thermal regimes in northern high-latitude permafrost regions. Biogeosciences, 15(17), 5287-5313.

Luce, C.H., Tarboton, D.G. and Cooley, K.R., 1998. The influence of the spatial distribution of snow on basin-averaged snowmelt. Hydrological Processes, 12, 1671–1683.

Lund, M., Lafleur, P. M., Roulet, N. T., Lindroth, A., Christensen, T. R., Aurela, M., Chojnicki, B., Flanagan, L., Humphreys, E., Laurila, T., Oechel, W., Olejnik, J., Rinne, J., Schubert, P., & Nilsson, M. B. (2010). Variability in exchange of CO_2 across 12 northern peatland and tundra sites. Global Change Biology, 16(9), 2436-2448.

Mack, M. C., Schuur, E. A., Bret-Harte, M. S., Shaver, G. R., & Chapin III, F. S. (2004). Ecosystem carbon storage in arctic tundra reduced by long-term nutrient fertilization. Nature, 431(7007), 440-443.

Magnani, M., Baneschi, I., Giamberini, M., Raco, B., & Provenzale, A. (2022). Microscale drivers of summer CO_2 fluxes in the Svalbard High Arctic tundra. Scientific Reports, 12(1), 1-14.

Marsh, P., Bartlett, P., MacKay, M., Pohl, S., & Lantz, T. (2010). Snowmelt energetics at a shrub tundra site in the western Canadian Arctic. Hydrological Processes, 24(25), 3603-3620.

Martin, J. P., & Germain, D. (2017). Large-scale teleconnection patterns and synoptic climatology of major snow-avalanche winters in the Presidential Range (New Hampshire, USA). International Journal of Climatology, 37, 109-123.

McGuire, A.D., Anderson, L.G., Christensen, T.R., Dallimore, S., Guo, L., Hayes, D.J., Heimann, M., Lorenson, T.D., Macdonald, R.W. and Roulet, N. (2009). Sensitivity of the carbon cycle in the Arctic to climate change. Ecological Monographs, 79(4), 523-555.

McGuire, A. D., Wirth, C., Apps, M., Beringer, J., Clein, J., Epstein, H., Kicklighter, D. W., Bhatti, J., Chapin III, De Groot, B., & Efremov, D. (2002). Environmental variation, vegetation distribution, carbon dynamics and water/energy exchange at high latitudes. Journal of Vegetation Science, 13(3), 301-314.

Mioduszewski, J. R., Rennermalm, A. K., Robinson, D. A., & Mote, T. L. (2014). Attribution of snowmelt onset in Northern Canada. Journal of Geophysical Research: Atmospheres, 119(16), 9638-9653.

Mu, C.C., Abbott, B.W., Zhao, Q., Su, H., Wang, S.F., Wu, Q.B., Zhang, T.J. and Wu, X.D. (2017). Permafrost collapse shifts alpine tundra to a carbon source but reduces N_2O and CH_4 release on the northern Qinghai-Tibetan Plateau. Geophysical Research Letters, 44(17), 8945-8952.

Musselman, K. N., Clark, M. P., Liu, C., Ikeda, K., & Rasmussen, R. (2017). Slower snowmelt in a warmer world. Nature Climate Change, 7(3), 214-219.

Natali, S. M., Schuur, E. A., & Rubin, R. L. (2012). Increased plant productivity in Alaskan tundra as a result of experimental warming of soil and permafrost. Journal of Ecology, 100(2), 488-498.

Natita, W., Wiboonsak, W., & Dusadee, S. (2016). Appropriate learning rate and neighborhood function of self-organizing map (SOM) for specific humidity pattern classification over Southern Thailand. International Journal of Modeling and Optimization, 6(1), 61.

Neff, J. C., & Hooper, D. U. (2002). Vegetation and climate controls on potential CO_2, DOC and DON production in northern latitude soils. Global Change Biology, 8(9), 872-884.

Newton, B. W. (2018). An evaluation of winter hydroclimatic variables conducive to snowmelt and the generation of extreme hydrologic events in western Canada. Doctoral dissertation, University of Victoria.

Nobrega, S., & Grogan, P. (2008). Landscape and ecosystem-level controls on net carbon dioxide exchange along a natural moisture gradient in Canadian low arctic tundra. Ecosystems, 11(3), 377-396.

Overland, E., Hanna, E., Hanssen-Bauer, I., Kim, S.J., Walsh, J.E., Bhatt, U.S., Thoman, R.L. (2015). Surface Air Temperature. Arctic Report Card 2015.

Pedersen, S. H., Liston, G. E., Tamstorf, M. P., Westergaard-Nielsen, A., & Schmidt, N. M. (2015). Quantifying episodic snowmelt events in Arctic ecosystems. Ecosystems, 18(5), 839-856.

Peterson, B. J., R. M. Holmes, J. W. McClelland, C. J. Vörösmarty, R. B. Lammers, A. I. Shiklomanov, I. A. Shiklomanov, and S. Rahmstorf. (2002). Increasing river discharge to the Arctic Ocean, Science, 298, 2171 – 2173.

Pohl, S., & Marsh, P. (2006). Modelling the spatial–temporal variability of spring snowmelt in an arctic catchment. Hydrological Processes, 20(8), 1773-1792.

Pulliainen, J., Aurela, M., Laurila, T., Aalto, T., Takala, M., Salminen, M., and Laaksonen, A. (2017). Early snowmelt significantly enhances boreal springtime carbon uptake. Proceedings of the National Academy of Sciences, 114(42), 11081-11086.

Rahmstorf, S. (2002). Oceanic circulation and climate during the past 120,000 years, Nature, 419, 207 – 214.

Randazzo, N. A., Michalak, A. M., & Desai, A. R. (2020). Synoptic Meteorology Explains Temperate Forest Carbon Uptake. Journal of Geophysical Research: Biogeosciences, 125(2), e2019JG005476.

Reyes, W. M., Epstein, H. E., Li, X., McGlynn, B. L., Riveros-Iregui, D. A., & Emanuel, R. E. (2017). Complex terrain influences ecosystem carbon responses to temperature and precipitation. Global Biogeochemical Cycles, 31(8), 1306-1317.

Reynolds, J. F., & Tenhunen, J. D. (1996). Ecosystem response, resistance, resilience, and recovery in Arctic landscapes: Introduction. In J. F. Reynolds, & J. Tenhunen (Eds.), Landscape function and disturbance in Arctic Tundra. Ecological Studies, vol. 120 (pp. 3 – 18). Heidelberg: Springer

Rudeva, I., Boschat, G., Lucas, C., Ashcroft, L., Pepler, A., & Hope, P. (2023). Atmospheric trends explained by changes in frequency of short-term circulation patterns. Communications Earth & Environment, 4(1), 127.

Sheridan, S. C., & Lee, C. C. (2011). The self-organizing map in synoptic climatological research. Progress in Physical Geography, 35(1), 109-119.

Schmidt, C. R., Rey, S. J., & Skupin, A. (2011). Effects of irregular topology in spherical self-organizing maps. International Regional Science Review, 34(2), 215-229.

Schneider von Deimling, T., Grosse, G., Strauss, J., Schirrmeister, L., Morgenstern, A., Schaphoff, S., Meinshausen, M. and Boike, J. (2015). Observation-based modelling of permafrost carbon fluxes with accounting for deep carbon deposits and thermokarst activity. Biogeosciences, 12(11), 3469-3488.

Schuur, E. A., Vogel, J. G., Crummer, K. G., Lee, H., Sickman, J. O., & Osterkamp, T. E. (2009). The effect of permafrost thaw on old carbon release and net carbon exchange from tundra. Nature, 459(7246), 556-559.

Semiletov, I., Pipko, I., Gustafsson, Ö., Anderson, L. G., Sergienko, V., Pugach, S., & Shakhova, N. (2016). Acidification of East Siberian Arctic Shelf waters through addition of freshwater and terrestrial carbon. Nature Geoscience, 9(5), 361-365.

Stigter, E. E., Litt, M., Steiner, J. F., Bonekamp, P. N., Shea, J. M., Bierkens, M. F., & Immerzeel, W. W. (2018). The importance of snow sublimation on a Himalayan glacier. Frontiers in Earth Science, 6, 108.

Stone, R. S., Dutton, E. G., Harris, J. M., & Longenecker, D. (2002). Earlier spring snowmelt in northern Alaska as an indicator of climate change. Journal of Geophysical Research: Atmospheres, 107(D10), ACL-10.

Stow, D. A., Hope, A., McGuire, D., Verbyla, D., Gamon, J., Huemmrich, F., & Hinzman, L. (2004). Remote sensing of vegetation and land-cover change in Arctic Tundra Ecosystems. Remote Sensing of Environment, 89(3), 281-308.

Sun, Y., Qu, F., Zhu, X., Sun, B., Wang, G., Yin, H., & Chen, Q. (2020). Non-linear responses of net ecosystem productivity to gradient warming in a paddy field in Northeast China. PeerJ, 8, e9327.

Tan, A., Adam, J. C., & Lettenmaier, D. P. (2011). Change in spring snowmelt timing in Eurasian Arctic rivers. Journal of Geophysical Research: Atmospheres, 116(D3).

Tarnocai, C., Canadell, J. G., Schuur, E. A. G., Kuhry, P., Mazhitova, G., and Zimov, S. (2009). Soil organic carbon pools in the northern circumpolar permafrost region. Global Biogeochemical Cycles, 23: doi:10.1029/2008GB003327

Verburg, P. S., Arnone III, J. A., Obrist, D., Schorran, D. E., Evans, R. D., Leroux-swarthout, D., & Coleman, J. S. (2004). Net ecosystem carbon exchange in two experimental grassland ecosystems. Global Change Biology, 10(4), 498-508.

Wehrens R and Kruisselbrink J. 2018. Flexible Self-Organizing Maps in kohonen 3.0. Journal of Statistical Software, 87(7), 1–18. doi: 10.18637/jss.v087.i07.

Welker, J. M., Fahnestock, J. T., Henry, G. H., O'Dea, K. W., & Chimner, R. A. (2004). CO_2 exchange in three Canadian High Arctic ecosystems: Response to long-term experimental warming. Global Change Biology, 10(12), 1981-1995.

Wilcox, E. J., Keim, D., de Jong, T., Walker, B., Sonnentag, O., Sniderhan, A. E., & Marsh, P. (2019). Tundra shrub expansion may amplify permafrost thaw by advancing snowmelt timing. Arctic Science, 5(4), 202-217.

Winchell, T. S., Barnard, D. M., Monson, R. K., Burns, S. P., & Molotch, N. P. (2016). Earlier snowmelt reduces atmospheric carbon uptake in midlatitude subalpine forests. Geophysical Research Letters, 43(15), 8160-8168.

Wipf, S., & Rixen, C. (2010). A review of snow manipulation experiments in Arctic and alpine tundra ecosystems. Polar Research, 29(1), 95-109.

Wookey, P. A., Aerts, R., Bardgett, R. D., Baptist, F., Bråthen, K. A., Cornelissen, J. H., ... & Shaver, G. R. (2009). Ecosystem feedbacks and cascade processes: understanding their role in the responses of Arctic and alpine ecosystems to environmental change. Global Change Biology, 15(5), 1153-1172.

Yang D, K., & Zhang T, Y. H. (2002). Siberian Lena river hydrologic regime and recent charge. Journal of Geophysical Research—Atmospheres, 107, 4694.

Yarnal, B., & Draves, J. D. (1993). A synoptic climatology of stream flow and acidity. Climate Research, 2, 193-202.

Zhang, T., Bowling, S. A., & Stamnes, K. (1997). Impact of the atmosphere on surface radiative fluxes and snowmelt in the Arctic and Subarctic. Journal of Geophysical Research: Atmospheres, 102(D4), 4287-4302.

Zhang, W., Miller, P. A., Smith, B., Wania, R., Koenigk, T., & Döscher, R. (2013). Tundra shrubification and tree-line advance amplify arctic climate warming: results from an individual-based dynamic vegetation model. Environmental Research Letters, 8(3), 034023.

Zhang, W., Wang, J., Jin, D., Oreopoulos, L., & Zhang, Z. (2018). A deterministic self-organizing map approach and its application on satellite data based cloud type classification. In 2018 IEEE International Conference on Big Data (Big Data) (pp. 2027-2034). IEEE.

Zhang, T., Xu, M., Xi, Y., Zhu, J., Tian, L., Zhang, X., Wang, Y., Li, Y., Shi, P., Yu, G. and Sun, X. (2015). Lagged climatic effects on carbon fluxes over three grassland ecosystems in China. Journal of Plant Ecology, 8(3), 291-302.

Zheng, L., Cheng, X., Chen, Z., Wang, S., Liang, Q., & Wang, K. (2022). Global Snowmelt Onset Reflects Climate Variability: Insights from Spaceborne Radiometer Observations. Journal of Climate, 35(10), 2945-2959.

Zhong, S., Yu, L., Heilman, W. E., Bian, X., & Fromm, H. (2020). Synoptic weather patterns for large wildfires in the northwestern United States—A climatological analysis using three classification methods. Theoretical and Applied Climatology, 141, 1057-1073.

Zhou, Y. M., Meng, G. L., Tai, Z. J., Han, J. Q., Deng, J. F., Wang, H. W., and Li, M. H. (2019). Effects of experimental warming on growing season temperature and carbon exchange in an alpine tundra ecosystem. Russian Journal of Ecology, 50, 474-481.

Zhou, X., Gao, T., Zheng, N., Yang, B., Li, Y., Yu, F., Awada, T. and Zhu, J. (2022). Accuracies of field CO_2–H_2O data from open-path eddy-covariance flux systems: assessment based on atmospheric physics and biological environment. Geoscientific Instrumentation, Methods and Data Systems, 11(2), 335-357.